


1-1-2016

# An Analysis Of Plasticity In The Rat Respiratory System Following Cervical Spinal Cord Injury And The Application Of Nanotechnology To Induce Or Enhance Recovery Of Diaphragm Function

Janelle Lorien Walker  
*Wayne State University,*

Follow this and additional works at: [https://digitalcommons.wayne.edu/oa\\_dissertations](https://digitalcommons.wayne.edu/oa_dissertations)

 Part of the [Nanoscience and Nanotechnology Commons](#), [Neurosciences Commons](#), and the [Physiology Commons](#)

---

## Recommended Citation

Walker, Janelle Lorien, "An Analysis Of Plasticity In The Rat Respiratory System Following Cervical Spinal Cord Injury And The Application Of Nanotechnology To Induce Or Enhance Recovery Of Diaphragm Function" (2016). *Wayne State University Dissertations*. 1602.

[https://digitalcommons.wayne.edu/oa\\_dissertations/1602](https://digitalcommons.wayne.edu/oa_dissertations/1602)

This Open Access Dissertation is brought to you for free and open access by DigitalCommons@WayneState. It has been accepted for inclusion in Wayne State University Dissertations by an authorized administrator of DigitalCommons@WayneState.

**AN ANALYSIS OF PLASTICITY IN THE RAT RESPIRATORY SYSTEM FOLLOWING  
CERVICAL SPINAL CORD INJURY AND THE APPLICATION OF NANOTECHNOLOGY TO  
INDUCE OR ENHANCE RECOVERY OF DIAPHRAGM FUNCTION**

by

**JANELLE WALKER**

**DISSERTATION**

Submitted to the Graduate School

of Wayne State University,

Detroit, Michigan

in partial fulfillment of the requirements

for the degree of

**DOCTOR OF PHILOSOPHY**

2016

MAJOR: ANATOMY AND CELL BIOLOGY

Approved By:

\_\_\_\_\_  
Advisor

\_\_\_\_\_  
Date

\_\_\_\_\_

\_\_\_\_\_

\_\_\_\_\_

\_\_\_\_\_

## **DEDICATION**

To the next generation of scientist  
especially Mallory

## **ACKNOWLEDGEMENTS**

First and foremost, I thank my mentor, Dr. Harry Goshgarian. His guidance, support, and advice have led to my success. The passion for his life's work has been contagious and I am honored to be a part of the story. His confidence in my abilities created an environment for me to explore, and for that I will forever be grateful.

I would like to thank my committee. Dr. Kwaku Nantwi for the time he invested to develop my surgical techniques and for always being available to discuss ideas. Dr. Dennis Goebel for his willingness to always talk with me when I needed the support. Dr. Jason Mateika for his input and advice towards my project. Dr. Guangzhao Mao for collaborating with our lab making a large piece of my work possible with the assistance of Dr. Yanhua Zhang and Fangchao Liu. I would also like to thank Dr. Paul Walker for his guidance and dedication to my success.

I would like to thank all of the individuals that make up the Division of Laboratory Animals Resources, specifically Dr. Tara Cotroneo and Kathy Baklarz. My chronic studies produced countless barriers and I could not have completed this work without their constant support. Also, Andrew Dayton for being there in the beginning and for helping me acclimate to the lab, and Dr. Zeljka Minic for always being a friend and sharing her knowledge of physiology. I would also like to thank Selina and Tonia for their work to make our department run as smooth as it does. I thank the Craig H. Neilsen Foundation and National Institutes of Health for funding my studies.

Finally, I would like to thank my family and friends that were there to celebrate my successes, encourage me when I needed the support, and made me laugh instead of losing my mind. Especially my parents Dan and Sharon Buttry for always supporting my quest for knowledge and nurturing my love of science.

## TABLE OF CONTENTS

Dedication .....	ii
Acknowledgements .....	iii
List of Tables .....	vi
List of Figures.....	vii
List of Abbreviations .....	x
Introduction .....	1
Chapter 1: WGA-Alexa Labeling in the Phrenic Motor System .....	8
Summary.....	8
Introduction .....	8
The pattern and extent of retrograde transsynaptic transport of WGA-Alexa 488 in the phrenic motor system is dependent upon the site of application..	11
Injection of WGA-Alexa 488 into the ipsilateral hemidiaphragm of acutely and chronically C2 hemisectioned rats reveal activity-dependent synaptic plasticity in the respiratory motor pathways .....	21
WGA-Alexa transsynaptic labeling in the phrenic motor system of adult rats: Intrapleural injection versus intradiaphragmatic injection .....	42
Closing Statement .....	61
Chapter 2: Recovery of Diaphragm Function in the Acutely Injured Spinal Cord Model Using a Retrograde Transsynaptic Theophylline Bound Nanoconjugate .....	63
Summary.....	63
Introduction .....	63
Visualization of the WGA-HRP-AuNP-proTHP nanoconjugate .....	68
Nanoconjugate synthesis .....	68
EMG response to WGA-HRP-AuNP-proTHP and control solutions .....	71
Phrenic nerve response to WGA-HRP-AuNP-proTHP and control solutions.	79
Discussion.....	88
Closing Statement .....	94

Chapter 3: Application of the Theophylline Bound Nanoconjugate in the Chronically Injured Spinal Cord Model.....	96
Summary.....	96
Introduction .....	96
Physiological response to WGA-HRP-AuNP-proTHP .....	98
Influence of spontaneous activity on recovery .....	100
Discussion.....	103
Overall Summary.....	105
Materials and Methods .....	110
Appendix: Nanoconjugate Patent Information.....	124
References.....	125
Abstract.....	144
Autobiographical Statement.....	146

## LIST OF TABLES

<b>Table 1:</b> Location of WGA-Alexa 488 labeling in the medulla and spinal cord of the acute C2Hx, chronic sham, and chronic C2Hx rats .....	30
<b>Table 2:</b> The 11 rats included in the intrapleural study and the locations and tracers injected into each rat .....	44
<b>Table 3:</b> Cell counts from 270 cervical spinal cord sections sampled from 5 rats .....	45
<b>Table 4:</b> Cell counts from a total of 82 medulla sections sampled from 6 rats .....	51
<b>Table 5:</b> Thermogravimetric analysis of WGA-HRP-AuNP-proTHP nanoconjugates .....	70
<b>Table 6:</b> Left phrenic nerve percent recovery on day 3 .....	81
<b>Table 7:</b> Left phrenic nerve percent recovery on day 7 .....	84
<b>Table 8:</b> Left phrenic nerve percent recovery on day 14 .....	84

## LIST OF FIGURES

<b>Figure 1:</b> Diagram of the bulbospinal pathway .....	2
<b>Figure 2:</b> EMG recording of the diaphragm immediately after C2Hx .....	3
<b>Figure 3:</b> Images from rats that had a left C2Hx followed by a contralateral (right) phrenicotomy and ipsilateral (left) intradiaphragmatic injection of WGA-HRP .....	7
<b>Figure 4:</b> WGA-Alexa 488 granulation in labeled neurons .....	13
<b>Figure 5:</b> Electromyogram of the diaphragm to confirm C2Hx .....	13
<b>Figure 6:</b> Labeling pattern following injection of 50 µl of 2% WGA-Alexa 488 into the left hemidiaphragm from a rat that was subjected to left C2Hx .....	14
<b>Figure 7:</b> Labeling pattern shown following WGA-Alexa 488 application for 1 h to the left phrenic nerve from a rat that was subjected to left C2Hx .....	16
<b>Figure 8:</b> Photographs of the surgical exposure of the left phrenic nerve and the application of WGA-Alexa 488 to the nerve for 1 h .....	17
<b>Figure 9:</b> EMG traces from the left and right hemidiaphragm immediately after a Sham C2Hx....	23
<b>Figure 10:</b> EMG traces from the left and right hemidiaphragm 22 weeks post C2Hx .....	23
<b>Figure 11:</b> EMG traces from the left and right hemidiaphragm 8 weeks after a Sham C2Hx .....	24
<b>Figure 12:</b> Spinal cord and medulla sections from an acute C2Hx rat following WGA-Alexa 488 Injection .....	25
<b>Figure 13:</b> C7 spinal cord sections from an acute and a chronic C2Hx rat .....	26
<b>Figure 14:</b> C4/C5 spinal cord sections of a chronic C2Hx rat .....	28
<b>Figure 15:</b> C8/T1 spinal cord sections from an acute and a chronic C2Hx rat .....	29
<b>Figure 16:</b> T4/T5 spinal cord sections from an acute and a chronic C2Hx rat .....	29
<b>Figure 17:</b> Drawings of the medulla summarizing all the locations of WGA-Alexa 488 in the acute C2Hx and Chronic C2Hx rats .....	31
<b>Figure 18:</b> Medulla sections from an acute and a chronic C2Hx rat .....	32
<b>Figure 19:</b> Medulla sections from a chronic C2Hx rat .....	32
<b>Figure 20:</b> Hypoglossal nuclei from an acute and a chronic C2Hx rat .....	33
<b>Figure 21:</b> Transverse sections of the cervical spinal cord at the level of the phrenic nuclei in the same rat following intrapleural and intradiaphragmatic injection.....	47



<b>Figure 22:</b> Sagittal section through the cervical spinal cord following intrapleural and intradiaphragmatic injection .....	48
<b>Figure 23:</b> T6 spinal cord section following intrapleural and intradiaphragmatic injection .....	49
<b>Figure 24:</b> High magnification of the NA and rVRG following intrapleural injection and vagus nerve injection .....	50
<b>Figure 25:</b> High magnification of the NA and rVRG following intrapleural, intradiaphragmatic and vagus nerve injection .....	52
<b>Figure 26:</b> Sagittal section of the medulla displaying the right rVRG and the intermingled cells of the right NA .....	55
<b>Figure 27:</b> NA and rVRG and ventrally extended cells following intrapleural, intradiaphragmatic and vagus nerve injection .....	56
<b>Figure 28:</b> Dorsal medulla following vagus nerve injection .....	57
<b>Figure 29:</b> NA and rVRG following vagus nerve injection and intradiaphragmatic injection .....	58
<b>Figure 30:</b> Schematic of the fabrication of the tripartite nanoconjugate .....	67
<b>Figure 31:</b> Cervical spinal cord and medulla sections displaying WGA labeling following nanoconjugate injection .....	69
<b>Figure 32:</b> EMG traces day 7 post injection 0.03mg/kg nanoconjugate .....	72
<b>Figure 33:</b> EMG traces day 2 and day 14 post injection of 0.07mg/kg nanoconjugate .....	73
<b>Figure 34:</b> EMG traces day 5 post injection 0.12mg/kg nanoconjugate .....	74
<b>Figure 35:</b> EMG traces day 2 post injection 0.14mg/kg dose .....	74
<b>Figure 36:</b> EMG traces from LHD day 7 post injection; 0.03mg/kg vs 0.07mg/kg .....	75
<b>Figure 37:</b> EMG traces post injection of control solutions .....	76
<b>Figure 38:</b> EMG traces day 5 post injection of proTHP 0.07mg/kg in diaphragm .....	76
<b>Figure 39:</b> EMG traces from the left and right hemidiaphragm day 7 post injection of saline.....	77
<b>Figure 40:</b> Percent Recovery Detected by EMG .....	78
<b>Figure 41:</b> Comparison of day 3 Nerve Recordings .....	80
<b>Figure 42:</b> Comparison of day 7 Nerve Recordings .....	82
<b>Figure 43:</b> Comparison of day 14 Nerve Recordings .....	83
<b>Figure 44:</b> Dose 0.03mg/kg Nerve Recordings .....	85

<b>Figure 45:</b> Dose 0.07mg/kg Nerve Recordings .....	86
<b>Figure 46:</b> Dose 0.14mg/kg Nerve Recordings .....	87
<b>Figure 47:</b> Chronic C2Hx model EMG response to nanoconjugate dose .....	99
<b>Figure 48:</b> Nerve recording dose comparison in chronically C2Hx .....	101
<b>Figure 49:</b> Effect of spontaneous recovery on nerve recordings in nanoconjugate injected chronically C2Hx rats .....	102
<b>Figure 50:</b> Intraoperative view of nanoconjugate injection sites .....	114
<b>Figure 51:</b> Example neurograms identifying the apneic and recruitment thresholds .....	119
<b>Figure 52:</b> Phrenic nerve tracing .....	123

## LIST OF ABBREVIATIONS

**Au:** gold

**C2Hx:** spinal cord hemisection at the second cervical spinal segment

**CTB:** cholera toxin subunit beta

**CPP:** crossed phrenic pathway

**DMX:** dorsal motor nucleus of vagus

**DSCT:** dorsal spinocerebellar tract

**EMG:** electromyogram

**im:** intramuscular

**ip:** intraperitoneal

**LHD:** left hemidiaphragm

**LPN:** left phrenic nerve

**NA:** nucleus ambiguus

**NP:** nanoparticle

**PMNs:** phrenic motoneurons

**PN:** phrenic nuclei

**PRN:** parvicellular reticular nuclei

**ProTHP:** pro-theophylline

**PRV-Bartha:** Pseudorabies virus Bartha strain

**RPN:** right phrenic nerve

**RST:** reticulospinal tract

**rVRGs:** rostral ventral respiratory groups

**sc:** subcutaneous

**SCI:** spinal cord injury

**TB:** True blue

**TGA:** Thermogravimetric analysis

**VSCT:** ventral spinocerebellar tract

**WGA-Alexa 488:** wheat germ agglutinin conjugated to Alexa 488

**WGA-Alexa 594:** wheat germ agglutinin conjugated to Alexa 594

**WGA-HRP:** wheat germ agglutinin conjugated to horseradish peroxidase

## INTRODUCTION

A high cervical spinal cord injury (SCI) in mammals often impairs respiratory motor function due to disruption of the bulbospinal pathway, the major pathway responsible for descending respiratory drive. The bulbospinal pathway transmits excitatory respiratory impulses from the right and left rostral ventral respiratory groups (rVRGs) in the medulla to depolarize the phrenic nuclei (PN) in the third through sixth cervical spinal segments (DeVries and Goshgarian, 1989). The PN then transmits the excitatory impulse to the diaphragm via the phrenic nerves. The surgical model used in the following studies is a left hemisection at the second cervical spinal segment (C2Hx). The left C2Hx disrupts the ipsilateral rVRG axonal connections to the left phrenic nucleus and causes ipsilateral (left) hemidiaphragm paralysis (Fig. 1). Electromyogram (EMG) recordings of the diaphragm immediately after injury verify the loss of diaphragm activity (Fig. 2).

A secondary latent pathway, the crossed phrenic pathway (CPP), consists of collateral axons from the contralateral and ipsilateral rVRGs that decussate rostral to or at the level of the PN (Fig. 1) (Porter, 1895; Moreno et al., 1992; for review Goshgarian, 2003). The axonal decussation is caudal to the C2Hx, and is therefore intact following injury. Under normal conditions the neurons involved in the CPP are in a latent state, meaning that they are not transmitting a signal from the rVRG to the PN to activate the diaphragm. In most cases, physiological evidence of the CPP can be demonstrated immediately after injury by the ability to produce an augmented breath (Fig. 2, arrows). An augmented breath occurs when descending respiratory drive from both rVRGs increase for a single breath. This activates the diaphragm bilaterally utilizing the non-injured pathway to the right hemidiaphragm and the CPP to the left hemidiaphragm (Fig. 1). An augmented breath is characteristically followed by a short period of apnea (Fig. 2) (Golder et al., 2001a).

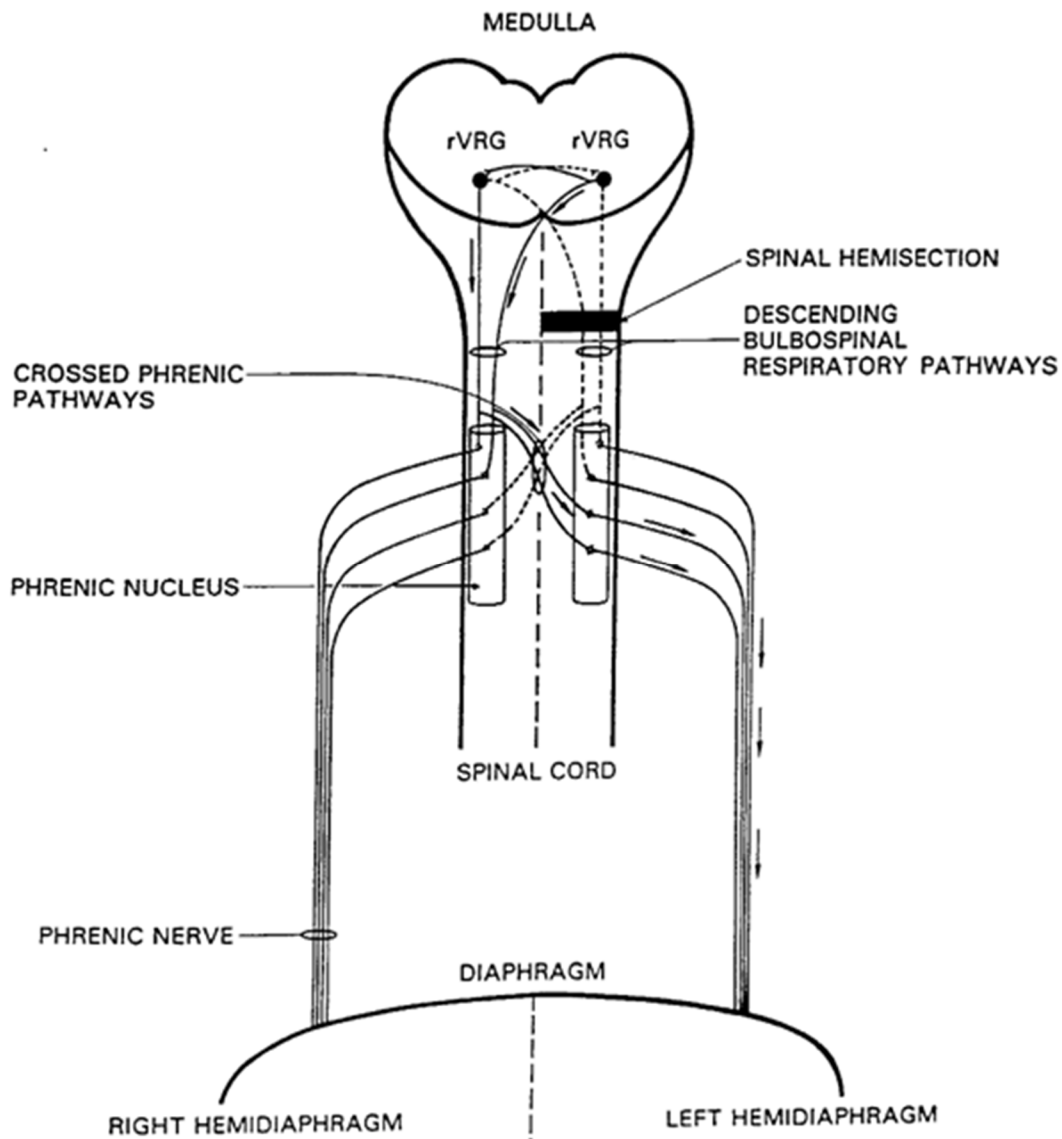


**Figure 1: Diagram of the bulbospinal pathway.** The descending respiratory drive is carried by the descending bulbospinal respiratory pathways. Pre-motor neurons in the rostral ventral respiratory groups (rVRGs) located in the ventral medulla send impulses to the motoneurons of the phrenic nucleus located in the 3<sup>rd</sup>-6<sup>th</sup> cervical spinal segments. The motoneurons in the phrenic nuclei then stimulate the diaphragm to contract via the phrenic nerve. The location of the spinal hemisection at the second cervical segment is rostral to the decussation of the latent crossed phrenic pathway leaving these axons uninjured following a C2Hx. Arrows indicate the pathway over which respiratory impulses travel upon activation of the crossed phrenic pathway to restore function to the paralyzed hemidiaphragm under certain conditions. Figure from Phillis and Goshgarian, 2001.

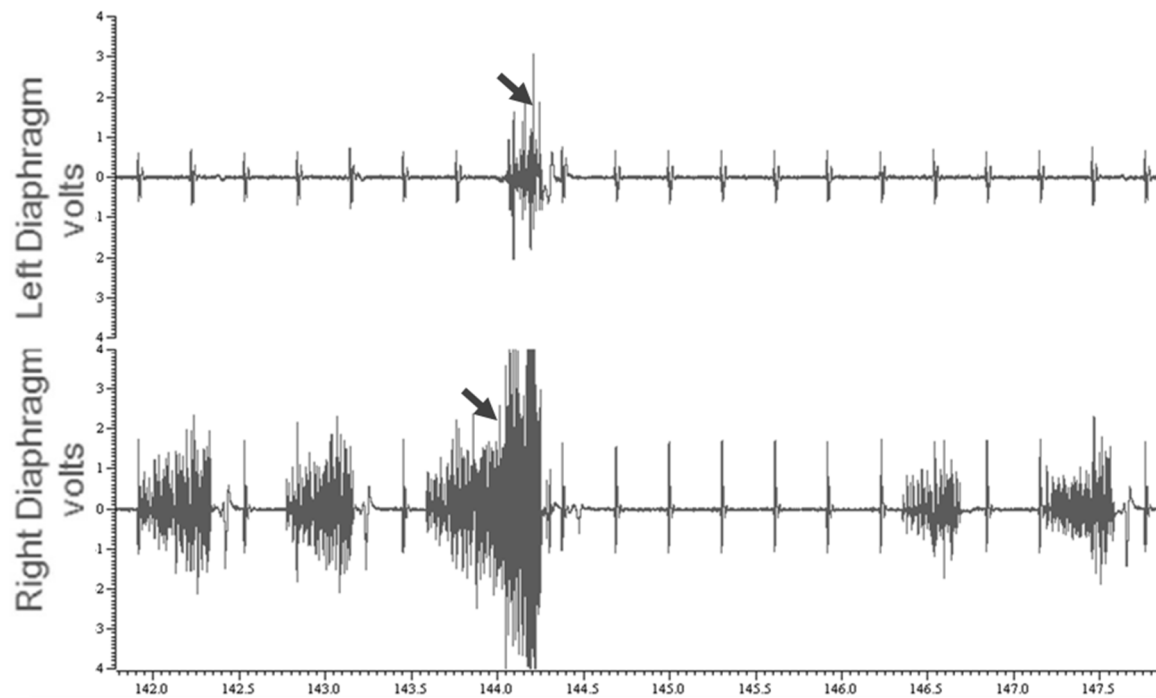


**Figure 2: EMG recording of the diaphragm immediately after C2Hx.** EMG recording of left (top panel) hemidiaphragm (ipsilateral to C2Hx) and right (bottom panel) hemidiaphragm immediately following a C2Hx. Note that the left hemidiaphragm is paralyzed (lack of bursts) following the C2Hx, while the right hemidiaphragm is actively contracting. An augmented breath is demonstrated (arrows) followed by a short period of apnea. The augmented breath confirms the crossed phrenic pathway is intact following the C2Hx and is capable of contacting the diaphragm. The spikes on the left and right are EKG (electrocardiogram) waves. Buttry and Goshgarian, 2014.

However, in the rat model following a SCI the ipsilateral phrenic nerve can spontaneously regain phasic function over time (6 weeks or more) by utilizing the CPP (Nantwi et al., 1999; Golder et al., 2001a; Fuller et al., 2008). In addition, recovery can occur in a relatively short time frame with pharmacological activation (Nantwi et al., 1996; Nantwi et al., 2003a; Kajana and Goshgarian, 2008a) or within minutes to hours with a contralateral phrenicotomy (Porter, 1895 (dog); Goshgarian, 1979 (rat)).

Pharmacological intervention following SCI to activate the latent CPP to regain diaphragm function holds great potential. Clinical use of theophylline (1,3-dimethylxanthine), a methylxanthine, in man has been reported as early as 1922 (Schultze-

Werninghaus and Meier-Sydow, 1982). Theophylline, acting as a bronchodilator, has been prescribed to treat symptoms of asthma, bronchitis, and emphysema (Aubier et al., 1981; Moro et al., 2006; Nantwi et al., 1996; Nantwi et al., 2002). Specifically, theophylline, a non-selective phosphodiesterase inhibitor (Butcher and Sutherland, 1962; Horn and McAfee, 1977), has been shown to enhance respiratory drive by acting as an adenosine receptor antagonist (Eldridge et al., 1983 and 1985; Nantwi and Goshgarian, 1998) that interferes with both A1 and A2 adenosine receptors (Nantwi et al., 1996). The return of diaphragm function can be transient or permanent based on the number and frequency of doses (Nantwi et al., 1996, 1x IV; Nantwi et al., 2003a, multiple oral).

In rats following a C2Hx, systemic (oral or intravenous) administration of theophylline stimulated the CPP increasing respiratory output and resulted in recovery of function for both the phrenic nerve and diaphragm (Nantwi et al., 1996; Nantwi and Goshgarian, 2002). However, there is limited documentation of clinical studies that investigate the use of theophylline in humans following SCI to increase respiratory drive (Ferguson et al., 1999; Bascom et al., 2005; Tzelepis et al., 2006). Lack of data in humans is due to the high therapeutic dose of theophylline required following SCI that can cause intolerable side effects including nausea, vomiting, nervousness, increased or irregular heartbeat, and insomnia (Aubier et al., 1981; Tzelepis et al., 2006; Barnes, 2013). These side effects are caused by a high concentration of the drug in the plasma leading to global phosphodiesterase inhibition and adenosine A1-receptor antagonism resulting in a hyperactive state of many non-targeted neurons (Barnes, 2013). Further efforts to investigate the clinical outcome of systemic theophylline administration have been abandoned due to intolerable side effects and lack of quality data.



Collectively, the past studies provide key information on the anatomy and function of the CPP that can be stimulated to re-direct the descending respiratory drive following SCI. In addition, several drugs capable of stimulating the CPP have been characterized *in vivo* with rodent models. Unfortunately, systemic administration of theophylline at a therapeutic dose causes intolerable side effects in humans. Therefore, an alternative method to administer theophylline was needed. Being able to target the drug to select respiratory nuclei holds the potential to greatly reduce the therapeutic dose and to reduce or eliminate unwanted side effects.

The key to delivering a drug to select populations of respiratory nuclei is wheat germ agglutinin (WGA). WGA is a lectin that has an affinity to sugars, specifically N-acetyl-d-glucosamine and sialic acid, which are components of glycoconjugates found on most neuronal cell membranes (Borges and Sidman, 1982; Fabian and Coulter, 1985; Robertson, 1990). These substances act as neuronal cell membrane receptors when WGA is injected into muscle (Borges and Sidman, 1982; Fabian and Coulter, 1985; Robertson, 1990). As a consequence of binding to these specific receptor sites on the motor nerve terminal membranes, WGA undergoes receptor-mediated endocytosis (Borges and Sidman, 1982). Subsequently WGA is retrogradely transported along the axon within vesicles, lysosomes, cisternae and tubules. Following transport to the cell body, the above membrane compartments fuse and the transported lectin is incorporated into lysosomes (Schwab et al., 1979; Ruda and Coulter 1982; Broadwell and Balin, 1985). In the electron microscopic studies of Schwab et al. (1979), the selective release of WGA from postsynaptic dendrites followed by the rapid uptake of the lectin into presynaptic nerve terminals was observed. However, after counting the number of presynaptic terminals labeled the authors concluded that the retrograde transsynaptic transport capability of WGA was far less than other

macromolecules such as tetanus toxin (Schwab et al., 1979). The precise mechanism for the release of WGA from postsynaptic dendrites into the synaptic cleft is still unknown.

Since the 1980s it has been suggested that there is a preferential release from postsynaptic dendrites of physiological active synaptic connections (Harrison et al., 1984, 1986; Jankowska, 1985). This was initially determined by observing the location and number of labeled motoneurons and propriospinal neurons in the spinal cord of cats and rats following the injection of wheat germ agglutinin conjugated to horseradish peroxidase (WGA-HRP) into motor nerves of chronically anesthetized and awake animals (Harrison et al., 1984; Jankowska, 1985). Furthermore, the extent of neuronal labeling was enhanced when the motor nerves were stimulated which facilitated synaptic activity to the motoneurons (Harrison et al., 1984; Jankowska, 1985). Commonly, as in these studies mentioned, WGA is conjugated with HRP in order to visualize the locations of WGA following injection. Phrenic motoneurons (PMNs) are unique in that they maintain a phasic discharge regardless of whether an animal is anesthetized or awake. Neurons in the rVRG are responsible for maintaining this discharge (Ellenberger and Feldman, 1988) and this is the presumed basis for the activity-dependent retrograde transsynaptic labeling of both PMNs and rVRG pre-motor neurons when WGA-HRP is injected into the diaphragm following a C2Hx (Moreno et al., 1992; Fig. 3).

Based on the demonstration of transsynaptic transport of WGA-HRP in the phrenic motor system following SCI (Moreno et al., 1992), WGA-HRP was utilized to target drug delivery to the motoneurons of the PN and pre-motor rVRG neurons involved in respiration. In order to bind theophylline (or drug of choice) to WGA-HRP a carrier was needed to facilitate the chemical conjugation. *In vivo* application of gold (Au) nanoparticles (NPs) has been established in the literature and are known their biocompatibility and for easy

attachment of various structures via chemical bonds to the Au (De Jong et al, 2008; Chen et al., 2009; Duncan et al., 2010; Jain 2010; Thakor et al., 2011; Dreaden et al., 2011, 2012; Zhou et al., 2013; Cheng et al., 2013; Mieszawska et al., 2013).

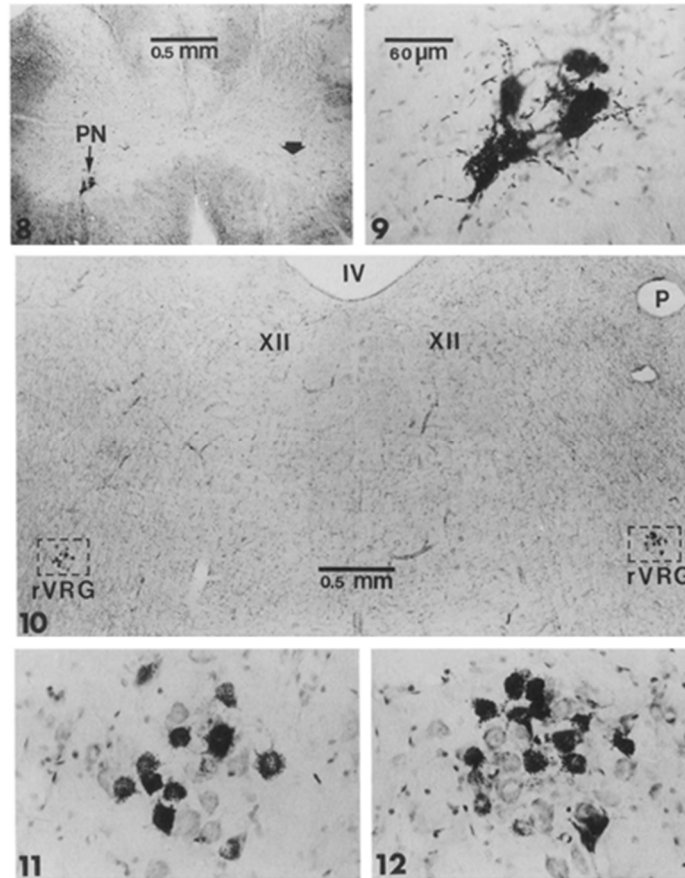


**Figure 3: Images from rats that had a left C2Hx followed by a contralateral (right) phrenicotomy and ipsilateral (left) intradiaphragmatic injection of WGA-HRP.** Fig. 8 Photomicrograph of transverse section through the C4 level of the spinal cord in the hemisected rat expressing the crossed phrenic reflex. Note the phrenic motoneurons in the left PN that have been retrogradely labeled with WGA-HRP. Also note the absence of any labeled neurons in the right phrenic nucleus (solid black arrow) Fig.9 High power magnification of the labeled motoneurons of the left phrenic nucleus shown in Fig. 8 Fig. 10 Photomicrograph of a transverse section through the medulla. In this spinal hemisected rat expressing the crossed phrenic reflex, note the neurons in both rVRGs (enclosed by rectangles) that have been transsynaptically labeled with WGA-HRP. P, pinhole. IV, fourth ventricle. XII, rostral pole of hypoglossal motor nucleus. Fig. 11 High power magnification of the area enclosed by the left rectangle in Fig. 10 showing transsynaptically labeled neurons of the left rVRG. Fig. 12 High power magnification of the area enclosed by the right rectangle in Fig. 10 showing transsynaptically labeled neurons of the right rVRG. Figure and caption from Moreno et al., 1992.

## **CHAPTER 1: WGA-ALEXA LABELING IN THE PHRENIC MOTOR SYSTEM**

### **Summary**

The purpose of this study was to identify and compare the spinal and medullary centers involved in the respiratory pathway that activate the diaphragm in acutely injured and chronically injured C2Hx rats. The identification of spinal and medullary centers was accomplished by the following approaches: i) ipsilateral intradiaphragmatic injection of WGA-Alexa in the acutely and chronically C2Hx injured rat model, ii) topical application of WGA-Alexa to the ipsilateral phrenic nerve in the acute C2Hx injured model and in non-injured rats, iii) unilateral intrapleural injection of WGA-Alexa in non-injured rats.

Both intradiaphragmatic and intrapleural injections resulted in bilateral retrograde labeling of the phrenic nucleus (PN) and bilateral retrograde transsynaptic labeling of the rostral ventral respiratory groups (rVRGs). Unexpectedly both intradiaphragmatic and intrapleural injections also resulted in bilateral nucleus ambiguus (NA) labeling. In addition, following intrapleural injection WGA-Alexa was detected bilaterally in the intercostal motor nuclei of the thoracic spinal cord. Interestingly topical application of WGA-Alexa to the phrenic nerve result in only retrograde transport to the ipsilateral PN suggesting transsynaptic transport is dependent upon the site of application.

Spinal and medullary labeling following Intradiaphragmatic injection of WGA-Alexa in the acutely C2Hx injured rats compared to the chronically C2Hx rats were strikingly different. These differences in WGA-Alexa labeling patterns demonstrate injury-induced spinal and supraspinal plasticity that may contribute to spontaneous recovery of the diaphragm following injury.

### **Introduction**

It has been well established that when WGA-HRP is injected into muscle it is transported in a retrograde fashion back to the motoneuron cell bodies and also transsynaptically to other neurons within the synaptic chain (Harrison et al., 1984, 1986; Porter et al., 1985; Moreno et al., 1992). In addition, it has been shown that the transsynaptic transport is selectively mediated across physiologically active connections rather than silent or less active connections (Harrison et al., 1984, 1986; Jankowska, 1985). To test the retrograde transsynaptic capability of WGA-HRP in the phrenic motor system, Moreno and colleagues (1992) injected WGA-HRP into the hemidiaphragm ipsilateral to a C2Hx after recovery of the hemidiaphragm was induced by cutting the contralateral phrenic nerve, activating the CPP. Moreno and colleagues found WGA-HRP labeling in the ipsilateral PMNs, and bilaterally in the medullary center that provides the excitatory drive to PMNs during inspiration, the rVRGs (Fig.3). Therefore, Moreno and colleagues (1992) demonstrated that retrograde transsynaptic transport of WGA-HRP also occurs in the phrenic motor system following cervical SCI.

In recent years, investigators have become interested in identifying the intracellular molecular mechanisms and intracellular pathways which may mediate respiratory plasticity and recovery of the diaphragm after spinal cord injury (Kajana and Goshgarian, 2008a, 2008b, 2009; MacFarlane and Mitchell, 2008; MacFarlane et al., 2009; Wilkerson and Mitchell, 2009). In order to study such intracellular molecular mechanisms, it would be advantageous to identify the physiologically active respiratory neurons in the spinal cord and brainstem that are most likely responsible for mediating the plasticity. This could be accomplished by using the retrograde transsynaptic transport capability of WGA-HRP following injections of the tracer into the hemidiaphragm. The identified neurons could then be isolated (e.g. by laser microdissection) and subjected to intracellular molecular analysis.

However, visualizing WGA-HRP requires exposure of the tissue sections to chemicals and reagents that may reduce the quality of the mRNA captured by laser microdissection (Gjerdrum et al., 2004; Mouledous et al., 2002; Wang et al., 2006). Several laboratories have documented this problem (Gjerdrum et al., 2004; Mouledous et al., 2002; Wang et al., 2006) and in our own laboratory we found this to be the case. Therefore, we set out to investigate an alternative tracer, WGA-Alexa Fluor®, which may have the same retrograde transsynaptic capabilities as WGA-HRP, but without the requirement of visualizing the tracer by histochemical staining. In this case, WGA is conjugated to a fluorochrome (Alexa 488 or Alexa 594) and can be visualized simply with a fluorescent microscope (Model et al., 2009).

The first aim of the present study was to determine if WGA-Alexa 488 would undergo retrograde transsynaptic transport in the phrenic motor system (i.e., labeling both PMNs and the rVRG) similar to WGA-HRP. To partly address the underlying mechanism for transsynaptic transport, the second aim was to investigate the pattern and extent of labeling that occurs when WGA-Alexa 488 is applied to the phrenic nerve isolated in the cervical region as compared to intradiaphragmatic injection. In the former case, the tracer diffuses into the exposed phrenic axons, while in the latter; WGA-Alexa 488 is actively taken up at the phrenic myoneural junction by WGA receptor-mediated endocytosis.

In the third aim, intradiaphragmatic injections of WGA-Alexa 488 were used to compare the anatomical pathways that innervate the diaphragm in acutely injured C2Hx rats to chronically injured C2Hx rats. Based on the observation that WGA-Alexa 488 is transsynaptically transported over select physiologically active synapses in the respiratory motor pathway, any changes in labeling pattern occurring over time after injury would primarily be due to changes in physiologically active synapses in the chronically injured

C2Hx rat. In addition, the changes in labeling pattern may reveal compensatory routes over which spontaneous recovery of the diaphragm is achieved after chronic spinal cord injury (Nantwi et al., 1999).

Due to the invasive nature of the laparotomy procedure required for intradiaphragmatic injections, the fourth and final aim was designed to investigate a less invasive labeling technique, intrapleural injection. In 2009 Mantilla and colleagues introduced a new method of labeling PMNs by injecting cholera toxin subunit beta (CTB) conjugated to Alexa 488 bilaterally into the intrapleural space. Unfortunately, Mantilla and colleagues only presented data pertaining to the spinal cord; presumably because CTB-Alexa 488 is not a transsynaptic tracer (Cabot et al., 1994, Lee et al., 2009) therefore one would not expect CTB-Alexa 488 to be identified in the rVRGs. The possibility of transsynaptic transport of a neuronal tracer to the rVRGs in the medulla following intrapleural injection remained unresolved. To verify the effectiveness of intrapleural injections versus intradiaphragmatic, each rat received injections in the intrapleural space and intradiaphragmatic injections allowing for the comparison of the two techniques. The studies detailed in the following 3 sections have already been published (Goshgarian and Buttry, 2014; Buttry and Goshgarian, 2014, 2015).

#### **The pattern and extent of retrograde transsynaptic transport of WGA-Alexa 488 in the phrenic motor system is dependent upon the site of application**

Due to the damaging histochemical techniques required to visualize HRP, an alternative to the neuronal tracer WGA-HRP was needed to visualize the phrenic motor system following SCI. WGA conjugated to a fluorochrome, Alexa 488 was selected based on the characteristic that it can be visualized immediately after sectioning with a fluorescent microscope (Model et al., 2009). WGA-Alexa tracers are well established, exceptionally bright, and are excellent for tracing axonal pathways in the central nervous system (Reeber

et al., 2011a, 2011b; Yamazaki et al., 2009; Panchuk-Voloshina et al., 1999). In addition, WGA-Alexa 488 labeled cells have distinct granules that are clearly identifiable at higher magnifications (Fig. 4). Both anterograde (Reeber et al., 2011 a, 2011b) and retrograde (Yamazaki et al., 2009) track tracing studies have been conducted with WGA-Alexa 488. Transneuronal/transsynaptic transport of WGA-Alexa 488, however, has never been demonstrated in vivo. Thus, the first aim of the present study was to determine if WGA-Alexa 488 would undergo retrograde transsynaptic transport in the phrenic motor system similar to WGA-HRP. In addition to partly address the underlying mechanism for WGA mediated transsynaptic transport, the second aim of the present study was to investigate the pattern and extent of labeling that occurs when WGA-Alexa 488 is applied to the cervical phrenic nerve as compared to intradiaphragmatic injection.

### *Results*

All rats used to produce the following data received a left C2Hx or a sham C2Hx (see methods for details). Rats that received a C2Hx were included in the study only if they had complete left hemidiaphragm paralysis as confirmed by EMG analysis (Fig. 5). A minimum survival period of 2 days was sufficient to obtain strong labeling in both the PN and rVRG.

In all rats that received left hemidiaphragmatic injections of WGA-Alexa 488, bilateral labeling of the PN was observed (Fig. 6A). Furthermore, the observed spinal cord labeling was restricted to the PN only; there were no other labeled motoneurons, propriospinal neurons or dorsal horn neurons identified at the C3–C6 level of the spinal cord (Fig. 6A). The lack of WGA-Alexa 488 in the cervical spinal tissue with the exception of the PN demonstrates the selective uptake of WGA following intramuscular injection.



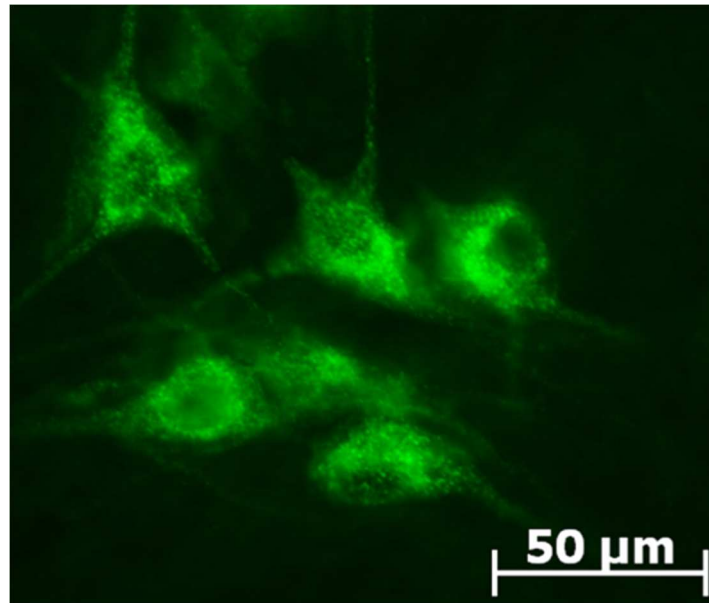


**Figure 4: WGA-Alexa 488 granulation in labeled neurons.** A high magnification of phrenic nuclei motoneurons displaying the granulation appearance of the WGA-Alexa 488 neuronal tracer. Note the specks or granules visible within the cell bodies, axons and dendrites of the labeled neurons.

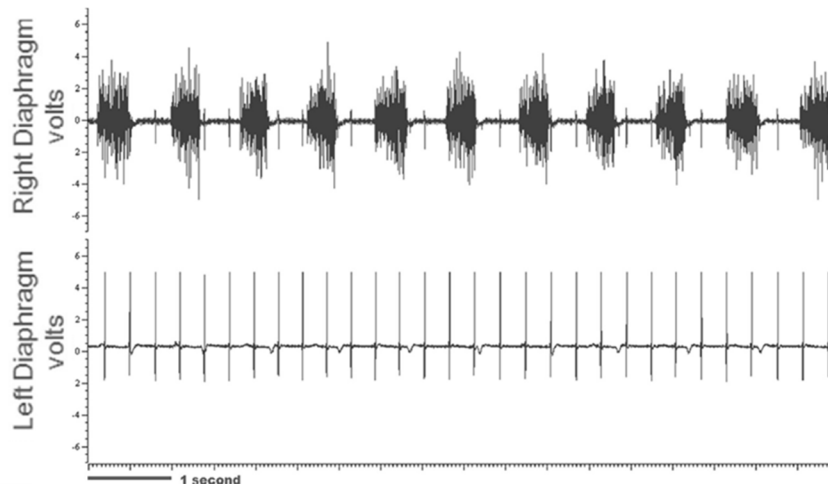


**Figure 5: Electromyogram of the diaphragm to confirm C2Hx.** Electromyograms taken from both sides of the diaphragm from a rat that was subjected to left C2 spinal cord hemisection. Note that the right hemidiaphragm is not significantly affected by the hemisection and displays EMG bursting every time the rat takes a breath. The left hemidiaphragm, however, is completely paralyzed and does not display EMG activity. The spikes on the left and right are EKG (electrocardiogram) waves. Calibration bar: 1 s. Goshgarian and Buttry, 2014.

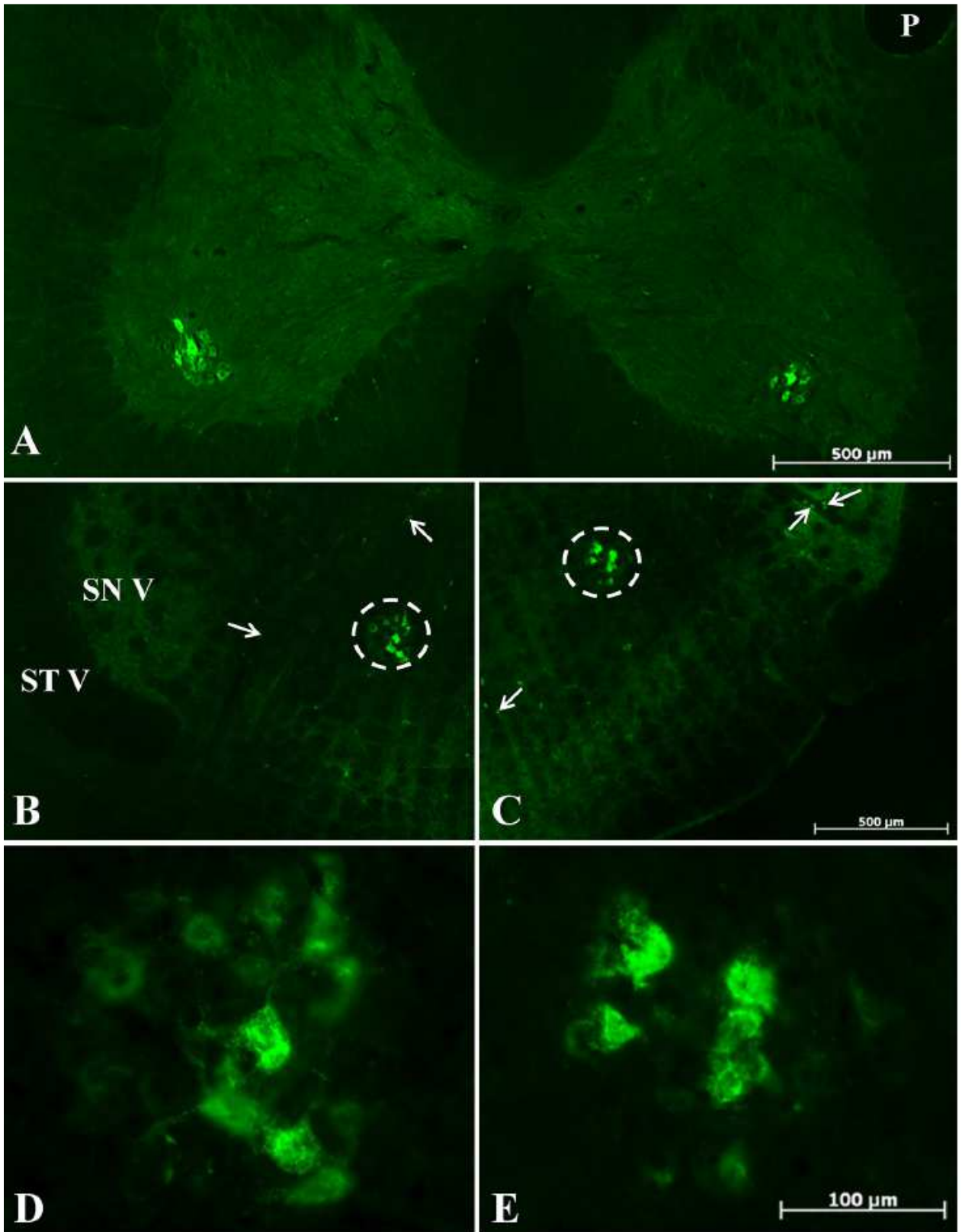


**Figure 6: Labeling pattern following injection of 50  $\mu$ l of 2% WGA-Alexa 488 into the left hemidiaphragm from a rat that was subjected to left C2Hx.** (A) Low power view of a section through the C3 level of the spinal cord, displaying bilateral phrenic nucleus labeling. Note that there is no other neuron labeling in the spinal cord gray matter and suggests that the tracer diffuses across the midline of the diaphragm to label both phrenic nuclei. This same pattern of labeling was seen in all rats with a left hemidiaphragm injection. The pinhole (P) marks the right side (contralateral to injection). (B) and (C) Each rat receiving intradiaphragmatic injections of WGA-Alexa 488 also displayed bilateral labeling of the rVRG indicating retrograde transsynaptic transport. (B) Low power view of the labeled left rVRG (circled area). SNV, spinal nucleus of V, STV, spinal tract of V is indicated as landmarks. (C) Same magnification as in (B) showing the right rVRG (circled area) in the same rat. Note that there is no other medullary center labeled. Small arrows in both (B) and (C) point to small labeled non-neuronal cells associated with blood vessels. Calibration bar in (C), also pertains to (B). (D) Higher power view of the labeled left rVRG shown in (B). (E) Higher power view of the right rVRG shown in (C). Note granulation in both rVRG centers indicating positively labeled cells. Calibration bar shown in (E) also pertains to (D). Goshgarian and Buttry, 2014.

In addition, intradiaphragmatic injection of WGA-Alexa 488 resulted in bilateral labeling of the rVRGs in the medulla. The left (ipsilateral to injection) rVRG is shown in Fig. 6B and D while the right rVRG (contralateral to injection) in the same rat is shown in Fig. 6C and E. Note also the selectivity of the medullary labeling. The area of the rVRG is the only location labeled. Moreover, the rVRG was always labeled bilaterally (Fig. 6B and C). In particular, note the absence of labeling in neither gigantocellular reticulospinal neurons nor raphe neurons known to project to the phrenic nucleus (Dobbins and Feldman, 1994).

In contrast, when WGA-Alexa 488 was applied to the intact isolated left phrenic nerve, only ipsilateral phrenic nucleus labeling was observed (Fig. 7A). Isolated ipsilateral phrenic nucleus labeling was observed in all rats. Contralateral phrenic motoneuron labeling was never observed, nor was there any other spinal cord neurons labeled at the level of the phrenic nucleus (C3–C6, Fig. 7A). During the pilot studies various methods were tested to label the phrenic motor system with WGA-Alexa 488; (i) injected the transected or intact phrenic nerve with the tracer, (ii) applied WGA-Alexa 488-soaked gelfoam to the exposed phrenic nerve or (iii) attempted to isolate the phrenic nerve with Parafilm® before applying

the tracer. All of these attempts yielded spurious labeling of phrenic and non-phrenic neurons in the cervical spinal cord. It was only when we isolated the phrenic nerve and contained the tracer in a cup (Fig. 8) that we achieved consistent ipsilateral phrenic nucleus labeling exclusively.

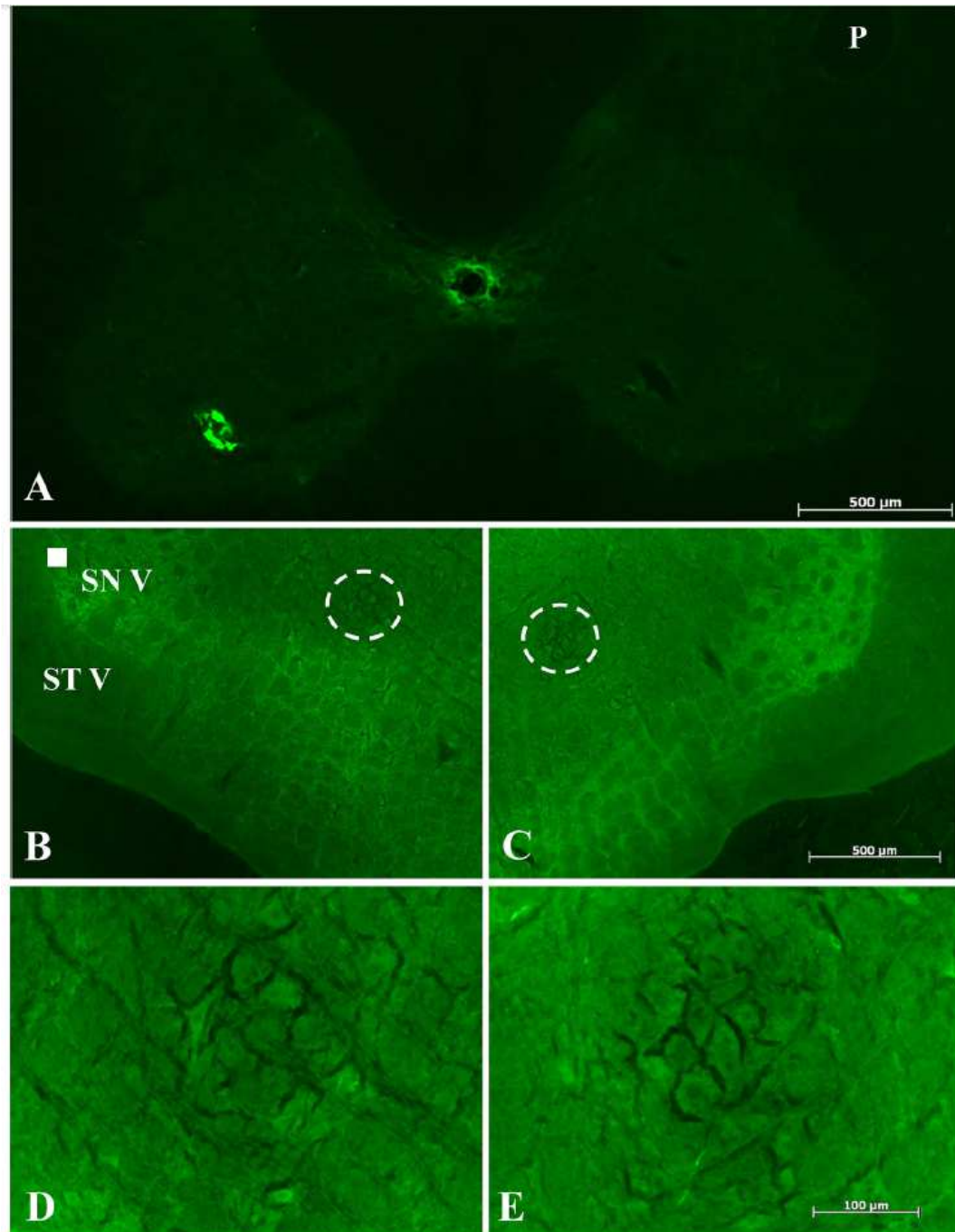


**Figure 7: Labeling pattern shown following WGA-Alexa 488 application for 1 h to the left phrenic nerve from a rat that was subjected to left C2Hx.** (A) Low power view of the C4 level of the spinal cord showing phrenic nucleus labeling only on the left side (ipsilateral to nerve application). The pinhole (P) marks the right side of the spinal cord. Note that no other neurons are labeled in the spinal cord other than the ipsilateral PN. Also note that the PN is as intensely labeled as it is following diaphragm injection of the tracer (compare this figure with Fig. 6A). Left (B) and right (C) sides of the medulla at the level of the rVRG (circled areas in both (B) and (C)). Note that the rVRGs are not labeled suggesting that retrograde transsynaptic transport does not occur when the tracer is applied to the phrenic nerve. SNV, spinal nucleus of V; STV, spinal tract of V is included as landmarks. These sections are comparable to the sections shown in Fig. 6B and C. Magnification in (B) is the same as in (C). (D) Higher power view of the rVRG shown in (B) (circled area). (E) Higher power view of the rVRG shown in (C) (circled area). Note that there is no granulation in the rVRG neurons indicating that they are not labeled. In order to see these unlabeled centers, the intensity of the fluorescent scope was increased substantially. Compare background intensity shown in Fig. 6D and E with these figures. Magnification of (D) is the same as (E). Goshgarian and Buttry, 2014.

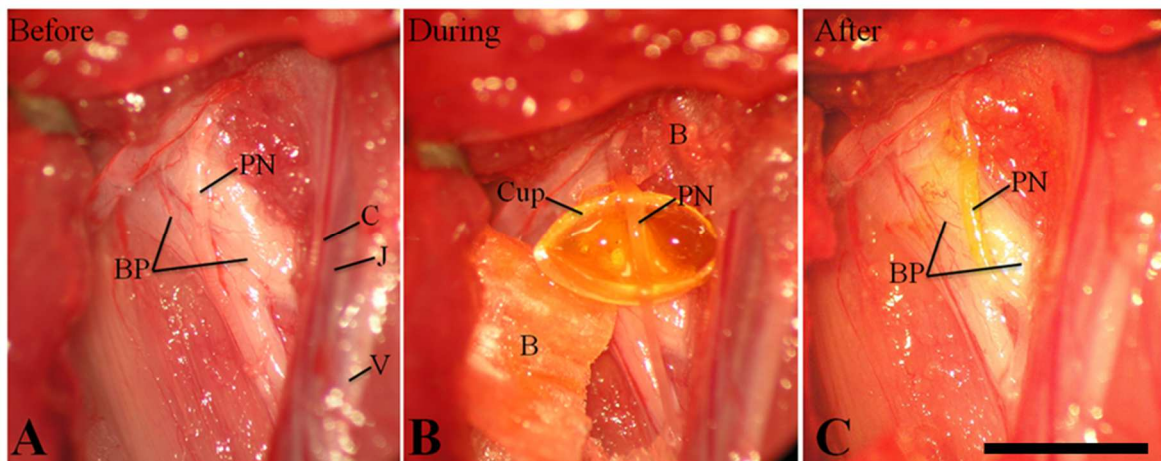


**Figure 8: Photographs of the surgical exposure of the left phrenic nerve and the application of WGA-Alexa 488 to the nerve for 1 h.** In all photographs, caudal is at the top, rostral is at the bottom, lateral is to the left and medial is to the right. (A) Surgical exposure of the phrenic nerve (PN) as it lays on the ventral surface of the brachial plexus (BP) before the application of the tracer. V, vagus nerve; C, carotid artery; J, jugular vein. (B) During the application of the tracer, a cup containing 1.5  $\mu$ l of 2% WGA-Alexa 488 is placed so that the nerve is bathed in the solution. Bench top paper (B) is placed in the surrounding tissue to absorb fluid from the rat during the application period. (C) After the 1 h application period, the cup and the bench top paper is removed and the tissue is gently swabbed. Note that the phrenic nerve (PN) has a yellow color indicating that the tracer diffused into the nerve. Scale bar is 3 mm. Goshgarian and Buttry, 2014.

Interestingly, following the application of WGA-Alexa 488 to the isolated phrenic nerve, there was no retrograde transsynaptic labeling to the rVRGs or any other medullary neuronal center observed in any of the rats (Fig. 7B–E). Fig. 7B and C is a section through the rVRG from a rat in which the phrenic nerve was soaked in WGA-Alexa 488. The unlabeled left and right rVRG can be seen at low magnification (Fig. 7B and C respectively) and a higher power view of each is shown (Fig. 7D and E). The medullary level is comparable to the level showing the labeled rVRGs in (Fig. 6B–E) in which WGA-Alexa 488 was injected into the diaphragm. Initially, because of the activity-dependent nature of transsynaptic transport using WGA-HRP (Harrison et al., 1984, 1986; Moreno et al., 1992), we thought there may be a difference in the labeling pattern occurring when WGA-Alexa 488 was applied to the quiescent phrenic nerve (i.e. ipsilateral to a C2 hemisection) versus an active phrenic nerve (ipsilateral to sham hemisection). However, there was no notable difference between the C2Hx group and the sham group. Following nerve application, the only labeled neurons detected were ipsilateral phrenic neurons regardless of whether the phrenic nerve was quiescent or active.

### *Discussion*

The ability to transsynaptically label PMNs and pre-motor rVRG neurons responsible for descending respiratory drive (Ellenberger and Feldman, 1988) provides an anatomical picture to compare various states of the phrenic motor system following spinal cord injury (Goshgarian et al., 1991). This study shows that retrograde transsynaptic transport of WGA-Alexa 488 occurs in the phrenic motor system (i.e., bilaterally labeling PMNs and rVRG pre-motor neurons) when the tracer is injected intradiaphragmatically similar to WGA-HRP. The bilateral phrenic nucleus labeling was most likely due to WGA-Alexa 488 diffusing within the muscle across the midline from the left hemidiaphragm to the

right and being taken up by the axon terminals in both phrenic nerves since peripheral crossing of phrenic axons has not been demonstrated in the rat diaphragm (Laskowski and Sanes, 1987). The right phrenic nerve (RPN) was not cut in the present study as it was in a previous study investigating WGA-HRP (Moreno et al., 1992). The primary reason the RPN was not cut was based on the observation that the crossed phrenic phenomenon (induced by C2Hx and contralateral phrenicotomy) contributes little to the overall ventilation of the animal (Fuller et al., 2006) and thus, we did not want to subject the experimental animals to unnecessary respiratory stress.

Bilateral PN labeling following an ipsilateral diaphragm injection is not a unique finding. Boulenguez et al. (2007) showed that dependent upon the monosynaptic retrograde fluorescent tracer injected unilaterally in the rat diaphragm, PMNs would be labeled either bilaterally, ipsilateral, or not at all. Very similar results were observed after horseradish peroxidase (HRP) injection. Interestingly, injection of the dextran amine, fluororuby and the carbocyanine, DiAsp, into one hemidiaphragm, always resulted in the exclusive labeling of ipsilateral PMNs. The authors suggested that the lipophilic properties of DiAsp and the high molecular weight of fluororuby may prevent their diffusion to adjacent tissues and into the bloodstream which may have caused the artifactual labeling observed with Fluorogold and HRP (Boulenguez et al., 2007). The present results show that WGA-Alexa 488 is an excellent retrograde transsynaptic fluorescent tracer in the phrenic motor system, however there is consistent diffusion of the tracer in the diaphragm. To prevent bilateral PN labeling, the addition of a contralateral phrenicotomy to the surgical procedure remains a feasible option.

Exposure of WGA-Alexa 488 directly to the left phrenic nerve in both C2 hemisected and sham-hemisected rats was used to assess possible differences between quiescent and

functionally active PMNs. In spite of the observation that there was WGA-Alexa 488 labeling isolated to ipsilateral PMNs following application of the tracer to the nerve, there was no observed transsynaptic labeling to the rVRG in either the C2Hx or sham-hemisected groups. Based on past studies utilizing alternative tracers in the phrenic motor system (e.g. HRP, Goshgarian and Rafols, 1981, 1984; CT-HRP, Furicchia and Goshgarian, 1987; and WGA-HRP, Moreno et al., 1992), a difference in labeling pattern dependent on the site of tracer administration (i.e. nerve versus diaphragm) has never been reported. The reason for this difference in labeling pattern may be due to the differences in the mechanisms of uptake and transport of WGA in the nervous system when the tracer is injected into muscle versus tracer application to the nerve. Since the phrenic nerve was stripped of its epineurium and WGA-Alexa 488 was applied directly to the nerve, the tracer may have entered the nerve primarily by simple diffusion (i.e., not by a receptor-mediated uptake mechanism). Once within the nerve, the retrograde transport of the tracer back to the cell body may have occurred as described by Schwab et al. (1979), however, transsynaptic transport did not occur. Since it has been shown that lectin binding sites are not distributed uniformly on individual neurons (Hatten et al., 1979), it is possible that WGA-Alexa 488 must be applied at the phrenic myoneural junction where there may be a high concentration of WGA receptors in order for transsynaptic transport to occur (Fabian and Coulter, 1985; Robertson, 1990). The result of the present study is that HRP is not necessary for retrograde transsynaptic transport in the phrenic motor system; WGA alone, or in this case WGA conjugated to Alexa, is sufficient to mediate the transport (suggested by Borges and Sidman, 1982).



### **Injection of WGA-Alexa 488 into the ipsilateral hemidiaphragm of acutely and chronically C2 hemisected rats reveal activity-dependent synaptic plasticity in the respiratory motor pathways**

Based on the data obtained from the acute C2Hx injury model it is suggested that WGA-Alexa 488 is capable of transsynaptic transport in vivo across select physiologically active synapses in the phrenic motor system (Goshgarian and Buttry, 2014) similar to that of WGA-HRP (Moreno et al., 1992). It is likely that the synaptic transfer occurs preferentially over the connections (i.e. rVRG synapses) that depolarize the PMNs during inspiration (Ellenberger and Feldman, 1988).

In contrast, Pseudorabies virus Bartha strain (PRV-Bartha), a retrograde transsynaptic neuronal tracer, demonstrates a diverse pattern of labeling compared to WGA-Alexa 488 when applied to the phrenic motor system. Following PRV-Bartha exposure to the diaphragm there is an increase in cell types positive for PRV-Bartha, compared to cell types positive for WGA-Alexa 488. This is likely due to the ability of PRV-Bartha to cross all synaptic connections; not just physiologically active synapses (Lane et al., 2008). Thus, the retrograde transsynaptic transport of PRV-Bartha does not differentiate plasticity occurring over physiologically active connections versus less active or inactive connections. Specifically, when PRV-Bartha is applied to the diaphragm after an acute C2Hx or in non-injured rats, the tracer is detected in ipsilateral PMNs within 48 h, interneurons bilaterally in laminae VII and X of the cervical cord at 64 h, and cells in the dorsal horn bilaterally at 72 h (Lane et al., 2008). These results are consistent with those documented by Dobbins and Feldman (1994) who injected PRV into the phrenic nerve. In the only major chronic study using PRV as a retrograde tracer in which C2Hx rats survived up to twelve weeks post C2Hx (Lane et al., 2009), the authors found that the ratio of interneurons to motoneurons in laminae VII and X both ipsilateral and contralateral to the

injury site were significantly reduced (though still present) in the chronically C2Hx rats. No other significant changes were detected after both qualitative and quantitative analyses.

Based on the previously observed transsynaptic labeling properties of WGA-Alexa 488 over select physiologically active synapses in the respiratory motor pathway in the acute C2Hx injury model; any changes in labeling pattern occurring over time after injury would primarily be due to changes in physiologically active synapses. Furthermore, the changes in labeling pattern may reveal compensatory routes over which spontaneous recovery of the diaphragm is achieved after chronic spinal cord injury (Nantwi et al., 1999). To determine if there are changes in physiologically active synapses in the chronically injured system, WGA-Alexa 488 labeling patterns were compared between acutely and chronically injured C2 hemisectioned rats.

### *Results*

Immediately following the C2Hx surgical procedure, an EMG of the diaphragm assessed the extent of hemidiaphragmatic paralysis (Fig. 2). Characteristic of C2Hx rats, an “augmented breath” (Fig. 2, arrows, Golder et al., 2001b) confirmed the presence of an intact crossed phrenic pathway (Moreno et al., 1992), over which spontaneous recovery of the C2Hx paralyzed hemidiaphragm is thought to occur (Nantwi et al., 1999). The sham C2Hx rats received a C2Hx procedure omitting the actual cut to the cervical spinal cord. The sham C2Hx rats showed no sign of diaphragm paralysis (Fig. 9).

A second EMG was assessed in the chronic C2Hx and sham rats at immediately prior to intradiaphragmatic injections of WGA-Alexa 488 to assess the extent of spontaneous recovery (Fig. 10). Sixty-two percent of the chronically C2Hx rats showed spontaneous diaphragm recovery based on the return of muscle contractions of the ipsilateral hemidiaphragm (Fig. 10, top trace). The chronic sham rats displayed right and

left hemidiaphragm activity similar to the initial EMG following the sham C2Hx procedure (Fig. 11).

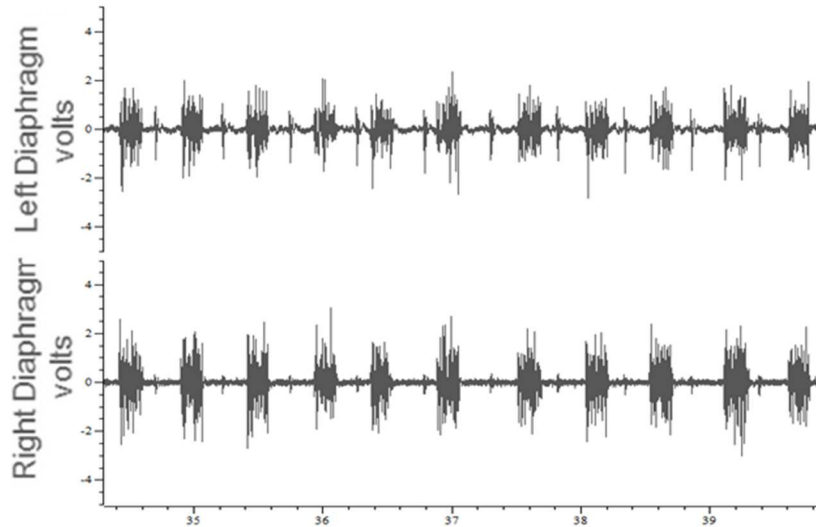


**Figure 9: EMG traces from the left and right hemidiaphragm immediately after a Sham C2Hx.** Note that the left hemidiaphragm (top trace) is still intact and functional and the bursting pattern matches the bursts of the right hemidiaphragm (bottom trace). The sharp spikes in all traces are EKG activity.

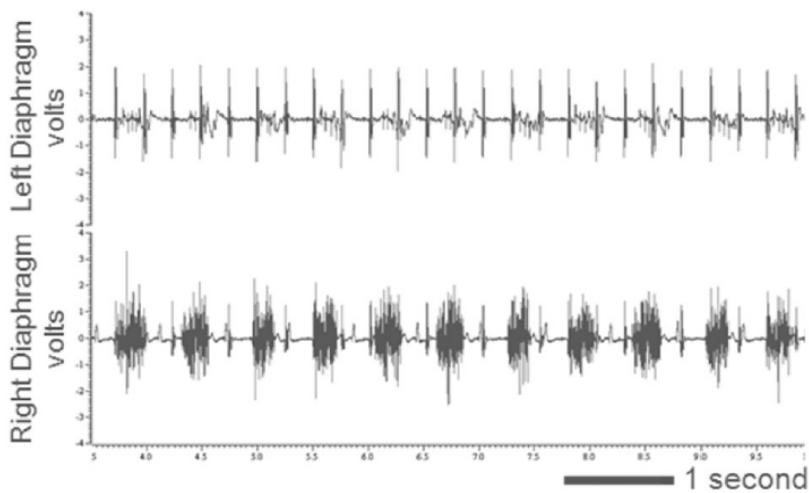


**Figure 10: EMG traces from the left and right hemidiaphragm 22 weeks post C2Hx.** This recording was taken from the same rat used in figure 2. There is a moderate return of the bursting pattern in the left hemidiaphragm (top trace) indicative of spontaneous recovery. The bursts in the left hemidiaphragm match those in the right hemidiaphragm (bottom trace). Buttry and Goshgarian, 2014.

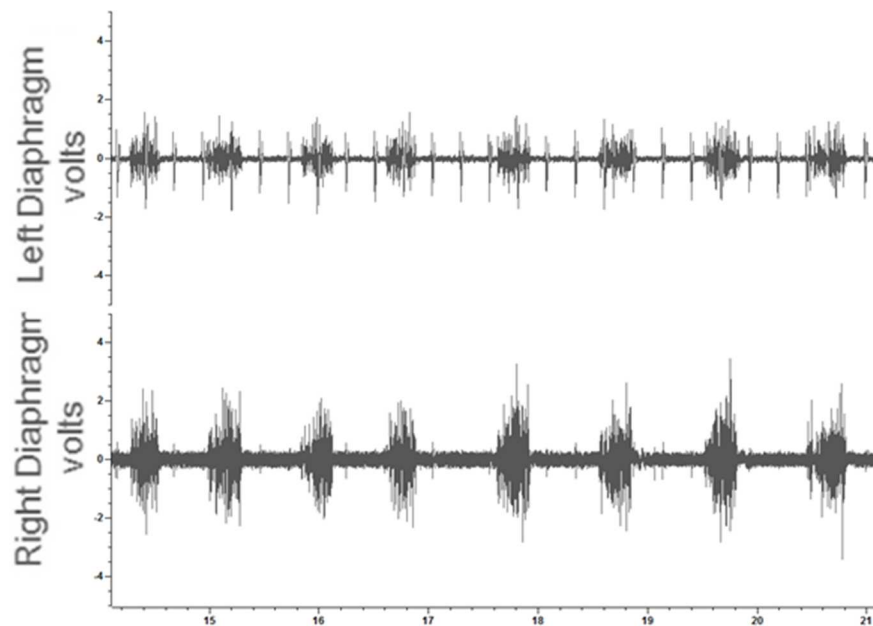


**Figure 11: EMG traces from the left and right hemidiaphragm 8 weeks after a Sham C2Hx.** Note that the left hemidiaphragm (top trace) is still intact and functional and the bursting pattern matches the bursts of the right hemidiaphragm (bottom trace). The sharp spikes in all traces are EKG activity. Right electrodes were producing excessive noise during the recordings resulting in a larger background signal.

Analysis of the spinal and medulla tissue from the acutely C2 hemisected rats was consistent with past studies (Goshgarian and Buttry, 2014). In the previous study only the cervical spinal cord at the level of the PN was examined, but in the present study, both cervical and thoracic spinal cord tissue was examined. The great majority of cells that contained WGA-Alexa 488 were PMNs at the C3-C6 levels of the spinal cord (Figs. 12A–C), and the rVRG pre-motor neurons in the medulla (Figs. 12D & E). There were no other neurons labeled at the C3–C6 levels of the spinal cord or in the medulla of the acute C2Hx rats. However, WGA-Alexa 488 labeling was found in non-neuronal cells associated with the blood vessels in the medulla (Figs. 12D&E arrows; Goshgarian and Buttry, 2014), as well as a small number of neurons along the medial ventral border of the ventral horn caudal to the PN at C7 (Fig. 13A).

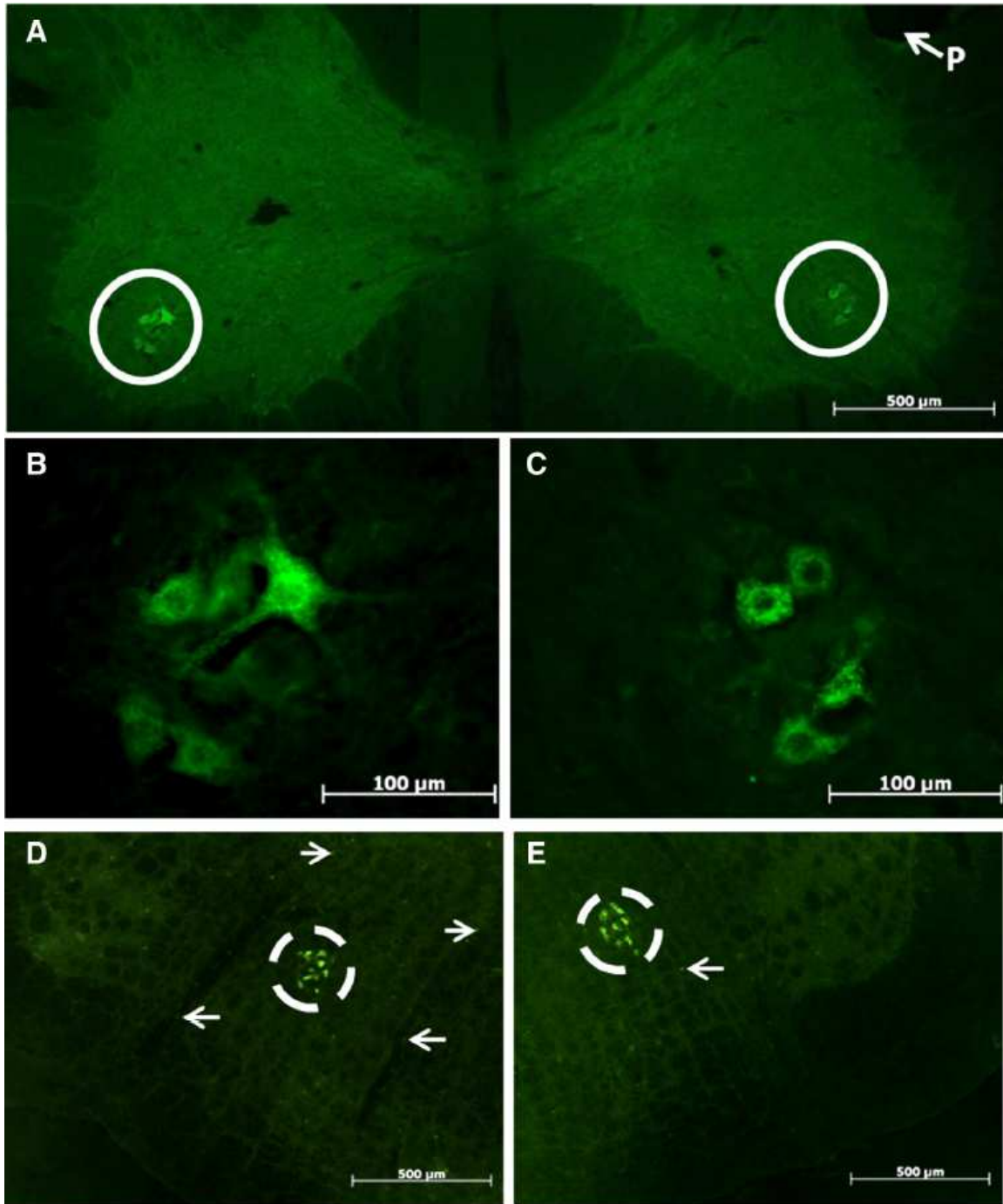


**Figure 12: Spinal cord and medulla sections from an acute C2Hx rat following WGA-Alexa 488 injection.** A, Spinal cord section at the C4 level showing bilateral WGA-Alexa 488 labeling in the phrenic nucleus (encircled areas). Note the absence of WGA-Alexa 488 in any other nuclei. P, pinhole marks contralateral to hemisection. B, Higher magnification of ipsilateral phrenic nucleus from A. C, Higher magnification of contralateral phrenic nucleus from A. D, Ipsilateral rVRG (dashed encircled area) in the medulla. E, Contralateral rVRG (dashed encircled area) in the medulla. Note the absence of WGA-Alexa 488 in any other neurons. Both D and E show some non-neuronal cells with WGA-Alexa 488 labeling associated with the blood vessels (arrows). Buttry and Goshgarian, 2014.

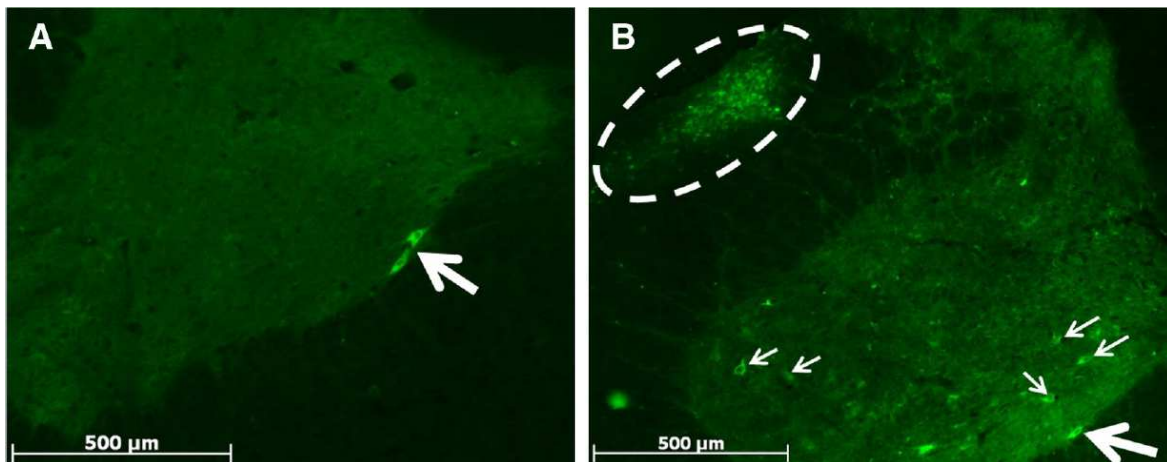


**Figure 13: C7 spinal cord sections from an acute and a chronic C2Hx rat.** A, Spinal cord section below the level of the phrenic nuclei at C7 of an acute C2Hx rat showing WGA-Alexa 488 labeled neurons (large arrow) along the ipsilateral medial ventral border of the ventral horn. Note the lack of any additional labeled nuclei. B, Spinal cord section at the C7 level of a chronic C2Hx rat with a WGA-Alexa 488 labeled neuron (large arrow) in the same area as the neurons shown in A. In addition, there is ipsilateral labeling of the dorsal spinocerebellar tract (dashed encircled area), and interneurons in laminae VII and VIII (small arrows). Buttry and Goshgarian, 2014.

After a minimum 7-week recovery period, the chronic sham rats were injected with WGA-Alexa 488 into the left hemidiaphragm. Analysis of the spinal and medulla tissues revealed bilateral WGA-Alexa 488 labeling in PMNs, neurons along the medial ventral border of the ventral horn in the cervical cord caudal to the PN, and the rVRG pre-motor neurons in the medulla were detected in all 3 chronic sham rats. In addition, there were bilateral WGA-Alexa 488 labeled interneurons primarily in laminae VII and VIII of the cervical and thoracic cord and bilateral WGA-Alexa 488 labeled intercostal motoneurons in

the thoracic cord. No other neurons or tracts were detected in the medulla, cervical or thoracic spinal cord of the chronic sham rats.

The chronically C2Hx rats received WGA-Alexa 488 intradiaphragmatic injections after a minimum 7-week recovery period. Five of the chronic C2Hx rats exhibited autophagy of the hind contralateral paw. Due to animal care policy, the severity of the autophagy determined the endpoint for these rats. Upon analysis of the spinal and medulla tissues there were no qualitative differences in the WGA-Alexa 488 labeling pattern regardless of the endpoint. Therefore, all rats were grouped together in a single chronic group.

All chronic C2Hx rats exhibited bilateral WGA-Alexa 488 labeling of PMNs at the levels of C3–C6 (Figs. 14A & C). In addition, chronic C2Hx rats displayed neurons along the medial ventral border of the ventral horn caudal to the PN at the C7 level of the spinal cord (Fig. 13B). WGA-Alexa 488 labeled interneurons were detected bilaterally throughout the gray matter in all sections examined, primarily in laminae VII and VIII in the C4–T5 region (Figs. 13B, 14, 15B & 16B). Unique to the chronic C2Hx rats was the labeled axons of the reticulospinal tract (RST) (Fig. 14C), ventral spinocerebellar tract (VSCT) (Fig. 14C), and dorsal spinocerebellar tract (DSCT) (Figs. 13B, 14C & 15B). All 3 tracts were labeled strictly ipsilateral to the injury. In all cases the DSCT and VSCT appeared as a fasciculated group of axons just lateral to the dorsal horn and just lateral to the ventrolateral sulcus, respectively. The DSCT was identified as far caudal as T5. The RST had a scattered appearance of axons throughout the lateral funiculus and was present in the upper and mid cervical regions of the spinal cord. Caudal to the PN in the region of C8/T1, motoneurons were identified in the motor nuclei for the triceps brachii and were bilaterally labeled with WGA-Alexa 488 (Fig. 15B). In addition, the motoneurons for the manus (hand) and/or forearm extensors were bilaterally labeled (Fig. 15B). The rostral/caudal transition from

forearm to manus could not be clearly identified with absolute certainty. In the thoracic cord of chronically hemisected rats, predominately at T3–T5, intercostal motoneurons were bilaterally labeled with WGA-Alexa 488 (Fig. 16B).

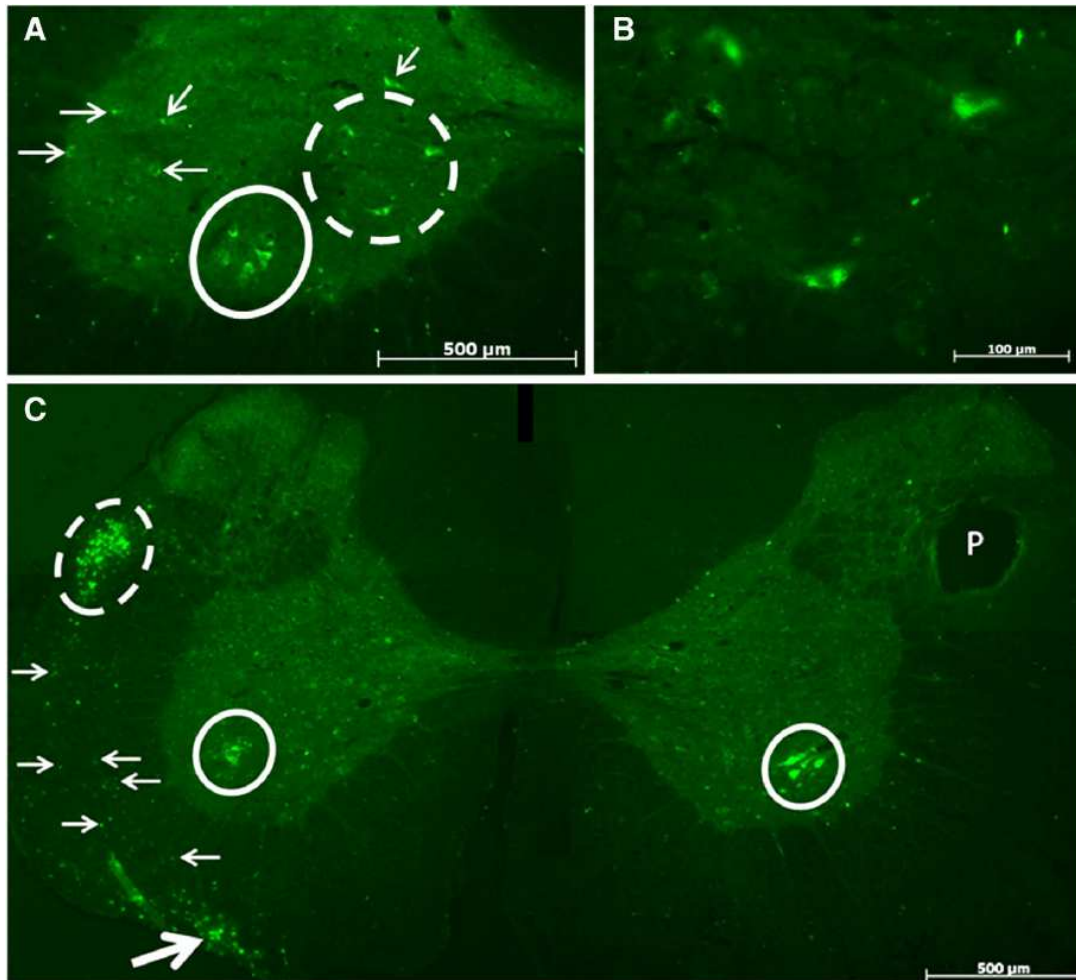


**Figure 14: C4/C5 spinal cord sections of a chronic C2Hx rat.** A, Spinal cord section at the C4/C5 level showing WGA-Alexa 488 labeling in the phrenic nuclei (solid encircled area) and labeling in neuronal cells throughout laminae VII and VIII (dashed encircled area and arrows). B, Higher magnification of dashed encircled area in A showing WGA-Alexa 488 labeling in neuronal cells located in laminae VII and VIII. C, Spinal cord section at the C3 level of a chronic C2Hx rat with bilateral phrenic nuclei (encircled areas) labeling in the ventral horn. Note also the ipsilateral labeling of the dorsal spinocerebellar tract (dashed encircled area), ventral spinocerebellar tract (large arrow), and reticulospinal tract (small arrows) in the lateral funiculus. Note the labeling of neuronal cells throughout laminae VII and VIII (compare to lack of labeling in Fig. 2A). P, pinhole marks contralateral to hemisection. Buttry and Goshgarian, 2014.



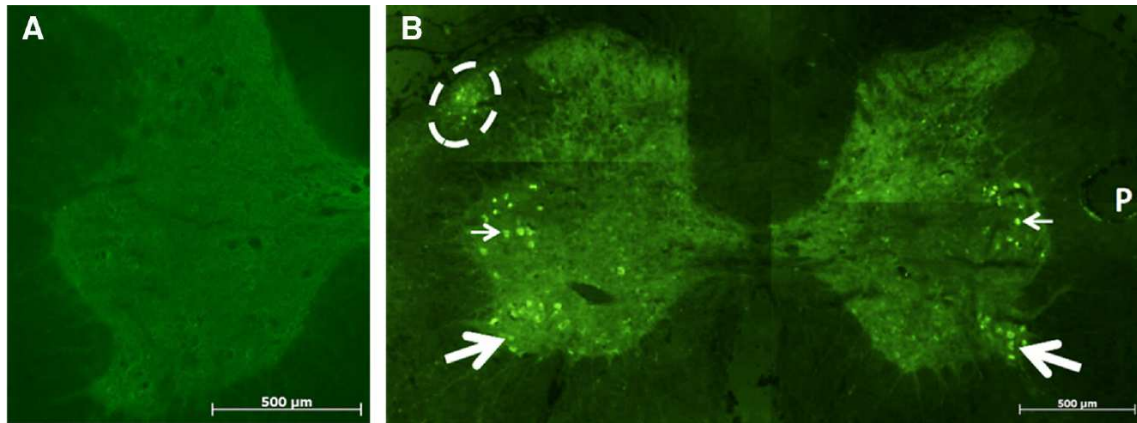


**Figure 15: C8/T1 spinal cord sections from an acute and a chronic C2Hx rat.** A, Spinal cord section at the C8/T1 level from an acute C2Hx rat showing a complete absence of WGA-Alexa 488 labeling. B, Spinal cord section at the C8/T1 level from a chronic C2Hx rat showing ipsilateral labeling of the dorsal spinocerebellar tract (dashed encircled area), as well as bilateral labeling of triceps brachii motoneurons (large arrows), and forearm/manus motoneurons (small arrows). Compare to lack of labeling in A. P, pinhole marks contralateral to hemisection. Buttry and Goshgarian, 2014.

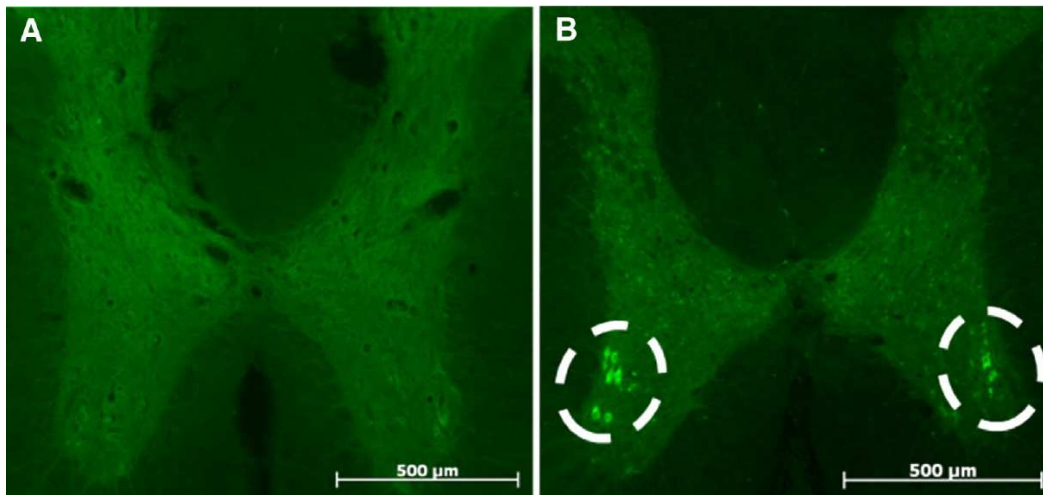


**Figure 16: T4/T5 spinal cord sections from an acute and a chronic C2Hx rat.** A, Spinal cord section at the T4/T5 level from an acute C2Hx rat showing a complete absence of WGA-Alexa 488 labeling. B, Spinal cord section at the T4/T5 level from a chronic C2Hx rat showing bilateral WGA-Alexa 488 labeled intercostal motoneurons (dashed encircled areas). Buttry and Goshgarian, 2014.

The chronic C2Hx rats displayed a very distinct bilateral pattern of medullary labeling that was consistently detected in all chronic C2Hx rats; a summary of the labeled areas for the acute C2Hx and chronic C2Hx rats is shown in Fig. 17. In addition to the rVRGs, chronic C2Hx rats displayed a scattering of raphe neurons that were bilaterally labeled along the midline (Fig. 18B). Neurons were also labeled in the gigantocellular reticular nuclei (Fig. 18B). The parvicellular reticular nuclei (PRN) were labeled and appeared as a column of neurons extending tangentially along the dorso-ventral plane (Figs. 18B & 19). The labeled neurons of the intermediate reticular nuclei were located dorsal to the rVRGs and in a grouping that at times reached just medial to the most dorsal portion of the labeled neurons in the PRN (Figs. 18B & 19). The spinal trigeminal nucleus had a scattering of labeled neurons throughout the nucleus (Fig. 18B). Lastly, neurons were bilaterally labeled throughout the hypoglossal nuclei (Fig. 20B). Interestingly, the sham rats showed labeling only in the rVRG. A summary of the anatomical results is presented in Table 1.

	rVRG	Raphe	Gigantocellular reticular nuclei	Parvicellular reticular nuclei	Intermediate reticular nuclei	Spinal trigeminal nuclei	Hypoglossal nuclei				
Acute C2Hx	•										
Chronic Sham	•										
Chronic C2Hx	•	•	•	•	•	•	•				
	Phrenic nuclei	C7 Medial ventral border of gray mater	Laminae VII & VIII	Reticulospinal tract	Ventral spinocerebellar tract	Dorsal spinocerebellar tract	Triceps brachii motor nuclei	Manus/forearm motor nuclei	Intercostal motor nuclei		
Acute C2Hx	•	•									
Chronic Sham	•	•	•						•		
Chronic C2Hx	•	•	•	•	•	•	•	•	•		

**Table 1: Location of WGA-Alexa 488 labeling in the medulla and spinal cord of the acute C2Hx, chronic sham, and chronic C2Hx rats.** Buttry and Goshgarian, 2014.

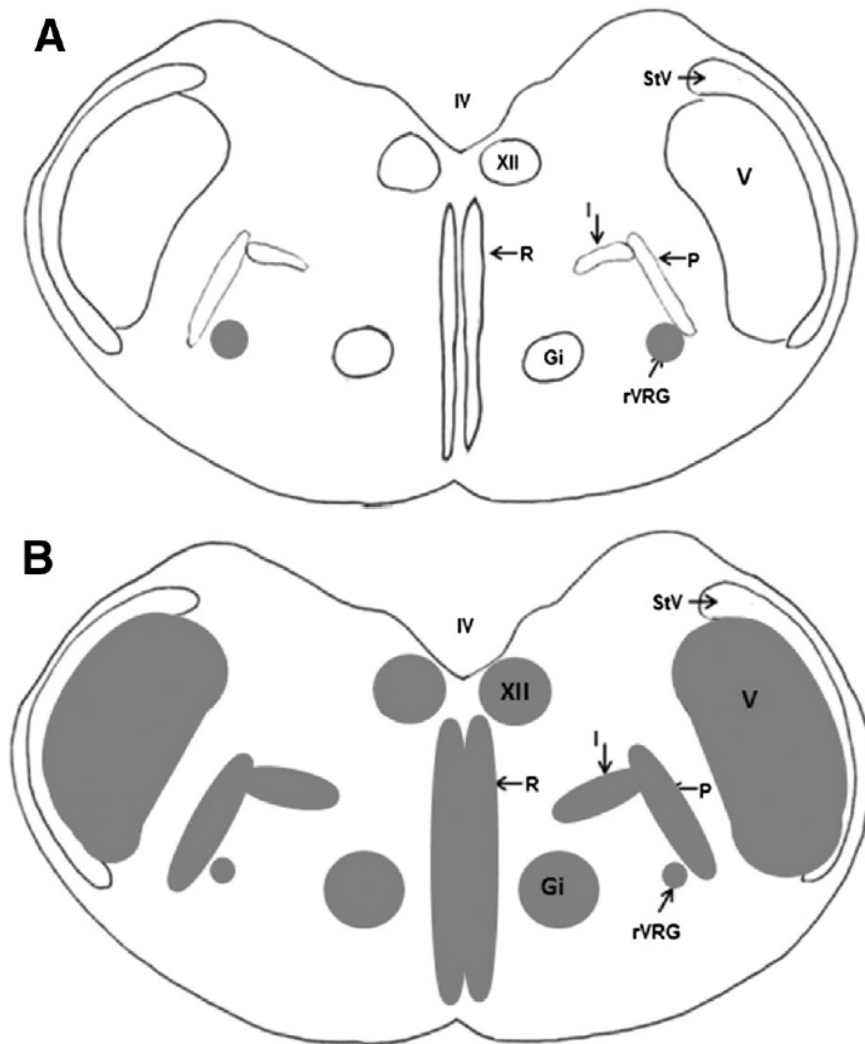


**Figure 17: Drawings of the medulla summarizing all the locations of WGA-Alexa 488 in the acute C2Hx and Chronic C2Hx rats.** WGA-Alexa 488 labeled cells and tracts (darkened areas) in the acute C2Hx rats (A) and in the chronic C2Hx rats (B). A, In the acute C2Hx rats only the rVRG is labeled bilaterally. B, In the chronic C2Hx rats bilateral labeling is seen in: rVRG, rostral ventral respiratory group; XII, hypoglossal nucleus; R, raphe nucleus; Gi, gigantocellular reticular nucleus; I, intermediate reticular nucleus; P, parvicellular reticular nucleus; V, spinal trigeminal nucleus. IV, fourth ventricle and StV, spinal tract of V noted as landmarks. Buttry and Goshgarian, 2014.

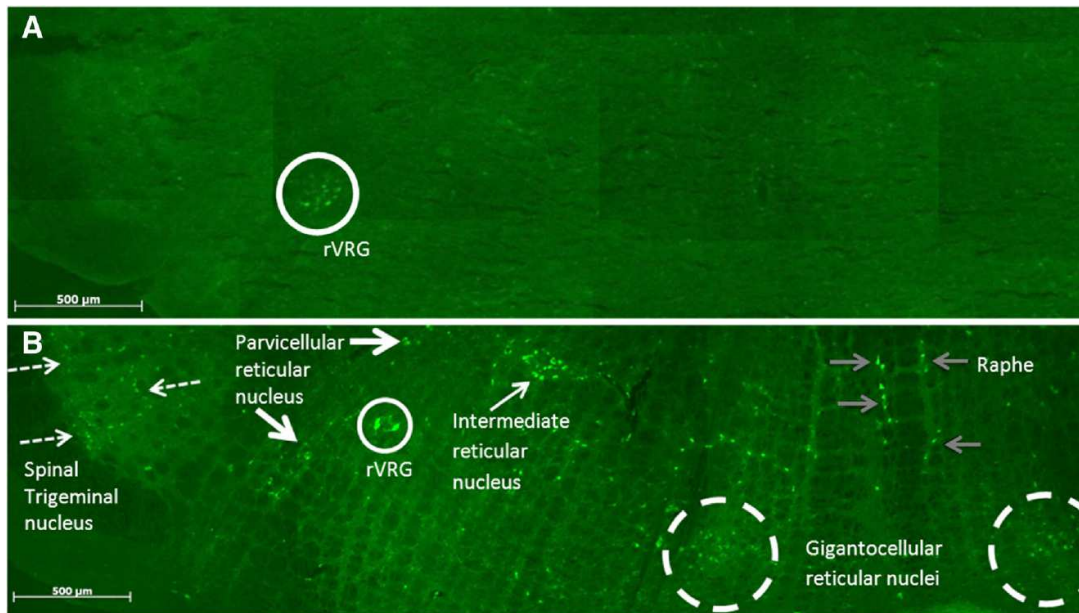


**Figure 18: Medulla sections from an acute and a chronic C2Hx rat.** A, Section from an acute C2Hx rat showing the medulla with WGA-Alexa 488 labeling in the ipsilateral rVRG. The contralateral rVRG is not shown at this magnification. B, Section from a chronic C2Hx rat showing the medulla with WGA-Alexa 488 labeling in the intermediate reticular nucleus (small white arrow), parvicellular reticular nucleus (large white arrows), rVRG (solid encircled area), raphe (gray arrows), spinal nucleus of V (small dashed arrows), and gigantocellular reticular nuclei (dashed encircled area). Buttry and Goshgarian, 2014.

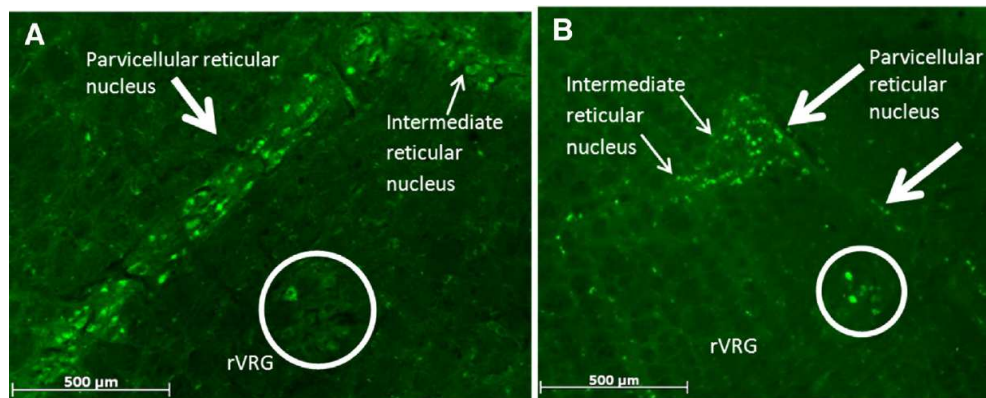


**Figure 19: Medulla sections from a chronic C2Hx rat.** A, Section from a chronic C2Hx rat medulla with ipsilateral WGA-Alexa 488 labeling in the intermediate reticular nucleus (small arrows), parvicellular reticular nucleus (large arrows), and rVRG (encircled area). B, Section from the same chronic C2Hx rat medulla as A with contralateral WGA-Alexa 488 labeling in the intermediate reticular nuclei (small white arrow), parvicellular reticular nuclei (large arrow), and part of the rVRG (encircled area). Buttry and Goshgarian, 2014.

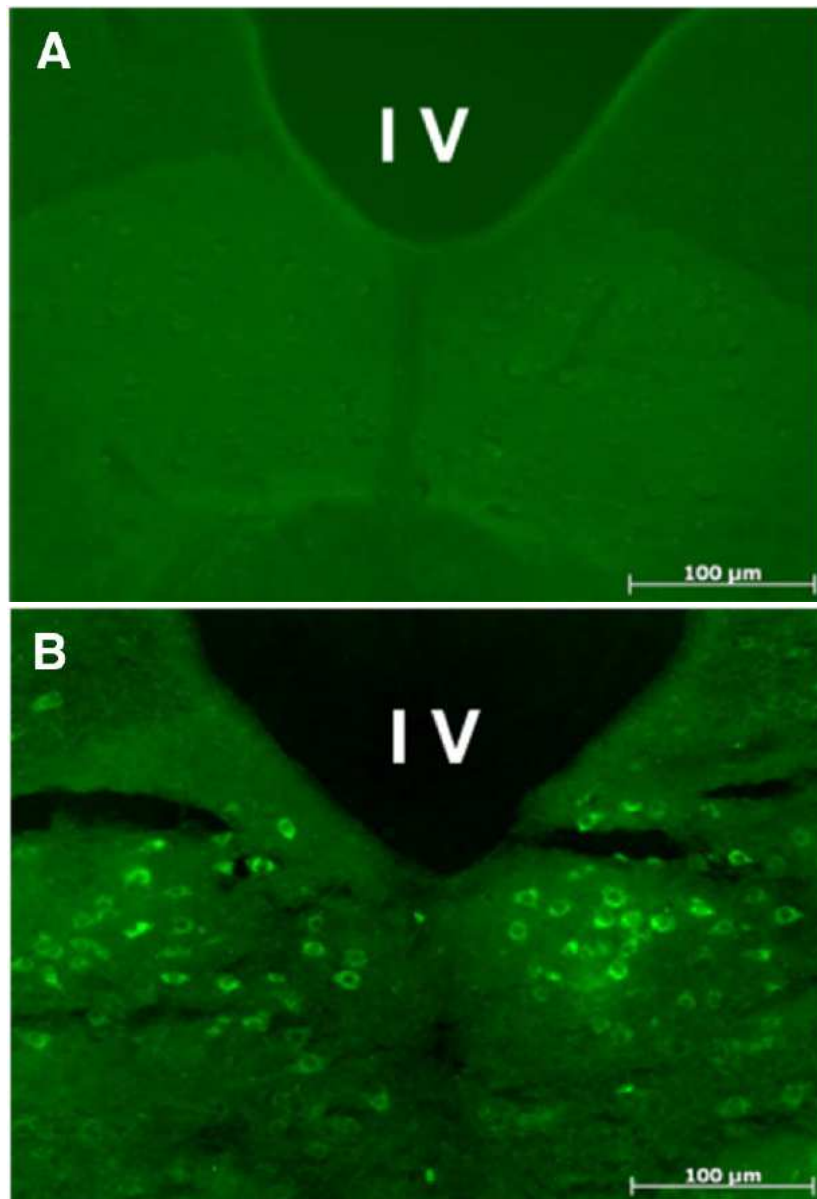


**Figure 20: Hypoglossal nuclei from an acute and a chronic C2Hx rat.** A, Section from an acute C2Hx rat showing the medulla with a complete lack of WGA-Alexa 488 within the hypoglossal nuclei. B, Section from a chronic C2Hx rat showing the same level of the medulla (caudal to the rVRG) with bilateral hypoglossal nuclei WGA-Alexa 488 labeling. IV, fourth ventricle noted as a landmark. Buttry and Goshgarian, 2014.

### *Discussion*

The isolated PN and rVRGs labeling of the phrenic motor system following intradiaphragmatic injection of WGA-Alexa 488 in the acutely injured C2Hx model demonstrates the selective transsynaptic transport of WGA bound tracers over physiologically active synapses as previously described in other motor systems (Harrison et al., 1984, 1986; Jankowska, 1985; Schwab et al., 1979). It has been shown that WGA selectively binds to N-Acetyl-D-glucosamine and sialic acid on the neuronal cell membrane and undergoes receptor mediated endocytosis (Fabian and Coulter, 1985; Robertson, 1990; Schwab et al., 1979). In addition, following injection of WGA-HRP, the number and location of WGA-HRP labeled motoneurons and propriospinal neurons in the spinal cord were compared between two groups; awake animals and chronically anesthetized animals. Two studies concluded that motor activity of the injected nerve was necessary for transsynaptic transport to occur from the motoneurons to the propriospinal neurons (Harrison et al., 1986 and Jankowska, 1985). Specifically, if the animals were chronically anesthetized and immobilized, the transsynaptic transport was minimal, whereas transsynaptic transport increased upon motor nerve stimulation (Harrison et al., 1984; Harrison et al., 1986; Jankowska, 1985) In contrast, alternative neuronal tracers that are transported independent of nerve activity have displayed labeling of additional medullary nuclei and cervical spinal interneurons in C2Hx rat models. For example, injection of Fluorogold, a monosynaptic tracer, into the phrenic nucleus post-C2Hx or sham C2Hx, results in bilateral labeling of the rVRGs, Böttinger complex, gigantocellular reticular nucleus, nuclei of the tractus solitarius, raphe nuclei, and the vestibular nuclei (Boulenguez et al., 2007). Although the Fluorogold was injected into the phrenic nucleus and not injected intradiaphragmatically, Fluorogold still demonstrates the synaptic relationship between the

neurons at the level of the PN and medullary centers that coordinate respiration, including diaphragmatic function. Similarly, application of PRV, a transsynaptic neuronal tracer applied to the diaphragm or phrenic nerve in non-injured or acute C2Hx rats labels the ipsilateral PMNs, interneurons in laminae VII and X bilaterally, cervical interneurons in the dorsal horn bilaterally, and the rVRGs (Dobbins and Feldman, 1994; Lane et al., 2008). The comparison of various tracers resulting in different patterns of neuronal labeling emphasizes the importance of the WGA component of WGA-Alexa 488 that is responsible for the selective transport of the tracer across physiologically active synapses (Goshgarian and Buttry, 2014), similar to that of WGA-HRP (Harrison et al., 1984, 1986; Jankowska, 1985). The importance of the selectivity of WGA-Alexa 488 is further demonstrated when comparing the pattern of labeling in the spinal cord and medulla of acutely injured C2Hx rats versus chronically injured C2Hx rats. The application of WGA-Alexa 488 reveals injury induced plasticity that alters physiologically active connections within the respiratory motor pathways.

Initially for the chronic sham model WGA-Alexa 488 was expected to be isolated to the PN and rVRGs since the hemisection of the cervical spinal cord was omitted. However, the chronic sham tissue displayed bilateral WGA-Alexa 488 labeled interneurons primarily in laminae VII and VIII of the cervical and thoracic cord and bilateral WGA-Alexa 488 labeled intercostal motoneurons in the thoracic spinal cord in addition to phrenic and rVRG labeled cells. This implies that the sham C2Hx surgery including laminectomy of C2, durotomy, and laparotomy had an impact on the spinal cord environment. This is not surprising since the traumatic effects of a laminectomy and durotomy (without a hemisection) has been previously documented and is linked to pseudomeningocele, hypovolemia, activation of astroglia, herniation of the spinal cord and nerve roots, ischemia, scar tissue, and neuronal

cell death (Hadley and Goshgarian, 1997; He et al., 1995; Hershman et al., 2013; Hosono et al., 1995; Macki et al., 2014). In addition, laparotomy has been shown to depress respiration (Barbalho-Moulim et al., 2011; Sieck and Fournier, 1989). Any of the stated side effects or a combination of these effects has the potential to disrupt the normal spinal cord circuitry and provoke spinal plasticity. Interestingly, the sham surgical procedure induces changes only in the spinal cord. The supraspinal components of the phrenic motor pathway appear to be unaffected by the sham surgery based on the observation that WGA-Alexa 488 labeling was restricted to the rVRG in the medulla in the sham rats. Therefore, implying a C2Hx must be carried out to induce supraspinal changes in the respiratory circuitry.

In the chronically injured model, when rats are provided a survival time of at least 7 weeks following a C2Hx, ipsilateral intradiaphragmatic injection of WGA-Alexa 488 followed by a 48-hour survival time results in the labeling of phrenic, intercostal and forelimb motoneurons, interneurons in the cervical and thoracic spinal cord, and the ipsilateral RST, DSCT, and VSCT. Comparison of the WGA-Alexa 488 labeling pattern in each experimental group suggests that the labeled neurons unique to the chronic C2Hx model (forelimb motoneurons, RST, DSCT, and VSCT) may participate in newly established or more likely strengthened synaptic connections to the diaphragm in response to the C2Hx. However, the anatomical data alone cannot confirm if the WGA-Alexa 488 labeled neurons unique to the chronic C2Hx rats are responsible for the time-associated functional recovery detected at the level of the diaphragm in 62% of the chronic C2Hx rats. Regardless, based on the WGA-Alexa 488 labeled nuclei and tracts in the spinal cord unique to the chronic C2Hx model, there is an undeniable difference of connectivity in the acute C2Hx model and chronic sham model compared to the chronic C2Hx model.



The WGA-Alexa 488 labeled neurons in the spinal cord of the chronically C2Hx rats are discussed as follows. Several motor nuclei throughout the cervical spinal cord were bilaterally labeled with WGA-Alexa 488 in addition to the motoneurons within the PN. Starting at the most rostral aspect and moving in the caudal direction, motor nuclei containing WGA-Alexa 488 labeled motoneurons that supply the triceps brachii, and the manus (hand) and/or forearm extensors were identified (Watson et al., 2009). As stated previously, at this time we cannot confirm the role of each neuronal cell type labeled in the chronic C2Hx spinal cord system. However, there is a physiological change in the synaptic connections as demonstrated by the selective transsynaptic transport of WGA-Alexa 488 across physiologically active synapses in the acute C2Hx model and chronic sham model compared to the chronic C2Hx model. Based on previous work demonstrating reciprocal interactions between respiration and locomotion generators in the cervicothoracic cord (Viala and Freton, 1983), one potential role of forelimb motoneurons in the chronically C2Hx spinal cord could be increased involvement in the coordination of accessory respiratory muscles to aid in the maintenance of respiration while walking. The coordination of respiration while walking may become more critical in the chronically C2Hx rat, requiring additional feedback and corrective measures. This could account for the strengthening of existing synapses between the respiratory pathway and pathways involved in the coordination of respiration with motility.

Continuing in the caudal direction, WGA-Alexa 488 labeling was located in the nuclei containing the intercostal motoneurons in the thoracic spinal cord of the chronic C2Hx rats and chronic sham rats. It has been established that intercostal motoneurons have existing connections to the rVRGs to coordinate respiration with movement of the intercostal muscles (Feldman et al., 1985; Hilaire and Monteau, 1997) in both the non-injured system

and following cervical spinal cord injury (Bellingham, 1999; Tian and Duffin, 1996). The appearance of WGA-Alexa 488 labeling in the intercostal motoneurons in the thoracic spinal cord of the chronic C2Hx rats and chronic sham rats suggests a modification to strengthen existing synapses in response to the trauma related to the surgical exposures, but not necessarily the hemisection. Another possibility is, because the hemidiaphragm is atrophied in the chronic C2Hx rats, the tracer could leak into the intrapleural cavity and directly label intercostal neurons. However, this would not explain intercostal neuron labeling in the chronic sham rats demonstrating spontaneous recovery in which the hemidiaphragm is not atrophied.

In addition to motoneurons, three ipsilateral white matter tracts were identified with axons containing WGA-Alexa 488 in the chronically C2Hx rats. The RST, DSCT, and VSCT were identified based on their anatomical location in the ipsilateral funiculi; the tracts were consistently displayed in all chronic C2Hx rat spinal cords, but not in the chronic sham rats. The DSCT and VSCT are well established as the pathway to transmit information of unconscious proprioception of the ipsilateral trunk/thorax and lower/hind limb to the cerebellum (Bosco and Poppele, 2001; Matsushita and Gao, 1997; Soja et al., 1995; Stecina et al., 2013; Valle et al., 2000). VSCT neurons located in lamina VII have been shown to monitor activity of spinal interneuronal networks and descending commands to the spinal motoneurons and interneurons (Shrestha et al., 2012; Stecina et al., 2013). In addition, it has been demonstrated that a population of DSCT neurons located in the thoracic cord in laminae VII and VIII (Tanaka et al., 1990) carries information of chest wall movements to the cerebellum. Recordings from spinocerebellar tract neurons showed either rhythmic activity matching that of artificial ventilation or with phrenic nerve activity

demonstrating a role in feedback and reflex pathways (Hirai et al., 1988; Tanaka and Hirai, 1994).

In our chronically C2Hx model, the axons of the ipsilateral DSCT and ipsilateral VSCT were consistently labeled with WGA-Alexa 488, suggesting an increase in communication by the sensory tracts to relay information about the current state of the thoracic cavity's peripheral wall. Sensory information from the thoracic cavity could play a feedback role in the coordination of accessory muscles to aid in the compensation of the lost hemidiaphragm function. Vinit and Kastner (2009) suggested that after a chronic partial SCI, there is a strategy to by-pass the injury that will consist of redistribution and rewiring of the descending pathways within the spinal cord through the development of accessory pathways. Based on the WGA-Alexa 488 labeling present in the chronic C2Hx model, the DSCT and VSCT could be involved in a strategy to by-pass the injured pathway.

The RST carries the primary descending bulbospinal respiratory pathway; RST axons had a scattered appearance throughout the lateral and ventromedial funiculi with the majority of the fibers terminating in the cervical enlargement (Feldman et al., 1985; Lipski et al., 1994; Nathan, 1963; Nathan et al., 1996; Peterson et al., 1975). Interestingly the RST was identifiable with WGA-Alexa 488 labeling in the chronically C2Hx model but was not easily detected in the acutely C2Hx model. A possible explanation to the WGA-Alexa 488 detected in the reticulospinal axons could involve spinal hyper-reflexia that is documented in chronic (1–12 months) spinal cord injury patients. Spinal hyper-reflexia is caused by new synapse growth of long-axoned neurons or competitive and activity-dependent synapse growth (Ditunno et al., 2004). An increase in synaptic activity or an increase in the number of axons communicating respiratory impulses documented in spinal hyper-reflexia could account for the WGA-Alexa 488 labeling within the ipsilateral RST axons.

In the chronic C2Hx rats and chronic sham rats, WGA-Alexa 488 labeled interneurons were identified throughout the cervical and thoracic spinal cord. The interneurons were predominately located in laminae VII and VIII. Previous studies have presented data describing how spinocerebellar tract (DSCT and VSCT) neurons located in laminae VII and VIII convey information of the central respiratory generator (Matsushita and Gao, 1997; Qin et al., 2002; Tanaka et al., 1990). In addition, the role of interneurons in the non-injured or injured spinal cord, specifically within the phrenic motor system involving communication between the medullary respiratory centers and/or the right and left PN have been considered (Darlot et al., 2012; Dougherty et al., 2012a, 2012b; Lane et al., 2008; Lipski et al., 1993; Qin et al., 2002; Saywell et al., 2011). In this study, WGA-Alexa 488 labeled interneurons in the chronic C2Hx and chronic sham spinal cord compared to the complete lack of interneurons in the acutely C2Hx spinal cord demonstrates injury induced plasticity that may alter the synaptic function in the chronic C2Hx and chronic sham spinal cord environment. However, the precise contribution of interneurons remains unclear and requires further investigation to gather precise details in respect to respiratory function and the role of interneurons.

WGA-Alexa 488 labeling in the medulla of acutely C2Hx rats compared to the medulla of chronically C2Hx rats demonstrates injury-induced supraspinal plasticity that may alter physiologically active synapses within the medulla. Following intradiaphragmatic injection of WGA-Alexa 488, the acute C2Hx model (and sham) demonstrates isolated WGA-Alexa 488 labeling of the rVRGs bilaterally. However, in the chronic C2Hx model in addition to the rVRGs, raphe, hypoglossal, spinal trigeminal, parvicellular reticular, gigantocellular reticular, and intermediate reticular nuclei, which importantly have all been demonstrated previously to be associated with respiratory control in acutely hemisected or

non-injured rats, were consistently labeled bilaterally with WGA-Alexa 488. The labeled nuclei and possible respiratory-based interactions of these nuclei in the chronic C2Hx model are as follows.

Raphe neurons were identified along the midline of the medulla. Midline serotonergic raphe neurons are associated with respiration by influencing respiratory associated nuclei including the hypoglossal, rVRGs, and PN (Manaker et al., 1992; Barker et al., 2009; Richerson, 2004 for review). Raphe neurons, rVRG connections to the trigeminal, and to the gigantocellular nuclei could have a possible role in spontaneous recovery in the chronically C2Hx model based on the presence of WGA-Alexa 488. All of the previously listed nuclei have been described as having synaptic connections to one another (Dobbins and Feldman, 1994; Gaytán and Pásaro, 1998). In addition, it has been demonstrated that neurons within the gigantocellular nuclei innervate the hypoglossal (Yang et al., 1995) and have a connection to the C3–C4 region of the spinal cord (Boulenguez et al., 2007). Golder et al. (2001a) suggested supraspinal plasticity two months after spinal hemisection based on an altered response in hypoglossal motor output; rVRG respiratory premotor collaterals have been shown to project to the hypoglossal in addition to the PN (Lipski et al., 1994).

The parvicellular reticular nuclei (PRN) were labeled in the chronic C2Hx model and links the function of all of the additional WGA-Alexa 488 labeled nuclei together. The PRN contains pre-motor neurons with direct projections to the trigeminal that affect motor behavior of the jaw (orofacial motor control) (Notsu et al., 2008; Nozaki et al., 1993; Sahara et al., 1996). In addition, the PRN are a source of pre-motor neurons with projections to the hypoglossal (Shammah-Lagnado et al., 1992), to the intermediate reticular nucleus (laryngeal function Simonyan et al., 2012), and the gigantocellular among others to control

jaw and tongue movement during facial movements including those associated with respiration (Luo et al., 2006; Mogoseanu et al., 1993; Ter Horst et al., 1991; Travers and Norgren, 1983; Tsumori et al., 2010; Yasui et al., 2004; Zhang and Luo, 2003). Afferents to the PRN communicate information from sensory structures related to orofacial and gustatory control, including sensory information regarding respiration (Fay and Norgren, 1997; Minkels et al., 1991; Mogoseanu et al., 1993; Ter Horst et al., 1991; Yasui et al., 2004). These connections demonstrate the established neuroanatomical framework in a non-injured system for the participation of the medullary nuclei in respiration that appears to be in a hyperactive state based on the pattern of WGA-Alexa 488 in the chronically C2Hx model.

The exact role of each medullary center in respect to spontaneous recovery of hemidiaphragm function following a C2Hx is far from being completely understood. The use of WGA-Alexa 488 as a neuronal tracer to detect changes in physiologically active synapses post injury provides a valuable tool to identify areas of plasticity. The labeled nuclei provided a starting point to examine the chronic effects of a C2Hx and possible targets for intervention to regain functional abilities.

#### **WGA-Alexa transsynaptic labeling in the phrenic motor system of adult rats: Intrapleural injection versus intradiaphragmatic injection**

Injection of WGA-Alexa 488 into the diaphragm consistently labels cell populations involved in the innervation of the diaphragm. Unfortunately, intradiaphragmatic injection requires a laparotomy, an invasive surgical exposure, shown to adversely affect respiration, therefore potentially altering functional outcomes (Sieck and Fournier, 1989; Barbalho-Moulim et al., 2011). In 2009 Mantilla and colleagues introduced a new method of labeling PMNs by injecting cholera toxin subunit beta (CTB) conjugated to Alexa 488 bilaterally into the intrapleural space. Delivery of a retrograde neuronal tracer by way of intrapleural

injection to label the phrenic motor system eliminates the need for anesthesia and the laparotomy required for intradiaphragmatic injections (Mantilla et al. 2009). Following intrapleural injection the authors reported labeling of PMNs as well as thoracic intercostal motoneurons and dorsal root ganglion neurons, but there was no evidence of transsynaptic labeling within the spinal cord tissue examined (Mantilla et al., 2009).

When investigating anatomical changes of the respiratory motor pathway following spinal cord injury, both the pre-motor neurons in the rVRGs that are responsible for descending respiratory drive as well as the motoneurons in the PN must be considered. Mantilla and colleagues (2009) did not report any evidence of transsynaptic transport in the medulla presumably because CTB-Alexa 488 is not a transsynaptic tracer (Cabot et al., 1994, Lee et al., 2009). Therefore, the possibility of transsynaptic transport of a neuronal tracer to the rVRGs in the medulla following intrapleural injection is still a question that has yet to be resolved.

The first aim of this study was to inject WGA-Alexa 488, a known retrograde transsynaptic tracer (Goshgarian and Buttry, 2014) into the intrapleural space to determine if transsynaptic labeling would occur. In carrying out this experiment we found it necessary to differentiate rVRG neurons from nucleus ambiguus (NA) neurons. The neurons of these two nuclei are intermingled in the ventrolateral medulla (Feldman and Ellenberger, 1988; Ellenberger and Feldman, 1990a, 1990b; Hayakawa et al., 2004; Spyer, 2009) and it is difficult to differentiate a rVRG neuron from a NA neuron by morphology alone. The identification of WGA-Alexa 488 labeled rVRG neurons would suggest retrograde transsynaptic labeling from the phrenic nuclei to the rVRG following intrapleural injection. However, since the NA innervates some targets in the thoracic cavity via the vagus nerve (lung parenchyma, Hadziefendic and Haxhiu, 1999; bronchus, Fontán et al., 2000; trachea,

Pérez Fontán and Velloff, 2001), this potential route of tracer uptake following intrapleural injection must be considered. Exposure of the vagus nerve or vagal nerve targets to WGA-Alexa 488 following intrapleural injection resulting in the labeling of NA cells would indicate retrograde labeling (not transsynaptic labeling). To identify the cell bodies that contribute to the vagus nerve, True blue, a retrograde tracer incapable of crossing synapses can be injected directly into the vagus nerve (Payne, 1987). The second aim of this study therefore was to differentiate labeled neurons identified as rVRG cells and NA cells. Three different tracers injected into three different locations were used to determine the extent of retrograde transsynaptic transport following intrapleural injection.

Several combinations of injections were administered to non-injured rats as detailed in Table 2. The various combinations were chosen to ensure the results were due to the location of the injections and not the injected substances themselves.

Animal ID	Weight	Vagus Injection (right)	Intrapleural Injection (right)	Intradiaphragmatic Injection (left)	Medulla Sectioned	Spinal Cord Sectioned
TB1	373	True Blue	WGA-Alexa 488	None	Transverse	Transverse
TB2	360	True Blue	WGA-Alexa 488	WGA-Alexa 594	Transverse	Transverse
TB3	379	True Blue	WGA-Alexa 488	WGA-Alexa 594	Sagittal	Sagittal
TB4	364	True Blue	WGA-Alexa 488	WGA-Alexa 594	Transverse	Transverse
TB5	358	True Blue	WGA-Alexa 488	WGA-Alexa 594	Coronal	Coronal
TB6	361	True Blue	WGA-Alexa 488	WGA-Alexa 594	Transverse	Transverse
TB7	372	True Blue	WGA-Alexa 488	WGA-Alexa 594	Transverse	Transverse
TB8	374	True Blue	WGA-Alexa 488	WGA-Alexa 594	Transverse	Transverse
TB9	351	True Blue	WGA-Alexa 488	WGA-Alexa 594	Transverse	Transverse
NA1	406	WGA-Alexa 594	None	WGA-Alexa 488	Transverse	None
NA2	473	WGA-Alexa 594	None	WGA-Alexa 488	Transverse	None

**Table 2: The 11 rats included in the intrapleural study and the locations and tracers injected into each rat.** Column 1 lists the Animal Identification. Column 2 lists the weight at the time of injection for each rat. Columns 3–5 list the tracers injected into each location. Columns 6 & 7 notes the anatomical plane the medulla and spinal cord tissue samples were sectioned. Buttry and Goshgarian, 2015.

## Results



Injection of WGA-Alexa 488 (green) into the right intrapleural cavity resulted in retrograde transport to produce bilateral labeling of PMNs in the cervical spinal cord (C3 – C6) in 7 of the 9 rats (Fig. 21A, 21E, Table 3). The remaining 2 rats lacked WGA-Alexa 488 labeling following intrapleural injection in all spinal sections examined. Lack of labeling in the 2 rats was likely due to an injection directly into the lung parenchyma, not the intrapleural space. At the time of perfusion, the 2 rats that lacked labeling displayed a site of trauma on the right upper portion of the lung and the lung tissue was notably yellow, the color of WGA-Alexa 488 in saline solution. Due to this observation, the 2 rats; TB4 and TB6, were excluded from quantitative analysis.

Animal ID	Right PN 594	Right PN 488	Right PN 594+488	Left PN 594	Left PN 488	Left PN 594+488	Total 594	Total 488	Total 594 +488
TB2	4	1	174	88	12	105	92	13	279
TB3	--	--	--	--	--	---	159	9	123
TB7	11	0	102	48	0	56	59	0	158
TB8	0	39	33	44	12	30	44	51	63
TB9	1	3	96	55	18	37	56	21	133
<b>TOTALS</b>	<b>16</b>	<b>43</b>	<b>405</b>	<b>235</b>	<b>42</b>	<b>228</b>	<b>410</b>	<b>94</b>	<b>756</b>

**Table 3: Cell counts from 270 cervical spinal cord sections sampled from 5 rats.** Column 1 lists the ID for each rat. Rats that received both intradiaphragmatic and intrapleural injections were included in this cell count. Column 2 lists the number of WGA-Alexa 594 labeled cells located in the right phrenic nucleus (PN). Column 3 lists the number of WGA-Alexa 488 labeled cells located in the right PN. Column 4 lists the number of dually labeled cells with WGA-Alexa 594 and WGA-Alexa 488 located in the right PN. Column 5 lists the number of WGA-Alexa 594 labeled cells located in the left PN. Column 6 lists the number of WGA-Alexa 488 labeled cells located in the left PN. Column 7 lists the number of dually labeled cells with WGA-Alexa 594 and WGA-Alexa 488 located in the left PN. Columns 8–10 list the total number of cells (right and left sides combined) labeled with WGA-Alexa 594, WGA-Alexa 488, or with a dual label of WGA-Alexa 594 and 488 respectively. The TB3 spinal cord was sectioned in a sagittal plane, left could not be differentiated from right therefore only total counts were recorded. TB1 was excluded from the count due the animal not receiving an intradiaphragmatic injection. TB4 and TB6 were excluded due to an unsuccessful intrapleural injection. Buttry and Goshgarian, 2015.

Intradiaphragmatic injection of WGA-Alexa 594 (red, N=8) or WGA-Alexa 488 (green, N=2) into the left hemidiaphragm also resulted in bilateral labeling of PMNs in all rats examined (Fig. 21A, 21E). At the level of the phrenic nuclei (C3 – C6), both intrapleural and intradiaphragmatic injection resulted in isolated labeling throughout the phrenic nuclei in all cervical spinal cord sections examined. There was no labeling in any other neuronal center at C3 – C6 (Fig. 21, 22). Moreover, there was no evidence of spinal interneurons labeled with either WGA-Alexa 488 or 594 following intrapleural or intradiaphragmatic injection. The lack of spinal interneurons confirms the findings in our previous studies examining WGA-Alexa 488 labeling following intradiaphragmatic injection (Goshgarian and Buttry, 2014; Buttry and Goshgarian, 2014). Of the WGA-Alexa 488 labeled cells observed in the PN following a right intrapleural injection,  $86 \pm 17.9\%$  displayed a dual label with WGA-Alexa 594 (left intradiaphragmatic injection) (Table 3). This data confirms that intrapleural injection is an effective method to label PMNs and is comparable to intradiaphragmatic injection (Mantilla et al., 2009). In addition, following intrapleural injection WGA-Alexa 488 was detected bilaterally in the thoracic spinal cord in the intercostal motor nuclei (Fig. 23A) confirming the findings of Mantilla and colleagues (2009). However, following intradiaphragmatic injection, neither WGA-Alexa 594 (red, N=8) or WGA-Alexa 488 (green, N=2) were detected in the thoracic spinal cord (Fig. 23B) confirming the results of our previous study (Buttry and Goshgarian, 2014). The labeling of intercostal motoneurons following intrapleural injection, but not after intradiaphragmatic injection indicates that the tracer is exposed to phrenic axons exclusively when injected into the diaphragm (Buttry and Goshgarian, 2014). In contrast, intrapleural injection results in the tracer being exposed to the entire intrapleural space, in which the tracer is able to diffuse

freely before coming into contact with multiple muscle targets including the diaphragm and intercostal muscles.

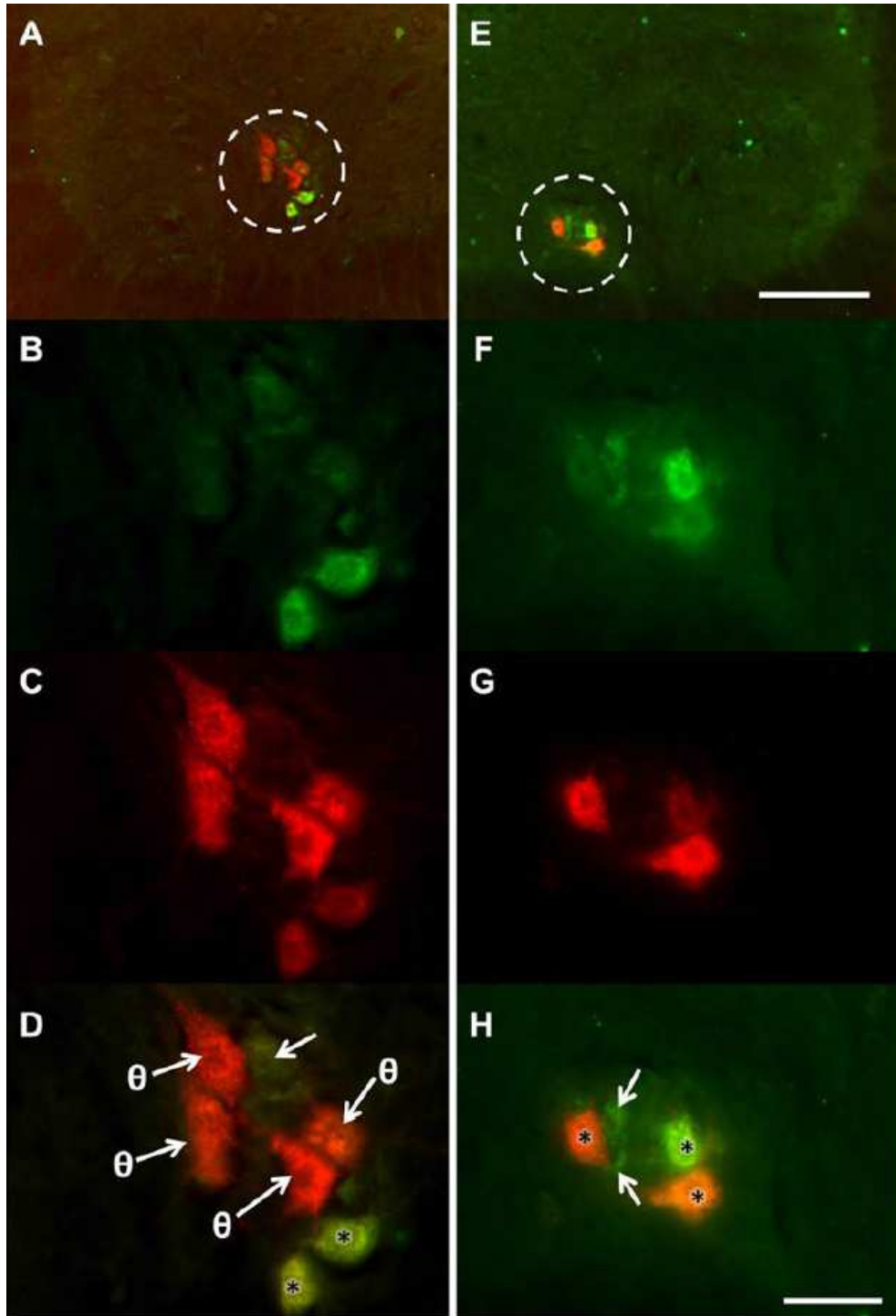


**Figure 21: Transverse sections of the cervical spinal cord at the level of the phrenic nuclei in the same rat following intrapleural and intradiaphragmatic injection.** A. displays a low magnification of the left phrenic nucleus (encircled), B-D display a higher magnification of A. B displays WGA-Alexa 488 (green filter) labeled cells following a right (contralateral) intrapleural injection of this tracer. C displays WGA-Alexa 594 (red filter) labeled cells following a left (ipsilateral) intradiaphragmatic injection. D is a merged image of B and C; note cells contain either WGA-Alexa 488 (arrow) or 594 alone ( $\theta$  arrow), or a mixture of both tracers (noted with \* in the nucleus). The dually labeled cells are easily identified in B and C. E displays a low magnification of the right phrenic nucleus (encircled), F-H display a higher magnification of E. F displays WGA-Alexa 488 (green) labeled cells following a right (ipsilateral) intrapleural injection. G displays WGA-Alexa 594 (red) labeled cells following a left (contralateral) intradiaphragmatic injection. H is a merged image of F and G; note cells contain either WGA-Alexa 488 (arrows) or a mixture of both tracers (noted with \* in the nucleus). Scale bars are 200 $\mu$ m (A and E) and 50 $\mu$ m (BD and F-H). Buttry and Goshgarian, 2015.

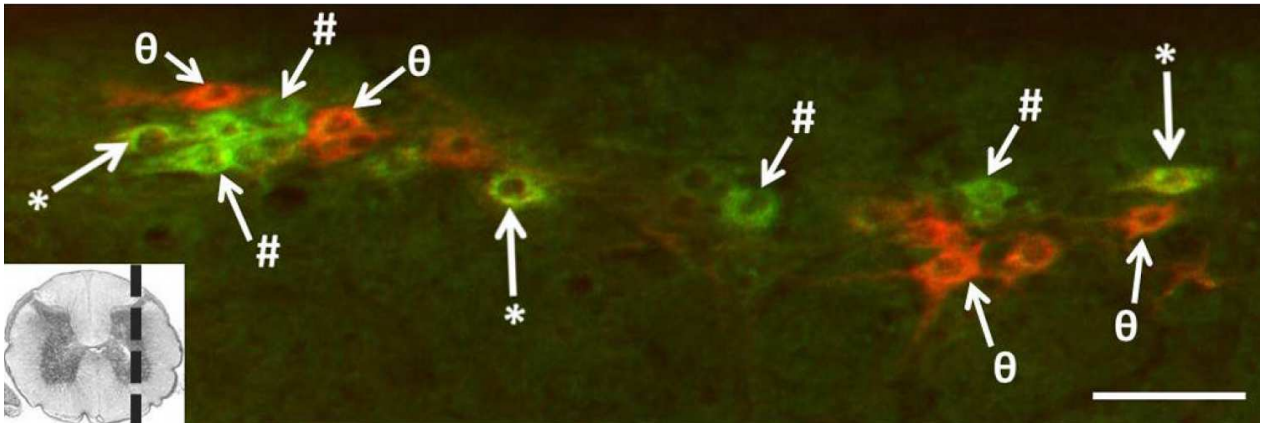


**Figure 22: Sagittal section through the cervical spinal cord following intrapleural and intradiaphragmatic injection** (insert of transverse section for reference). WGA-Alexa 488 (green filter) and WGA-Alexa 594 (red filter) labeling within the right phrenic nucleus following right intrapleural injection of WGA-Alexa 488 and left intradiaphragmatic injection of WGA-Alexa 594. Notice cells contain either WGA-Alexa 488 (green, examples noted with # arrow) or WGA-Alexa 594 (red, examples noted with  $\theta$  arrow) and cells with a dual label appear yellowish in color (examples noted with \* arrows). Scale bar is 100 $\mu$ m. Buttry and Goshgarian, 2015.

The first rat analyzed to validate if intrapleural injection was able to produce spinal cord and medullary labeling with WGA-Alexa 488 received a right intrapleural injection of WGA-Alexa 488 followed by an injection of True blue into the right vagus nerve. Forty-eight hours after injection the rat was sacrificed and the tissue was sectioned. The tissue samples from the medulla demonstrated labeled cells in the intermingled region of the NA and rVRG. Some cells were labeled with either WGA-Alexa 488 or True blue (Fig. 24). In addition, there were numerous cells dually labeled with both WGA-Alexa 488 and True blue demonstrating that intrapleural injection results in the labeling of NA cells.

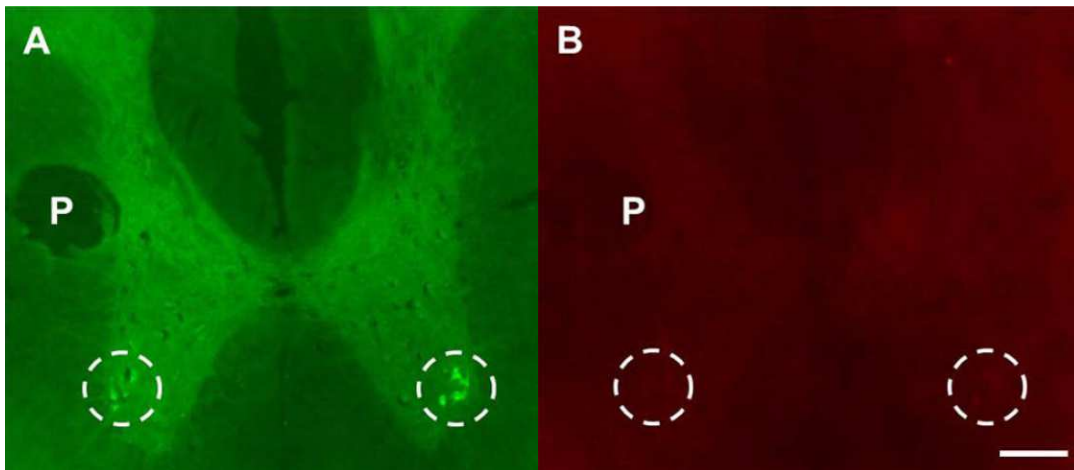


**Figure 23: T6 spinal cord section following intrapleural and intradiaphragmatic injection.** A, Low power magnification of a transverse section through the spinal cord at the T6 level showing bilateral WGA-Alexa 488 (green filter) labeling in the region of the intercostal motor nuclei (encircled areas) following right intrapleural injection of this tracer. B, image of the same section in A using the red filter to detect WGA-Alexa 594 following left intradiaphragmatic injection. The WGA-Alexa 594 label (red) is absent (encircled areas). Thus, intrapleural injection labels intercostal motoneurons, but Intradiaphragmatic injection does not. Scale bar is 200 $\mu$ m. P; pinhole marks left side. Buttry and Goshgarian, 2015.

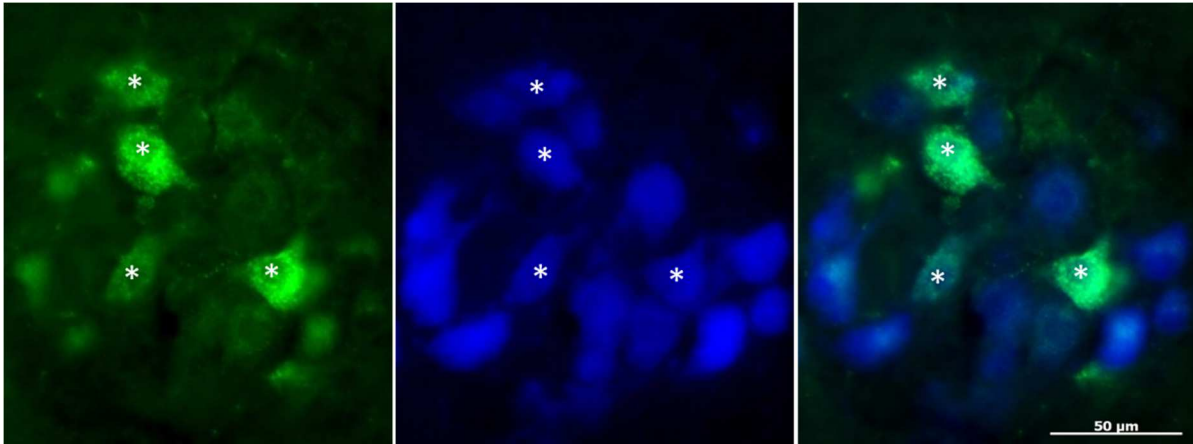


**Figure 24: High magnification of the NA and rVRG following intrapleural injection and vagus nerve injection.** This rat received a right intrapleural injection of WGA-Alexa 488 (green) followed by an injection of True blue into the right vagus nerve (blue). The merged image demonstrates the intermingled relationship between the two labeled cell populations. Some cells are labeled with either WGA-Alexa 488 or True blue as well as cells dually labeled with both WGA-Alexa 488 and True blue (noted with \* in the nucleus) demonstrating that intrapleural injection results in the labeling of NA cells.

To further investigate the route of tracer uptake by the NA cells, 8 rats were injected with 3 types of tracer in 3 different locations (Table 2). Six of the 8 rats that received 3 tracers displayed individually labeled, dual labeled and triple labeled cells in the region of the rVRG and NA (Fig. 25-27, Table 4). TB4 and TB6 were excluded due to the lack of WGA-Alexa 488 labeling in the spinal cord as mentioned previously. The following qualitative and quantitative data includes a total of 82 sections spanning the medulla from 6 rats (summary in Table 4). The left half of the medulla displayed WGA-Alexa 488 and WGA-Alexa 594 labeling isolated to the rVRG and NA following right intrapleural (WGA-Alexa 488) and left intradiaphragmatic (WGA-Alexa 594) injection. Of these cells  $18.1 \pm 10.8\%$  were observed with only WGA-Alexa 488 (green filter, Fig. 25A),  $13.6 \pm 7.1\%$  with only WGA-Alexa 594 (red filter, Fig. 25B), and  $68.2 \pm 8.9\%$  were dually labeled with both tracers (yellow in appearance, Fig. 25D). Left intradiaphragmatic injection of WGA-Alexa

594 resulted in uptake of the tracer by the phrenic nerve, retrograde transport to the phrenic nuclei, followed by transsynaptic transport to the rVRGs as demonstrated in our previous study investigating WGA-Alexa 488 (Goshgarian and Buttry, 2014). Cells containing WGA-Alexa 488 following intrapleural injection were labeled by one or more of the following three potential routes; 1) transsynaptic transport following tracer uptake by the phrenic nerve, 2) transsynaptic transport following tracer uptake by the intercostal nerves, or 3) retrograde transport following tracer uptake from the vagus nerve and its extensive branches that innervate targets in the thoracic cavity. It is important to note that there was a complete absence of True blue in the left half of the medulla following True blue injection into the right vagus nerve (Fig. 25C).

Animal ID	Right rVRG/NA 594	Right rVRG/NA 488	Right rVRG/NA 594+488	Right NA Trueblue	Right NA Trueblue+ 594	Right NA Trueblue+ 488	Right NA Trueblue+ 594+488	Left rVRG/NA 594	Left rVRG/NA 488	Left rVRG/NA 594+488
TB2	7	11	37	65	8	15	32	29	58	98
TB3	0	1	20	60	10	10	45	2	4	21
TB5	1	0	26	242	0	1	25	4	23	61
TB7	7	3	39	115	5	15	46	14	0	45
TB8	4	1	17	120	0	0	36	9	15	50
TB9	1	3	11	110	1	3	62	26	23	93
TOTALS	20	19	150	712	24	44	246	84	123	368

**Table 4: Cell counts from a total of 82 medulla sections sampled from 6 rats.** Column 1 lists the ID for each rat. Rats that received injections in all three locations (intradiaphragmatic, intrapleural and vagus nerve) were included in this cell count. Columns 2–8 list the numbers of labeled cells located in the right half of the medulla in the region of the NA and rVRG. Cells were identified as individually labeled (WGA-Alexa 594, WGA-Alexa 488, or True blue), dually labeled (any combination of 2 of the 3 tracers), or triple labeled (all 3 tracers in a single cell). Columns 9–11 list the numbers of labeled cells located in the left half of the medulla in the region of the NA and rVRG. Cells were identified as individually labeled (WGA-Alexa 594 or WGA-Alexa 488), or dually labeled with both WGA-Alexa 594 and WGA-Alexa 488. TB1 was excluded from the count due the animal not receiving an intradiaphragmatic injection. TB4 and TB6 were excluded due to an unsuccessful intrapleural injection. Buttry and Goshgarian, 2015.

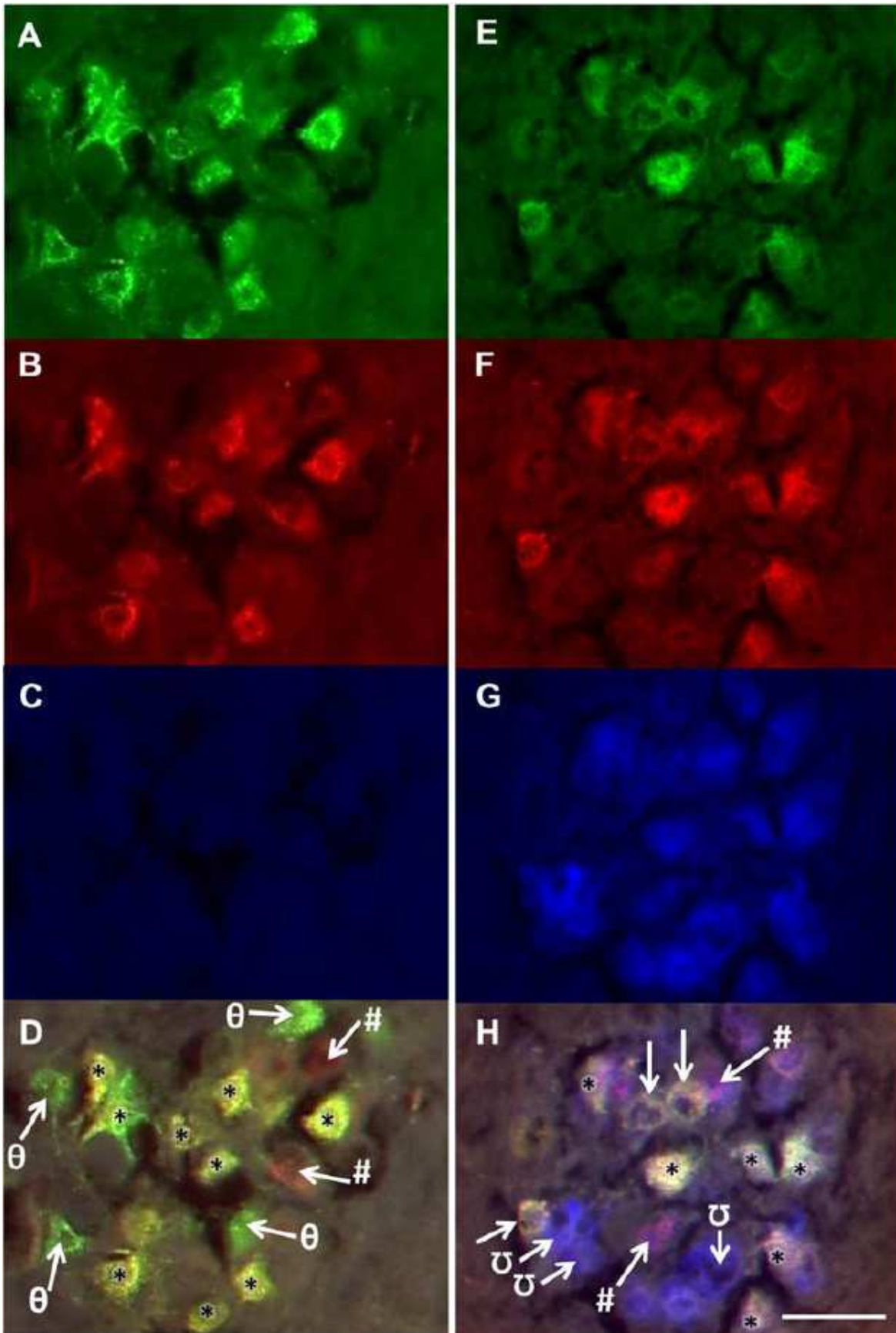




**Figure 25: High magnification of the NA and rVRG following intrapleural, intradiaphragmatic and vagus nerve injection.** High power magnification of a transverse section through the medulla displaying both the left (A-D) and right (E-H) rostral ventral respiratory groups and the nucleus ambiguus. A and E display WGA-Alexa 488 (green filter) labeled cells following a right intrapleural injection of this tracer (A and E captured with equal exposure times). B and F display WGA-Alexa 594 (red filter) labeled cells following a left intradiaphragmatic injection of this tracer (B and F captured with equal exposure times). C and G display the absence on the left and presence on the right of True blue (blue filter) labeled cells following a right vagus nerve injection of this tracer (C and G captured with equal exposure times). D is a merged image of A-C, notice cells contain either WGA-Alexa 488 (green,  $\theta$  arrow), WGA-Alexa 594 (red, # arrow), or a dual label and appear yellow in color (noted with \* in the nucleus). All rVRG cells are transsynaptically labeled. The image shows that not all rVRG cells are dually labeled; some are green only and some are red only. H is a merged image of E-G. Notice cells contain either True blue alone (nucleus ambiguus cells,  $\cup$  arrow) or a mixture of two or three of the labels in one cell. The yellow cells are dually labeled rVRG cells (WGA-Alexa 488 and WGA-Alexa 594, arrow), but the dually (True blue and WGA-Alexa 594, # arrow) and triple labeled cells (noted with \* in the nucleus) suggests that rVRG and NA cells not only intermingle, but they have a synaptic relationship. The cells marked with an asterisk in H can be seen with the green, red and blue filter in E-G respectively. Scale bar is 50 $\mu$ m. Buttry and Goshgarian, 2015.

In comparison, the right half of the medulla displayed WGA-Alexa 488 and WGA-Alexa 594 labeling isolated to the rVRG and NA (Fig. 25–27) following intrapleural (WGA-Alexa 488) and intradiaphragmatic (WGA-Alexa 594) injection. A total of 189 cells were identified as rVRG neurons based on the presence of WGA-Alexa 488 alone, WGA-Alexa 594 alone, or a dual label of 488 and 594 and a complete absence of True blue. Of the right rVRG cells,  $9.2 \pm 8.6\%$  were observed with WGA-Alexa 488 (green filter, Fig. 25E),  $9.3 \pm 6.9\%$  with WGA-Alexa 594 (red filter, Fig. 25F), and  $81.5 \pm 11.8\%$  were dually labeled with both WGA-Alexa 488 and WGA-Alexa 594 (yellow in appearance, Fig. 25H). However, unique to the right half of the medulla, True blue (TB) a retrograde tracer incapable of crossing synapses (Payne, 1987) was injected into the right vagus nerve to identify the ipsilateral NA cells (Fig. 25G & H). A total of 1026 NA cells contained TB. Of these NA cells,  $65.9 \pm 15.4\%$  contained TB alone,  $3.0 \pm 3.5\%$  contained TB with WGA-Alexa 594,  $5.1 \pm$

5.1%) contained TB with WGA-Alexa 488, and  $26.0 \pm 9.7\%$  contained all three tracers (Fig. 25H, 26D, 27). In addition to the right NA, TB alone was identified in a scattering of cells ventral to the NA (Fig. 26C, 26D, & 27), and in the dorsal motor nucleus of vagus (DMX) (Fig. 28), both isolated to the right side. The anatomical relationship of the rVRG and NA can be appreciated in both transverse (Fig. 25 & 27) and sagittal (Fig. 26) planes where both nuclei intermingle within the same cell column in the ventrolateral medulla as described previously (Feldman and Ellenberger, 1988; Ellenberger and Feldman, 1990a, 1990b; Hayakawa et al., 2004; Spyer, 2009).

To validate the result of identifying WGA-Alexa 594 in True blue labeled NA cells following intradiaphragmatic injection, two additional rats, NA1 and NA2 were added. True blue has a hazy appearance and can produce difficulties when examining tissue at the cellular level with a fluorescent microscope. In contrast WGA-Alexa fluorochromes have a distinct granulation resulting in easily identifiable labeled cells. NA1 and NA2 received right vagus nerve injections of WGA-Alexa 594 followed by left intradiaphragmatic injections of WGA-Alexa 488. Both rats displayed individually labeled cells of either WGA-Alexa 594 or WGA-Alexa 488, and dually labeled cells (Fig. 29). This again validates that intradiaphragmatic injection of WGA-Alexa fluorochromes results in both rVRG and NA labeled cells.

Following intradiaphragmatic injection of WGA-Alexa 594, the observation of NA cells containing both TB and WGA-Alexa 594 suggests that WGA-Alexa 594 was transsynaptically transported from rVRG neurons to NA neurons. It is important to stress that this is the first anatomical report of a direct synaptic relationship between rVRG and

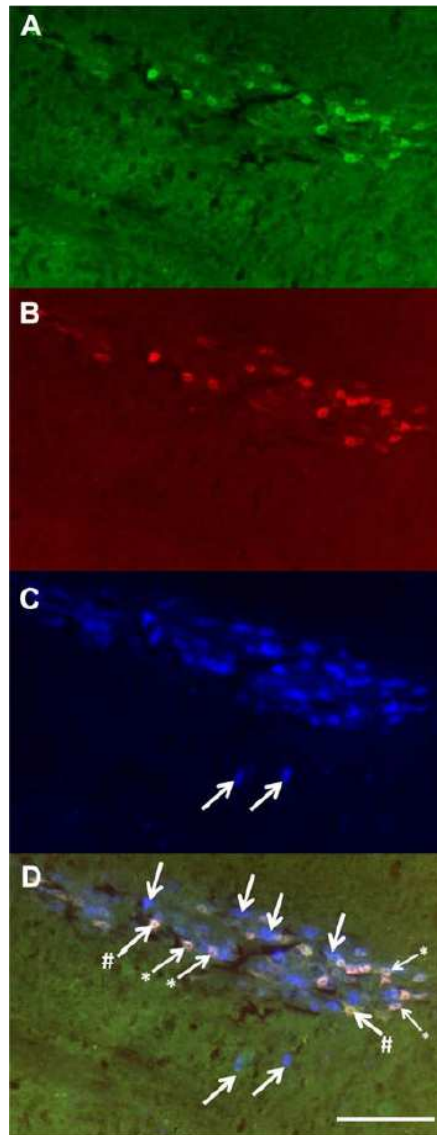


**Figure 26: Sagittal section of the medulla displaying the right rVRG and the intermingled cells of the right NA.** A displays WGA-Alexa 488 (green filter) labeled cells following a right (ipsilateral) intrapleural injection of this tracer. B displays WGA-Alexa 594 (red filter) labeled cells following a left (contralateral) intradiaphragmatic injection. C displays True blue (blue filter) labeled cells following a right (ipsilateral) vagus nerve injection. D is a merged image of A-C, note that the blue labeled NA cells (arrows) not only follow the main column of the rVRG, but there is also a scattering of cells ventral to the main nuclei (arrows in C and D). Note also that many of the cells in the main column are dually labeled rVRG cells (WGA-Alexa 488 and WGA-Alexa 594, # arrows) or triple labeled NA cells (\* arrows) demonstrating a synaptic relationship with the rVRG and NA cells. The ventrally extended cells (arrows in C and D) displayed only True blue label. Scale bar is 200 $\mu$ m. Buttry and Goshgarian, 2015.

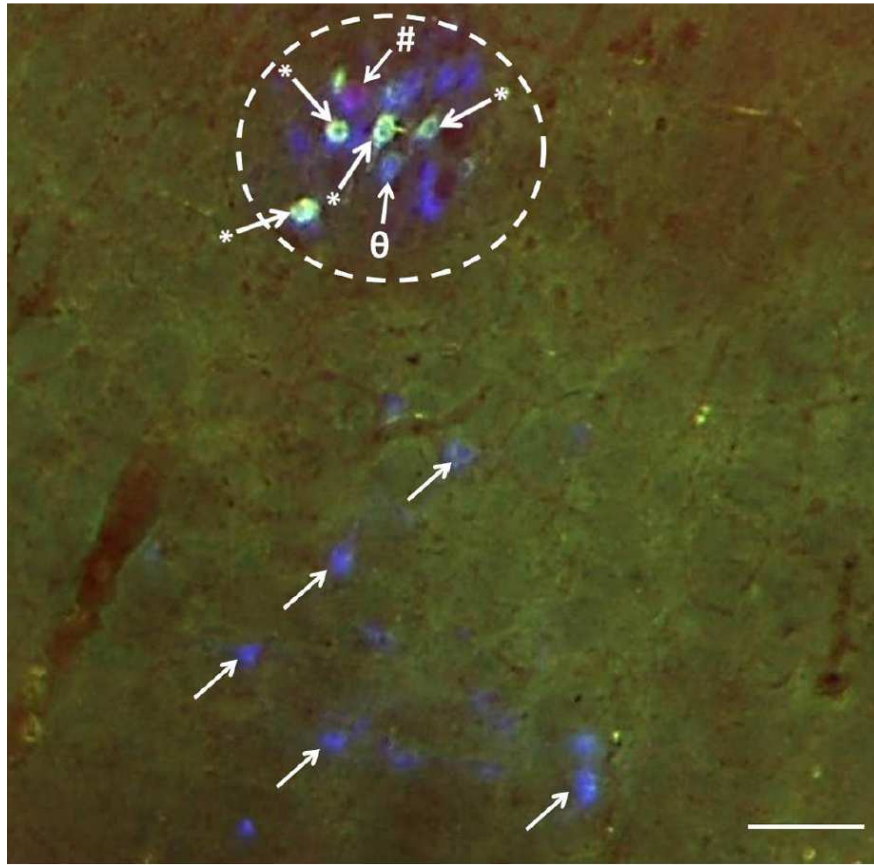


**Figure 27: NA and rVRG and ventrally extended cells following intrapleural, intradiaphragmatic and vagus nerve injection.** High power magnification of a transverse section through the medulla displaying the right rostral ventral respiratory group and the nucleus ambiguus (encircled) labeled after an ipsilateral intrapleural injection of WGA-Alexa 488 (green filter) and a contralateral intradiaphragmatic injection of WGA-Alexa 594 (red filter). True blue (blue filter) was injected into the ipsilateral vagus nerve to label the NA. The figure is a merged image of all three tracers; notice cells contain either True blue alone (NA cells; cells without arrows within the encircled area) or a mixture of two or three of the labels in one cell (# arrow, True blue and WGA-Alexa 594;  $\theta$  arrow, True blue and WGA-Alexa 488; \* arrow, triple label). Notice ventrally extended cells (arrows for examples), displaying True blue only, extend far ventral to the encircled NA and rVRG nuclei. Scale bar is 100 $\mu$ m. Buttry and Goshgarian, 2015.

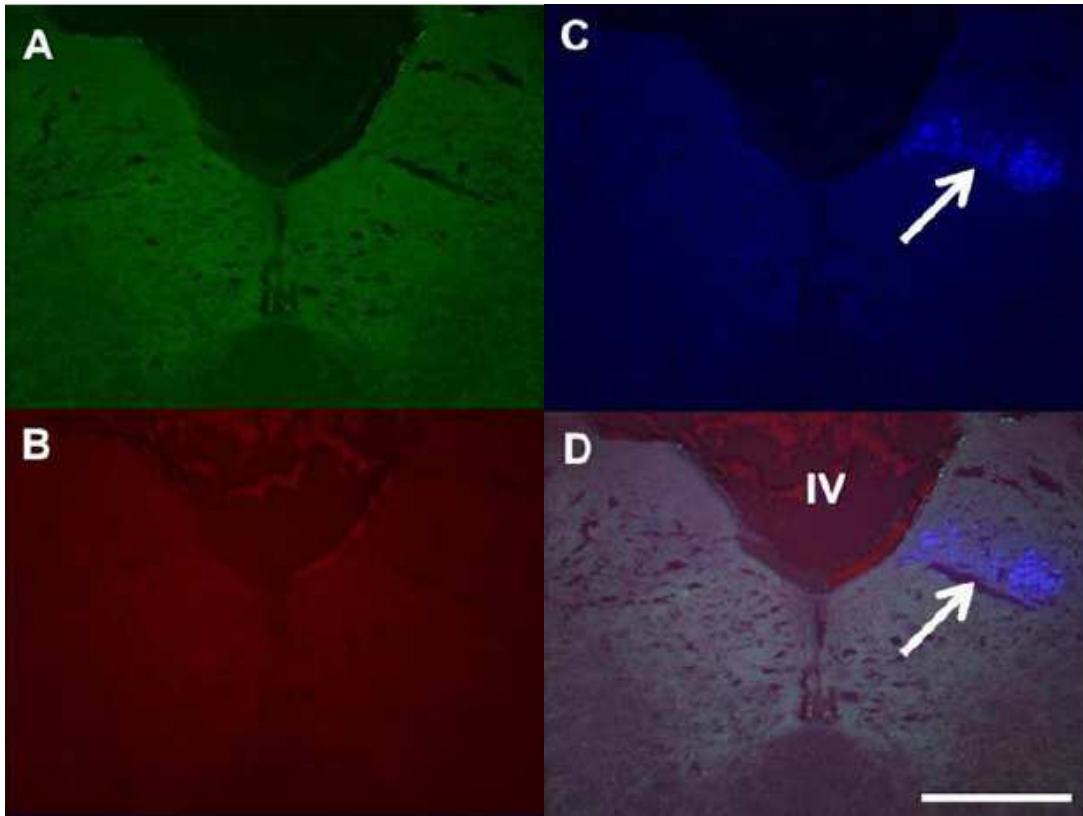


**Figure 28: Dorsal medulla following vagus nerve injection.** Low power magnification of a transverse section through the dorsal medulla displaying the right dorsal motor nuclei of vagus (DMX) labeled with True blue (blue filter) after ipsilateral injection of True blue into the vagus nerve. A displays a complete lack of WGA-Alexa 488 (green filter) labeled cells following a right (ipsilateral) intrapleural injection of this tracer. B displays a complete lack of WGA-Alexa 594 (red filter) labeled cells following a left (contralateral) intradiaphragmatic injection. C displays True blue (blue filter) labeled cells within the right DMX (arrow) following a right (ipsilateral) vagus nerve injection. D is a merged image of A-C. Notice WGA-Alexa 488 and 594 labeling is completely absent in the DMX. IV notes the 4th ventricle for reference. Scale bar is 500 $\mu$ m. Buttry and Goshgarian, 2015.

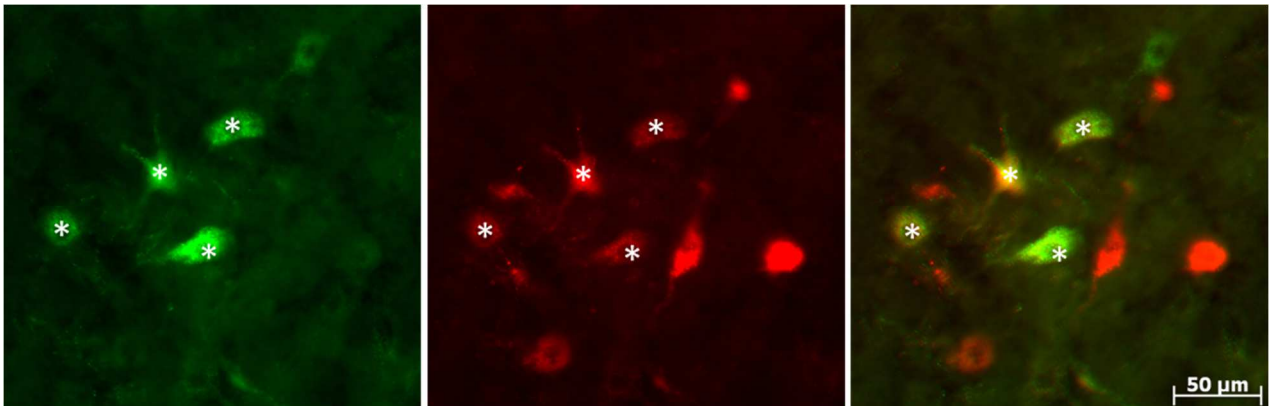


**Figure 29: NA and rVRG following vagus nerve injection and intradiaphragmatic injection.** High magnification of the medulla in the area of the NA and rVRG. This rat received right vagus nerve injections of WGA-Alexa 594 followed by left intradiaphragmatic injections of WGA-Alexa 488. Both rats displayed individually labeled cells of either WGA-Alexa 594 or WGA-Alexa 488, and dually labeled cells (noted with \* in the nucleus). This again validates that intradiaphragmatic injection of WGA-Alexa fluorochromes results in both rVRG and NA labeled cells.

select NA cells. Further support of the selectivity of this synaptic relationship is the observation that all other locations of TB labeled cells, i.e. the DMX (Fig. 28) and the cells scattered ventral to the main column of the NA and rVRG (Fig. 26C, 26D, and 27) had a complete lack of WGA-Alexa 594. Similar to intradiaphragmatic injection of WGA-Alexa 594, following intrapleural injection WGA-Alexa 488 was also absent in the DMX and in the region ventral to the NA suggesting that WGA-Alexa 488 was transsynaptically transported from the PN to the rVRG and then to only select cells of the NA.

### *Discussion*

In 2009, Mantilla and colleagues demonstrated retrograde transport of CTB-Alexa 488 to PMNs and intercostal motoneurons after intrapleural injection, but there was no evidence of transsynaptic transport. This study demonstrated that intrapleural injection of WGA-Alexa fluorochromes not only labels PMNs and intercostal motoneurons similar to

CTB-Alexa 488 (Mantilla et al., 2009), but is also transsynaptically transported in a retrograde fashion to the rVRG and select NA cells in the medulla.

The rVRG and NA have been described as an intermingled column of neurons in the ventrolateral medulla indistinguishable based on size or morphology (Feldman and Ellenberger, 1988; Ellenberger and Feldman, 1990; Hayakawa et al., 2004; Spyer, 2009). In order to distinguish the NA from the rVRG, True blue, a retrograde tracer incapable of crossing synapses, was injected into the right vagus nerve (Sawchenko and Swanson, 1981a, 1981b; Stuesse and Powell, 1982; Cunningham and Sawchenko, 1989). Following intrapleural injection, WGA-Alexa 488 was identified in both the rVRG and select NA cells. Right rVRG neurons were identified based on a dual label of WGA-Alexa 488 (intrapleural injection) and WGA-Alexa 594 (intradiaphragmatic injection) and a complete absence of TB (vagus nerve injection). NA cells were identified by TB labeling. Dual labeling of WGA-Alexa 488 (intrapleural injection) and TB was also identified. There are two potential mechanisms as to how the NA cells became labeled with WGA-Alexa fluorochromes following intrapleural injection; by retrograde transport via targets of the vagus nerve in the thoracic cavity or transsynaptic transport via the phrenic motor pathway.

Based on the observed locations of TB labeling, the latter mechanism is more probable. Following intrapleural injection of WGA-Alexa 488, select cells of the NA were labeled with WGA-Alexa 488 after transsynaptic transport within the phrenic motor pathway from the PN to the rVRG and subsequently to the NA. In support, WGA-Alexa 488 labeling was restricted to specific NA cells intermingled with rVRG cells. WGA-Alexa 488 was never identified in the other two locations of TB labeling: the DMX and the cells scattered ventral to the NA.

Following TB injection into the right vagus nerve, the right DMX and a scattering of cells ventral to the right NA were labeled with TB in addition to the right NA. The DMX has been shown to provide preganglionic parasympathetic innervation to the esophagus (Hadziefendic and Haxhiu, 1999; Hayakawa et al., 2002), larynx (Basterra et al., 1987; Kobler et al., 1994), trachea (Haxhiu and Loewy, 1996; Atoji et al., 2005), lung parenchyma (Hadziefendic and Haxhiu, 1999), and myocardium (Stuesse and Powell, 1982). The cells ventral to the NA are associated with the myocardium (Stuesse and Powell, 1982). These cells of the DMX and the area ventral to the NA are not related directly to respiration. If the only route of WGA-Alexa 488 transport to the NA was via uptake by the vagus nerve, the DMX and cells ventral to the NA would also be expected to exhibit a dual label of TB and WGA-Alexa 488. However, in all rats WGA-Alexa 488 was isolated to the rVRG and the intermingling cells of the NA demonstrating a functional significance of the transsynaptic transport of WGA-Alexa 488 from rVRG to select NA cells. Using physiological techniques, Ellenberger and Feldman (1990) demonstrated that some of the NA cells intermingled with the rVRG cells exhibit respiratory related discharge patterns. Previous studies demonstrate the selective characteristic of WGA-Alexa 488 to be transsynaptically transported over select physiologically active synapses of the respiratory motor pathway as compared in acute and chronic spinal cord injured rats (Buttry and Goshgarian, 2014). Following intradiaphragmatic injection of WGA-Alexa 488 into acutely C2Hx rats, the tracer was described as being located strictly in the PN and rVRG (Goshgarian and Buttry, 2014; Buttry and Goshgarian 2014). However, this study demonstrates the transsynaptic transport of WGA bound conjugates following intradiaphragmatic (as well as intrapleural) injection must be expanded beyond the rVRG to select cells of the NA in the non-injured rat. The connections between the NA and the rVRG have been described physiologically before



(Shannon and Freeman, 1981) and suggest a role in the coordination of respiration with muscle control over airflow (Ellenberger and Feldman, 1990; Spyer, 2009) mediated by pharyngeal and laryngeal muscles. Past studies speculated a role of interneurons relaying information between the NA and rVRG (Ellenberger and Feldman, 1990). However, based on the lack of interneuron labeling, this study provides anatomical evidence of a direct synaptic relationship between rVRG and select NA cells which further supports the contention that transsynaptic transport occurs over physiologically active connections. Moreover, this study demonstrates that transsynaptic transport of WGA-Alexa fluorochromes can occur over two synaptic connections linking PMNs with rVRG cells and subsequently select NA cells.

### **Closing Statement**

The results presented in Chapter 1 demonstrate that WGA-Alexa fluorochromes can be administered by means of intradiaphragmatic or intrapleural injection to selectively identify physiologically active connections between motor and pre-motor neurons in the respiratory circuitry. The importance of the selectivity of WGA-Alexa 488 is undoubtedly demonstrated when comparing the pattern of labeling in the spinal cord and medulla of acutely injured C2Hx rats versus chronically injured C2Hx rats. WGA-Alexa 488 reveals injury induced plasticity that alters physiologically active connections within the respiratory motor pathways detectable just weeks after injury. As a result, these studies provide investigators with a new method that eliminates the need of chemical reactions, to examine plasticity in the respiratory system after spinal cord injury. In addition, the differences between WGA-Alexa 488 labeling in the acutely vs. chronically injured system provide an extensive list of nuclei that can be investigated further to determine their role in recovery of the diaphragm. Depending on an investigator's needs, either intrapleural or

intradiaphragmatic injection proves to be an easily executed and dependable method to label neurons in the respiratory circuitry. Moreover, the application of WGA-Alexa fluorochromes may provide useful in investigating anatomy prior to and following injury to other motor systems.

## **CHAPTER 2: RECOVERY OF DIAPHRAGM FUNCTION IN THE ACUTELY INJURED SPINAL CORD MODEL USING A RETROGRADE TRANSSYNAPTIC THEOPHYLLINE BOUND NANOCONJUGATE**

### **Summary**

The primary descending respiratory drive, provided by the bulbospinal pathway, transmits an excitatory impulse from the rostral Ventral Respiratory Groups (rVRGs) in the medulla to the phrenic nuclei (PN) in the cervical spinal cord. The PN then stimulates the diaphragm via the phrenic nerves, resulting in contraction of the diaphragm during inspiration. Following a spinal cord hemisection at the second cervical segment (C2Hx) the ipsilateral hemidiaphragm is paralyzed due to the disruption of the rVRG axons descending to the ipsilateral phrenic nucleus. Systemically administered theophylline activates a functionally latent crossed phrenic pathway (CPP) which decussates caudal to the hemisection, activating phrenic motoneurons ipsilateral to the hemisection. The result is return of function to the paralyzed hemidiaphragm. Unfortunately, in humans systemically administered theophylline at a therapeutic dose produces many unwanted side effects. In order to eliminate the side effects of theophylline while still maintaining the ability to stimulate the CPP, a tripartite nanoconjugate was synthesized in which theophylline was bound to a neuronal tracer, WGA-HRP, using gold nanoparticles (AuNPs) as the coupler. Following intradiaphragmatic injection of the nanoconjugate, WGA-HRP selectively targets the nanoconjugate to phrenic motoneurons initially and then to the premotor neurons in the rVRG by transsynaptic transport. The ester bond between theophylline and AuNP degrades following injection, releasing theophylline. This method of targeted drug delivery results in a return of function to the once paralyzed hemidiaphragm.

### **Introduction**

According to the National Spinal Cord Injury Statistical Center (NSCISC, 2015) the number of people in the United States affected by SCI who were alive in 2014 is estimated to be approximately 276,000, (range of 240,000 to 337,000). The life span expectancy of these individuals after SCI is greatly reduced when the patient is ventilator dependent (NSCISC, 2015). The reduced life span is due to the fact that respiratory system complications are a major cause for re-hospitalization and death. The reported leading causes of death for individuals with a SCI are pneumonia, septicemia, other diseases of the respiratory system, and cardiovascular diseases (NSCISC, 2015, Yang et al., 2015). Increasing a patient's respiratory output with pharmacological intervention could lead to eliminating ventilator dependence and therefore reduce the chance of infection and untimely death.

Following a high cervical SCI, specifically a C2Hx, there is damage to the bulbospinal pathway that transmits an excitatory impulse from the rVRGs in the medulla to the PN in the cervical spinal cord (C3-C6, rat) (DeVries and Goshgarian, 1989). After injury the PN is unable to effectively stimulate the diaphragm via the phrenic nerves, resulting respiratory stress. However, the CPP, remains intact following a C2Hx since the CPP decussates caudal to the hemisection (Porter, 1895; Moreno et al., 1992; for review Goshgarian, 2003) (Fig. 1). In the rat model, pharmacological activation of the CPP has been shown to restore diaphragm function following systemic administration of theophylline (Nantwi et al., 1996; Nantwi et al., 2003a; Kajana and Goshgarian, 2008a).

Theophylline, acting as a bronchodilator, has an established clinical history as discussed in the introduction (page 1). However, when administered to humans systemically (oral or intravenous) at therapeutic doses equal to or greater than 20mg/mL (measured as plasma levels), there are unwanted side effects such as nausea, vomiting, nervousness,

increased or irregular heartbeat, restlessness, and insomnia (Tzelepis et al., 2006; Barnes, 2013). The side effects following systemic administration in humans are related to an elevated plasma concentration of the drug that causes global phosphodiesterase inhibition and adenosine A1-receptor antagonism, which affects numerous central nervous system centers (Barnes, 2013). Further efforts to investigate the clinical outcome of systemic theophylline administration have been abandoned due to intolerable side effects and lack of quality data.

Collectively, the past studies provide key information on the anatomy and function of the CPP that can be stimulated to re-establish diaphragm function following SCI. Due to the intolerable side effects of theophylline at a therapeutic dose in humans, an alternative to systemic administration was needed. Being able to target the drug to select respiratory nuclei has potential to greatly reduce the therapeutic dose and to decrease or eliminate unwanted side effects.

The key to delivering a drug to select populations of respiratory nuclei is wheat germ agglutinin (WGA). Commonly WGA is bound to horseradish peroxidase (WGA-HRP) as a means to visualize WGA following chemical reactions. WGA, a lectin, has an affinity to N-acetyl-d-glucosamine and sialic acid which are components of glycoconjugates is found on most neuronal cell membranes (Borges and Sidman, 1982; Fabian and Coulter, 1985; Robertson, 1990). These substances act as receptors when WGA-HRP is injected into muscle (Borges and Sidman, 1982; Fabian and Coulter, 1985; Robertson, 1990). Subsequently, WGA-HRP undergoes receptor-mediated endocytosis, and is retrogradely transported within the axon. In the electron microscopic studies of Schwab et al. (1979), the selective release of WGA-HRP from postsynaptic dendrites followed by the rapid uptake of

WGA-HRP into presynaptic nerve terminals was observed, thus demonstrating the retrograde transsynaptic transport of WGA-HRP.

Based on the demonstration of transsynaptic transport of WGA-HRP in the phrenic motor system following a C2Hx (Moreno et al., 1992), WGA-HRP was utilized to target drug delivery to the motoneurons of the PN and the pre-motor rVRG neurons involved in diaphragm function. In order to bind theophylline (or drug of choice) to WGA-HRP, a carrier was needed to facilitate the chemical conjugation. Gold (Au) nanoparticles (NPs) were chosen as a carrier. *In vivo* application of AuNPs has been established in the literature and are known for their biocompatibility, low toxicity, and easy attachment of various structures via chemical bonds to the AuNPs (De Jong et al, 2008; Chen et al., 2009; Duncan et al., 2010; Jain 2010; Thakor et al., 2011; Dreaden et al., 2011; Dreaden et al., 2012; Zhou et al., 2013; Cheng et al., 2013; Mieszawska et al., 2013).

Following a C2Hx, Minic and colleagues (2016) injected into the ipsilateral hemidiaphragm a nanoconjugate consisting of WGA-HRP, AuNP and 1,3-dipropyl-8-cyclopentylxanthine (DPCPX). DPCPX, a specific A<sub>1</sub> adenosine receptor antagonist has been shown to restore ipsilateral phrenic nerve activity following systemic administration (Nantwi et al., 1996; Goshgarian and Nantwi, 2001; Kajana and Goshgarian, 2008). Following injection of the DPCPX nanoconjugate, there was a return of activity to the ipsilateral phrenic nerve and hemidiaphragm. However, theophylline, not DPCPX, has been approved for use in humans to treat respiratory diseases. Therefore, the purpose of the following study was to investigate the possibility that a nanoconjugate could be synthesized with theophylline in place of DPCPX and used to induced recovery.

The nanoconjugate used in the following study consists of three parts; a transporter (WGA-HRP), a carrier (gold nanoparticle, AuNP), and a drug (proTHP) (Fig. 30). The

carrier, AuNP, was used to chemically link the drug to the transporter. To link theophylline a hydroxymethyl group was added to theophylline creating 7-(hydroxymethyl)-theophylline or “proTHP” (Zhang et al., 2016). ProTHP was then linked to the AuNP via a biodegradable ester bond to enable *in vivo* drug release (Zhang et al., 2016). The experimental nanoconjugate and all control nanoconjugates were synthesized by our collaborators in the Department of Chemical Engineering and Materials Science at Wayne State University, Dr. Guangzhao Mao, Dr. Yanhua Zhang, and Fangchao Liu.

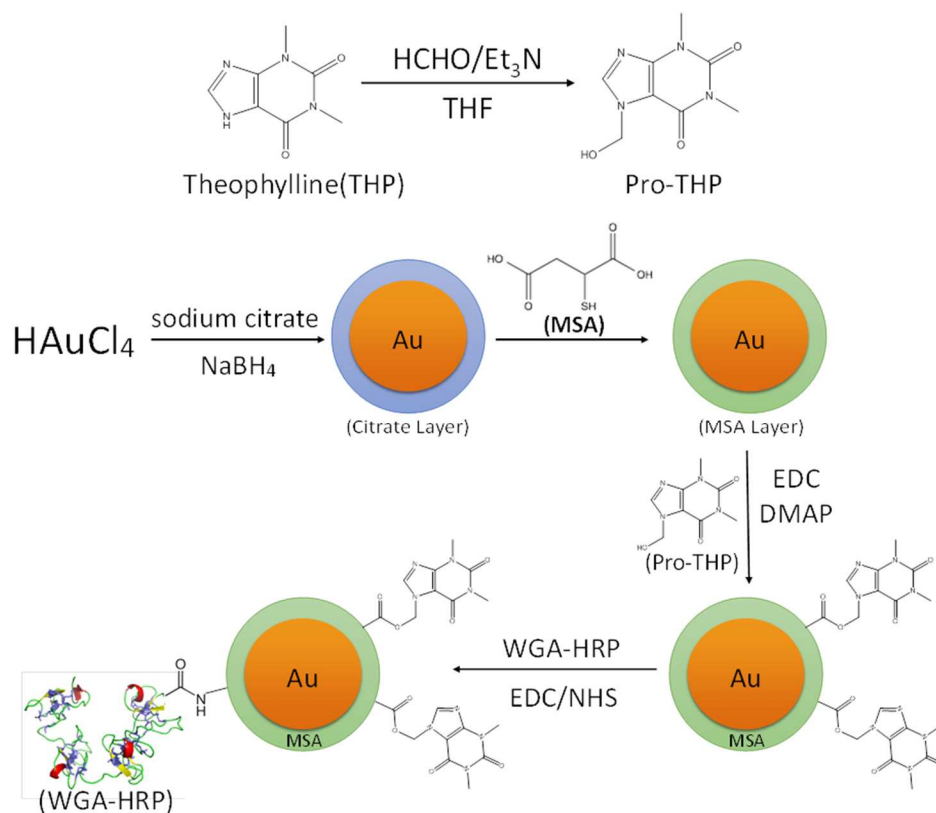


**Figure 30: Schematic of the fabrication of the tripartite nanoconjugate.** HCHO/Et<sub>3</sub>N; formaldehyde/triethylamine; THF, Tetrahydrofuran; HAuCl<sub>4</sub>, chloroauric acid; NaBH<sub>4</sub>, Sodium borohydride; Au, gold; MSA, mercaptosuccinic acid; EDC, 1-Ethyl-3-[3-dimethylaminopropyl] carbodiimide hydrochloride; DMAP, 4-Dimethylaminopyridine; WGA-HRP, wheat germ agglutinin-horseradish peroxidase; NHS, N-Hydroxysuccinimide. Zhang et al., 2016.

Following injection into the diaphragm, similar to WGA-HRP, the nanoconjugate is expected to undergo receptor mediated endocytosis. Once endocytosed, the nanoconjugate is expected to be transported in a retrograde manner to the PN in the spinal cord followed by retrograde transsynaptic transport to the rVRGs in the medulla. The ester bond linking the AuNP to proTHP is transient, resulting in the release of proTHP following injection (Zhang et al., 2016). In contrast the peptide (amide) bond between WGA-HRP and the AuNP is permanent.

### **Visualization of the WGA-HRP-AuNP-proTHP nanoconjugate**

A total of 5 rats underwent intradiaphragmatic injections to visualize the location(s) of the nanoconjugate following injection. An immunohistochemistry technique (see Methods) was utilized to visualize the WGA component of the nanoconjugate. The WGA-HRP-AuNP amide bond is permanent whereas the AuNP-proTHP ester bond is transient. Therefore, the location of WGA should also identify where the AuNPs are but not necessarily the proTHP. All 5 rats revealed the same results. WGA positive cells were identified in the ipsilateral phrenic nuclei in the spinal cord and bilateral in the rVRGs in the medulla (Fig. 31). These results suggest that the WGA-HRP portion of the nanoconjugate is capable of being transported to the PN and subsequently to the rVRGs following intradiaphragmatic injection.

### **Nanoconjugate synthesis**

All nanoconjugates used in this study were synthesized according to Zhang et al., 2016. To determine the drug concentration of each batch, thermogravimetric analysis (TGA) was completed on all nanoconjugate batches (Table 5). The variation of proTHP bound to each AuNP as demonstrated by TGA, highlights the importance of verifying every batch produced, even if identical protocols were used during synthesis. TGA provides information



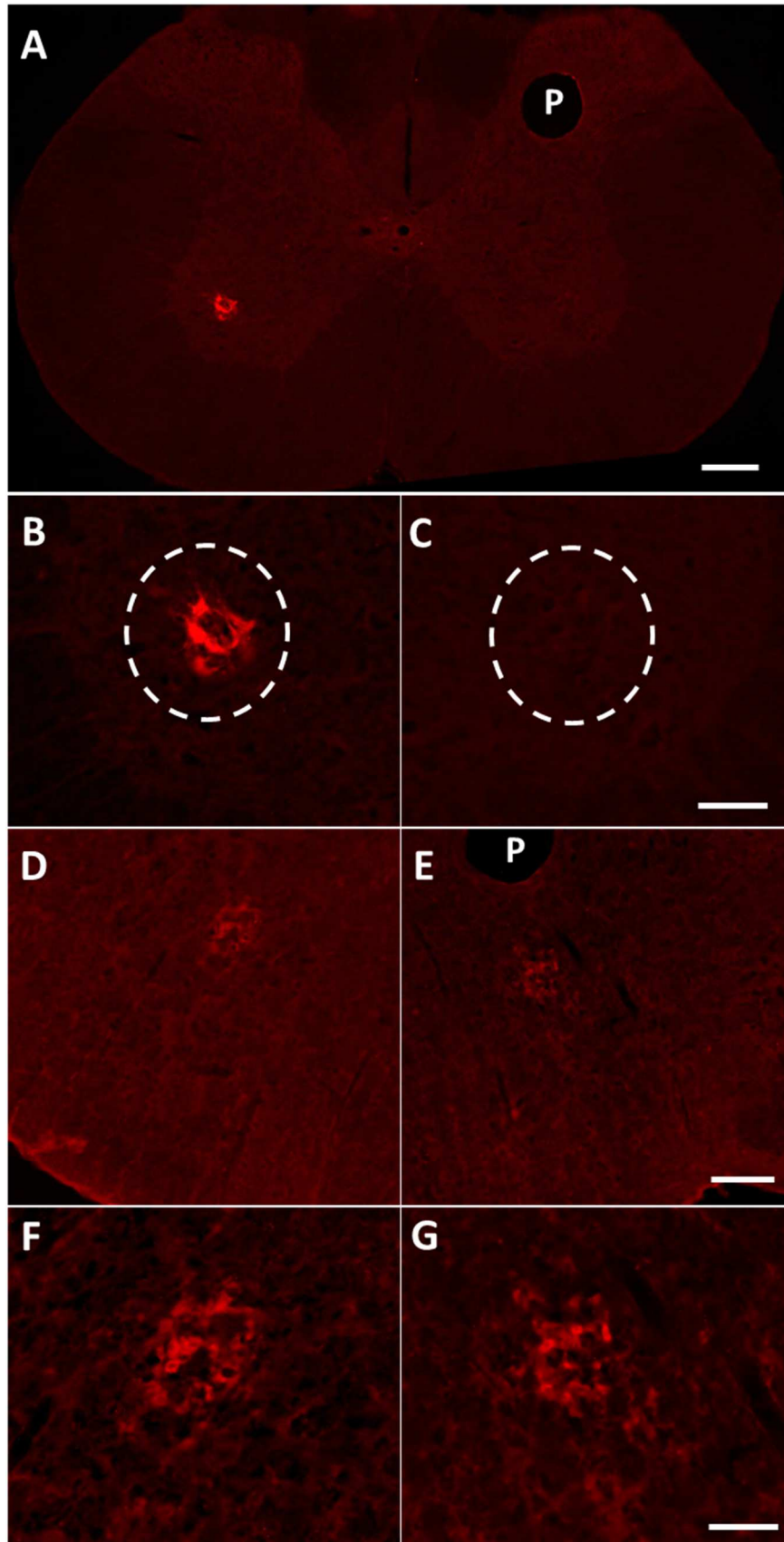


**Figure 31: Cervical spinal cord and medulla sections displaying WGA labeling following nanoconjugate injection.** (A) Transverse section of the cervical spinal cord displaying ipsilateral anti-WGA positive labeling in the phrenic nuclei (PN) following intradiaphragmatic injection of the WGA-HRP-Au-pro-THP nanoconjugate. There is a lack of labeling in the contralateral PN. Scale bar 200um, P notes pinhole to mark side contralateral to the injection. (B) Higher magnification of the ipsilateral PN shown in A displaying fluorescence from the anti-WGA antibody. (C) Higher magnification of the contralateral PN shown in A with a complete lack of WGA label. Scale bar 50um. (D and E) Transverse sections of the medulla at the level of the rVRGs from the same rat shown in A. (D) Ipsilateral rVRG displaying fluorescence from the anti-WGA antibody. (E) Contralateral rVRG displaying fluorescence from the WGA antibody. P notes pinhole to mark side contralateral to the injection. Scale bar 200um. (F) Higher magnification of the ipsilateral rVRG show in D. (G) Higher magnification of the contralateral rVRG shown in E. Scale bar 50um. Zhang et al., 2016

Synthesis Date	Average Amount of proTHP molecules per one AuNP	Concentration of proTHP (mg/ml) in nanoconjugate solution containing AuNP = 4mg/ml
2/17/2014	532.95	1.1508
3/14/3014	277.12	0.5984
4/4/2014	218.030	0.471
8/15/2014	341.54	0.7376
1/12/2015	768.15	1.6588
2/17/2015	330.076	0.713
3/2/2015	754.41	1.6416
6/8/2015	202.030	0.436
7/20/2015	248.212	0.536

**Table 5: Thermogravimetric analysis of WGA-HRP-AuNP-proTHP nanoconjugates.** Each batch underwent Thermogravimetric analysis (TGA) to determine the drug concentration of each solution. TGA detects how many proTHP molecules are bound to each AuNP. The drug concentration in mg/ml can be calculated using the concentration of the AuNP combined with the TGA data. TGA is necessary to ensure each rat is receiving the same dose of proTHP when multiple batches are being compared.

that can be applied to each nanoconjugate batch to calculate the exact volume needed to deliver a set dose. All nanoconjugate solutions had an AuNP concentration of 4mg/ml. For example, a nanoconjugate with 202 proTHP molecules per one AuNP results in a proTHP concentration of 0.436 mg/ml, whereas a nanoconjugate with 248 proTHP molecules per one AuNP has a proTHP concentration of 0.536 mg/ml. This leads to differences in the volume required to administer a set proTHP dose. To administer the dose of 0.03mg/kg proTHP for a 400-gram rat, 28 $\mu$ l of the solution containing 202 proTHP per AuNP must be administered. In contrast to administer the same dose of 0.03mg/kg proTHP for a 400-gram rat, 23 $\mu$ l of the solution containing 248 proTHP molecules per AuNP must be administered.

#### **EMG response to WGA-HRP-AuNP-proTHP and control solutions**

Five doses of the nanoconjugate based on proTHP concentration (0.03mg/kg, 0.07mg/kg, 0.12mg/kg, 0.14mg/kg, 0.25mg/kg) were analyzed by EMG (Minic et al., 2016) on days 2 through 14 post injection. All proTHP doses were confirmed with TGA analysis. EMG functional recovery of the diaphragm after a one-time injection of the nanoconjugate proTHP dose of 0.03mg/kg, was detected as early as day 2 post nanoconjugate injection and persisted up to 14 days in 65% of the rats (N=20) (Fig. 32). Similarly, the 0.07mg/kg proTHP nanoconjugate dose resulted in recovery in 57% of the rats (N=21) (Fig. 33), the 0.12mg/kg proTHP nanoconjugate dose resulted in recovery in 27% of the rats (N=11) (Fig. 34), the 0.14mg/kg proTHP nanoconjugate dose resulted in recovery in 44% of the rats (N=18) (Fig. 35), and the 0.25mg/kg proTHP nanoconjugate dose resulted in recovery in 14% of the rats (N=7). Nevertheless, there were some noticeable qualitative differences between the experimental groups. Rats that received a 0.03mg/kg dose often had weaker bursts compared to those observed in rats in the 0.07mg/kg dose group (Fig. 36). Rats from the 0.12mg/kg and 0.14mg/kg dose groups typically had stronger bursts similar to the

0.07mg/kg dose group. However, in several rats from the 0.12mg/kg and 0.14mg/kg dose groups, the LHD burst frequency was sporadic (non-phasic) and sometimes off rhythm compared to the right side, a possible effect of over stimulation (Fig. 35). Interestingly several rats from the 0.14mg/kg group presented challenges while trying to stabilize them under anesthesia. To reach the anesthetic plane for an EMG procedure, these rats required multiple supplemental doses of anesthesia compared to one dose needed in all other groups.

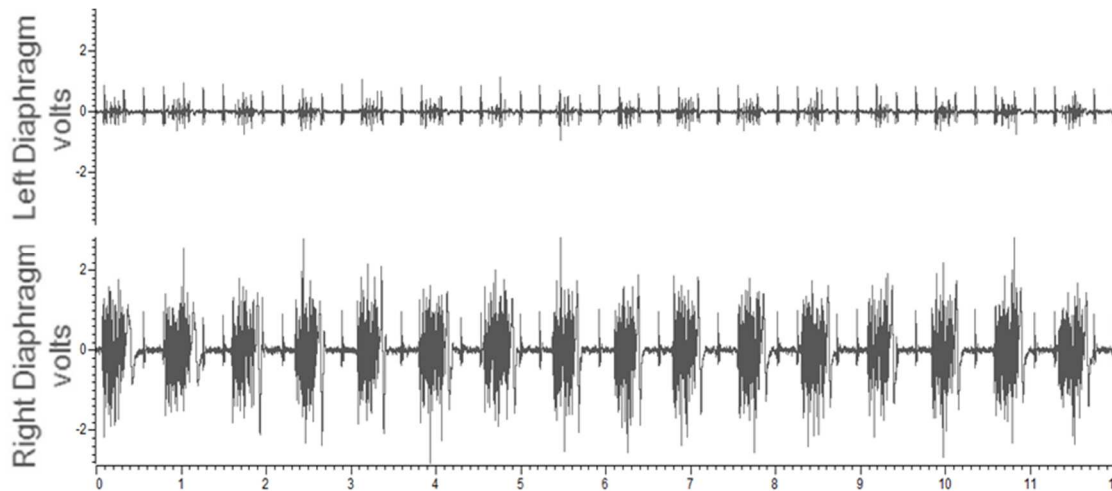


**Figure 32: EMG traces day 7 post injection 0.03mg/kg nanoconjugate.** Day 7 post injection of the 0.03mg/kg dose nanoconjugate. There is a return of the phasic bursting pattern from the left hemidiaphragm (top trace). The bursts from the left hemidiaphragm match those in the right hemidiaphragm (bottom trace). The sharp spikes in all traces are EKG activity.

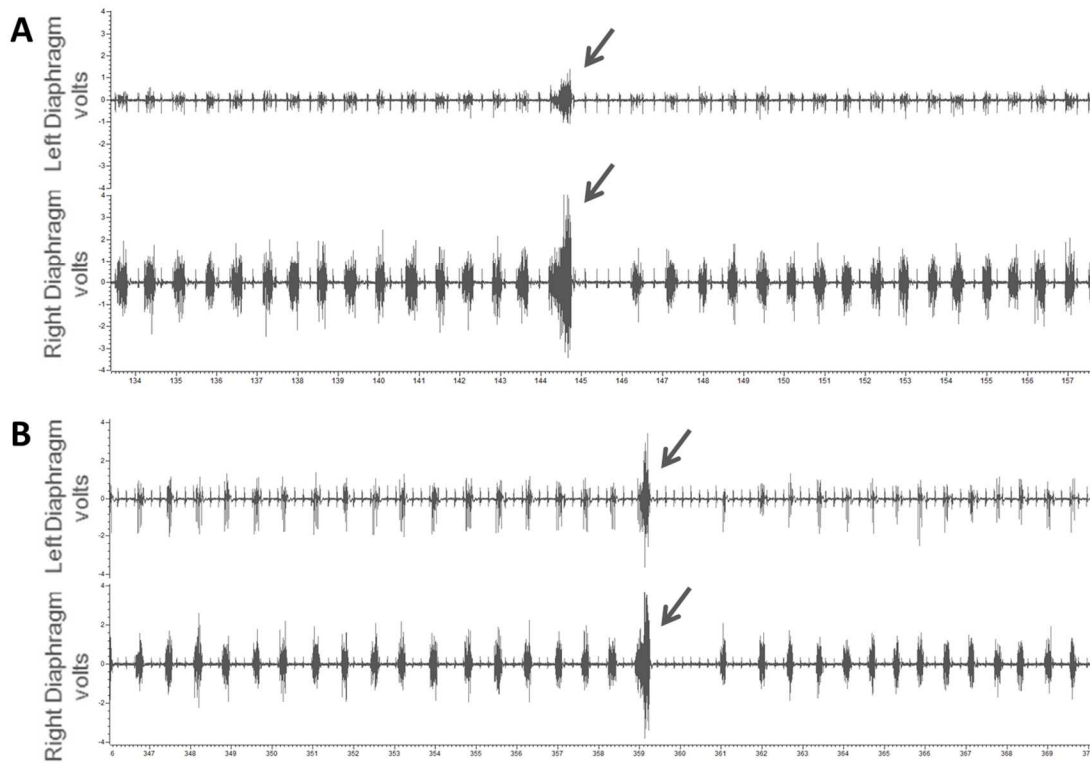


**Figure 33: EMG traces day 2 and day 14 post injection of 0.07mg/kg nanoconjugate.** Both recordings were obtained from the same rat. (A) Day 2 post injection of the 0.07mg/kg dose nanoconjugate there is a return of the phasic bursting pattern from the left hemidiaphragm (top trace). The bursts from the left hemidiaphragm match those from the right hemidiaphragm (bottom trace). (B) Day 14 post injection, the activity has persisted in the left hemidiaphragm (top trace) and remains phasic and synchronous with the right hemidiaphragm (bottom trace). In both traces an augmented breath is demonstrated (arrows) followed by a short period of apnea. This demonstrates that the CPP is intact and is functional. The sharp spikes in all traces are EKG activity.

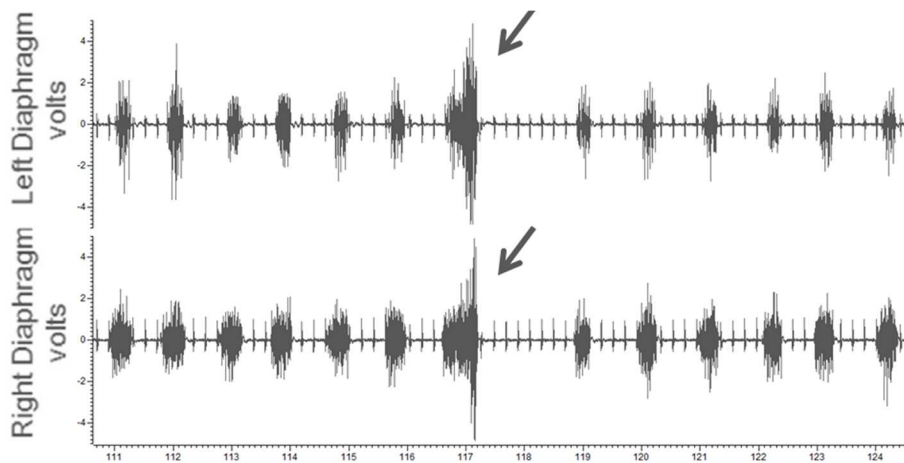


**Figure 34: EMG traces day 5 post injection 0.12mg/kg nanoconjugate.** Day 5 post injection of the 0.12mg/kg dose nanoconjugate there is a return of the phasic bursting pattern from the left hemidiaphragm (top trace). The bursts from the left hemidiaphragm match those from the right hemidiaphragm (bottom trace). In both traces an augmented breath is demonstrated (arrows) followed by a short period of apnea. The sharp spikes in all traces are EKG activity.

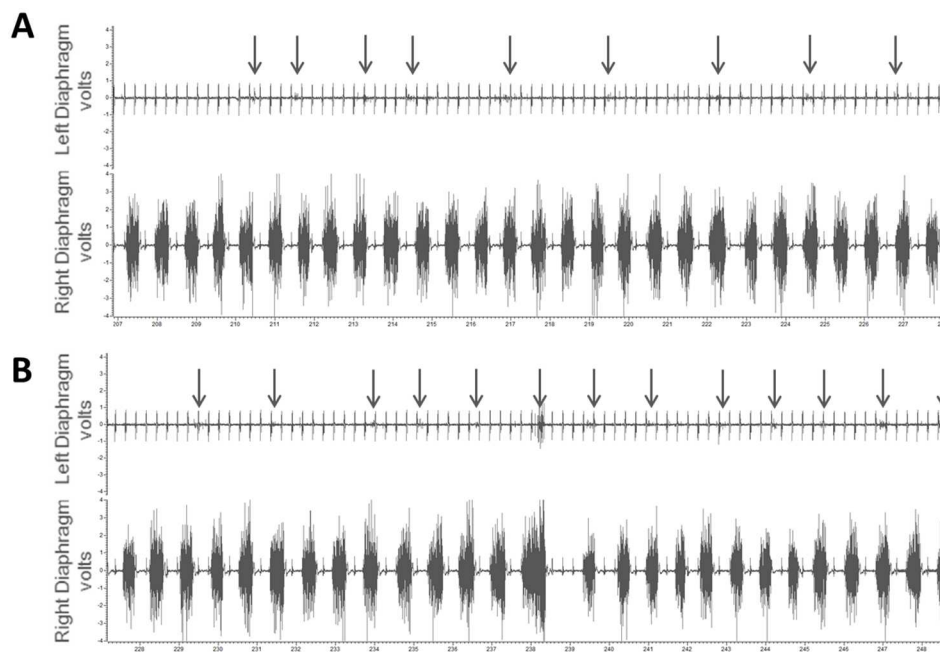


**Figure 35: EMG traces day 2 post injection 0.14mg/kg dose.** (A) and (B), day 2 post injection of the high dose (0.14mg/kg) nanoconjugate there is a small return of the bursting pattern (arrows) from the left hemidiaphragm (A and B top traces) but the pattern is sporadic (non-phasic) and out of sync with the right hemidiaphragm (A and B bottom traces). B, exhibits an augmented breath followed by a short period of apnea. The sharp spikes in all traces are EKG activity

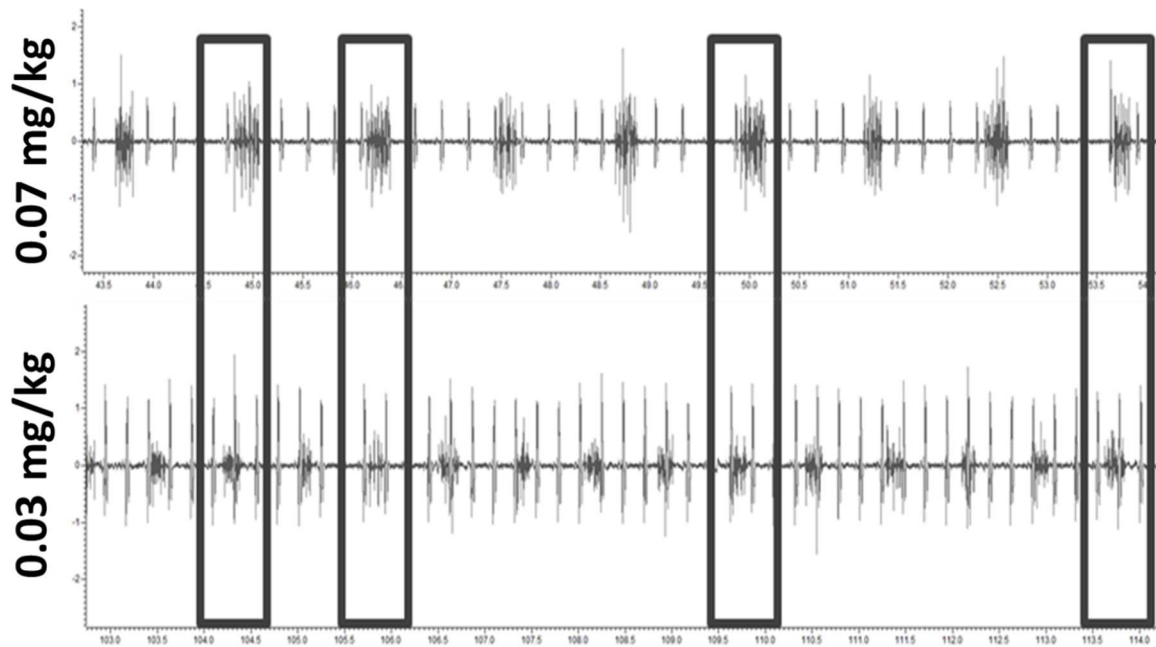


**Figure 36: EMG traces from LHD day 7 post injection; 0.03mg/kg vs 0.07mg/kg.** Traces from the left hemidiaphragm of a rat that received a 0.07mg/kg dose (top trace) and a rat that received a 0.03mg/kg dose (bottom trace). Note in the four areas highlighted that the burst from the 0.07mg/kg dose produces a more robust burst than the 0.03mg/kg dose.

Injection of a control solution containing a conjugate of AuNP-proTHP 0.03mg/kg (no WGA-HRP) (N=9), or WGA-HRP-AuNP (no proTHP) (N=8) failed to produced recovery of the LHD (Fig. 37). To determine the effectiveness of the nanoconjugate, proTHP (7-(hydroxymethyl)-theophylline, see methods) in saline (0.07mg/kg) was injected into the diaphragm. The proTHP dose of 0.07mg/kg resulted in recovery in 40% of the rats (N= 5) (Fig. 38). Two additional rats were injected with the same saline used to dissolve the proTHP. Both rats injected with saline lacked functional recovery in all follow up EMG recordings (Fig. 39).

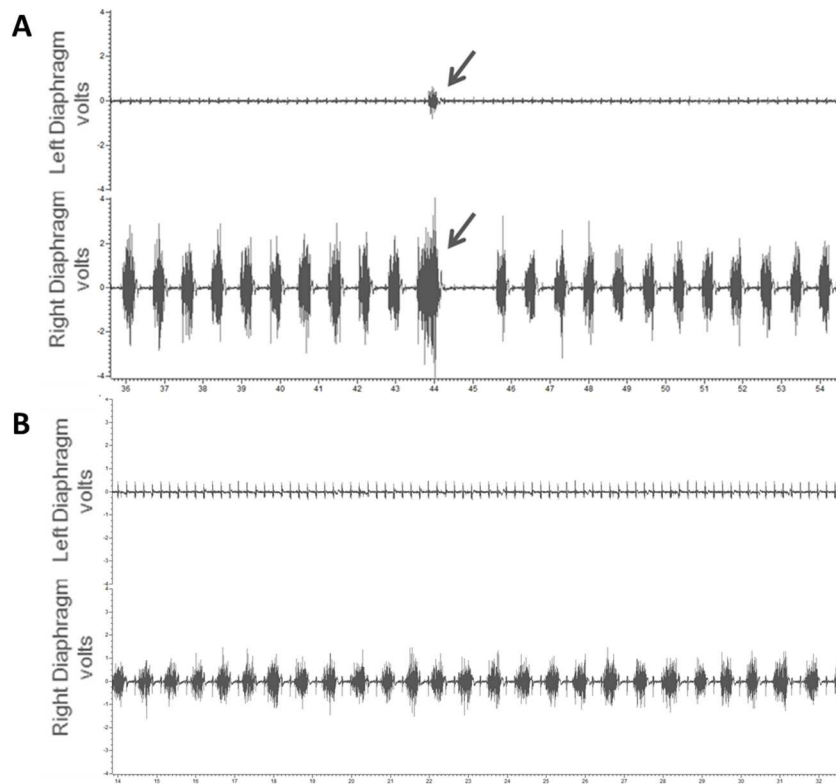


**Figure 37: EMG traces post injection of control solutions.** (A) Following injection of the WGA-HRP-AuNP control the left hemidiaphragm remains inactive (top trace) with the exception of the CPP demonstrated by the augmented breath (arrows). The right hemidiaphragm maintains phasic bursting activity (bottom trace). (B) Following injection of the 0.03mg/kg AuNP-proTHP control the left hemidiaphragm remains inactive (top trace) while the right hemidiaphragm maintains phasic bursting activity (bottom trace).

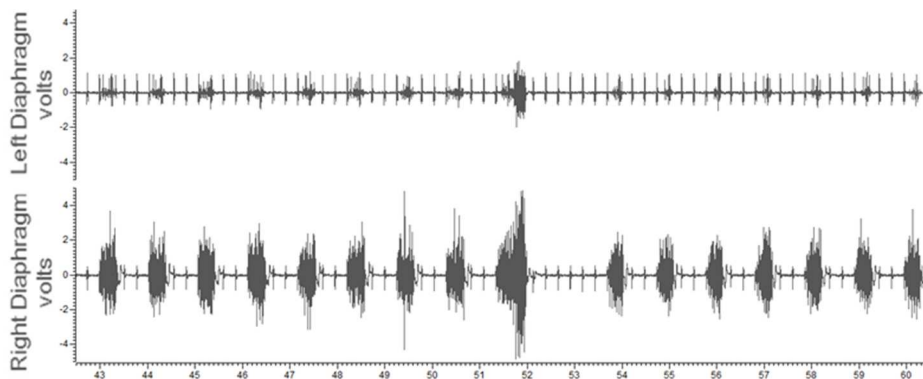


**Figure 38: EMG traces day 5 post injection of proTHP 0.07mg/kg in diaphragm.** Following injection of proTHP there is a return of the bursting pattern from the left hemidiaphragm (top trace) that matches the phasic bursts of the right hemidiaphragm (bottom trace).



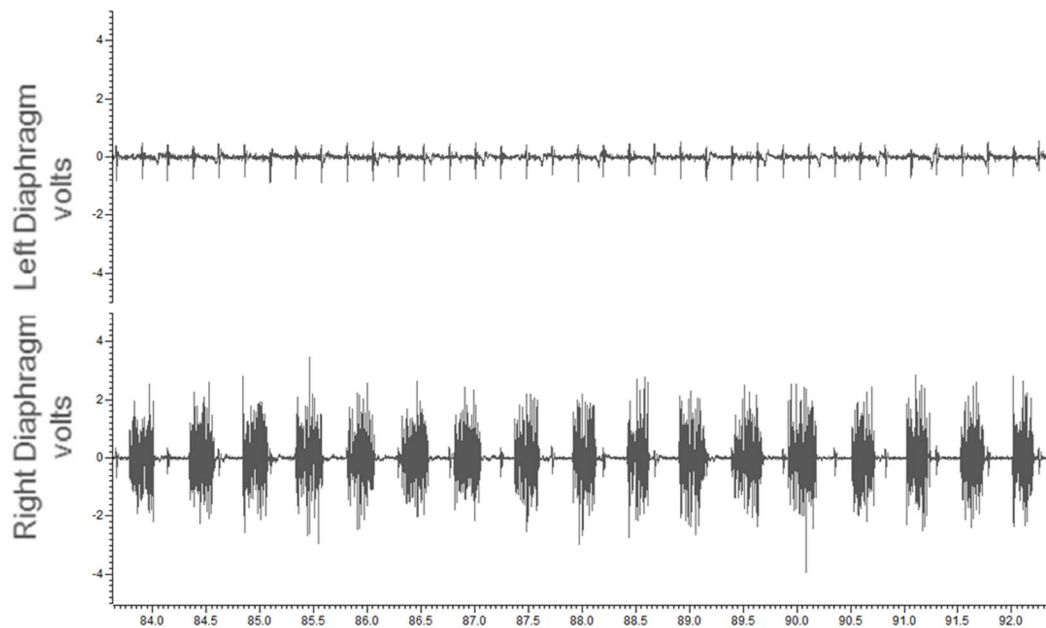


**Figure 39: EMG traces from the left and right hemidiaphragm day 7 post injection of saline.** Day 7 post injection of the saline control the left hemidiaphragm remains inactive (top trace). The right hemidiaphragm maintains phasic bursting activity (bottom trace).

Statistical significance of functional recovery occurrence, detected with EMG analysis, was determined using the Chi Square-Fisher's exact test followed by the Bonferroni adjustment (Fig 40, Minic et al., 2016). Treatment with 0.03mg/kg of the pro THP nanoconjugate resulted in significantly greater proportion of rats achieving functional recovery when compared to the 0.25mg/kg dose ( $p=0.033$ ). In addition, treatment with 0.03mg/kg, 0.07mg/kg, or 0.14mg/kg of the proTHP nanoconjugate resulted in a significantly greater proportion of rats achieving functional recovery when compared to the control 0.03mg/kg AuNP-proTHP; ( $p=0.002$ ), ( $p=0.009$ ), ( $p=0.031$ ) respectively. Treatment with 0.03mg/kg, 0.07mg/kg, or 0.14mg/kg also resulted in a significantly greater proportion of rats achieving functional recovery when compared to the control WGA-HRP-AuNP; ( $p=0.001$ ), ( $p=0.004$ ), ( $p=0.026$ ) respectively.

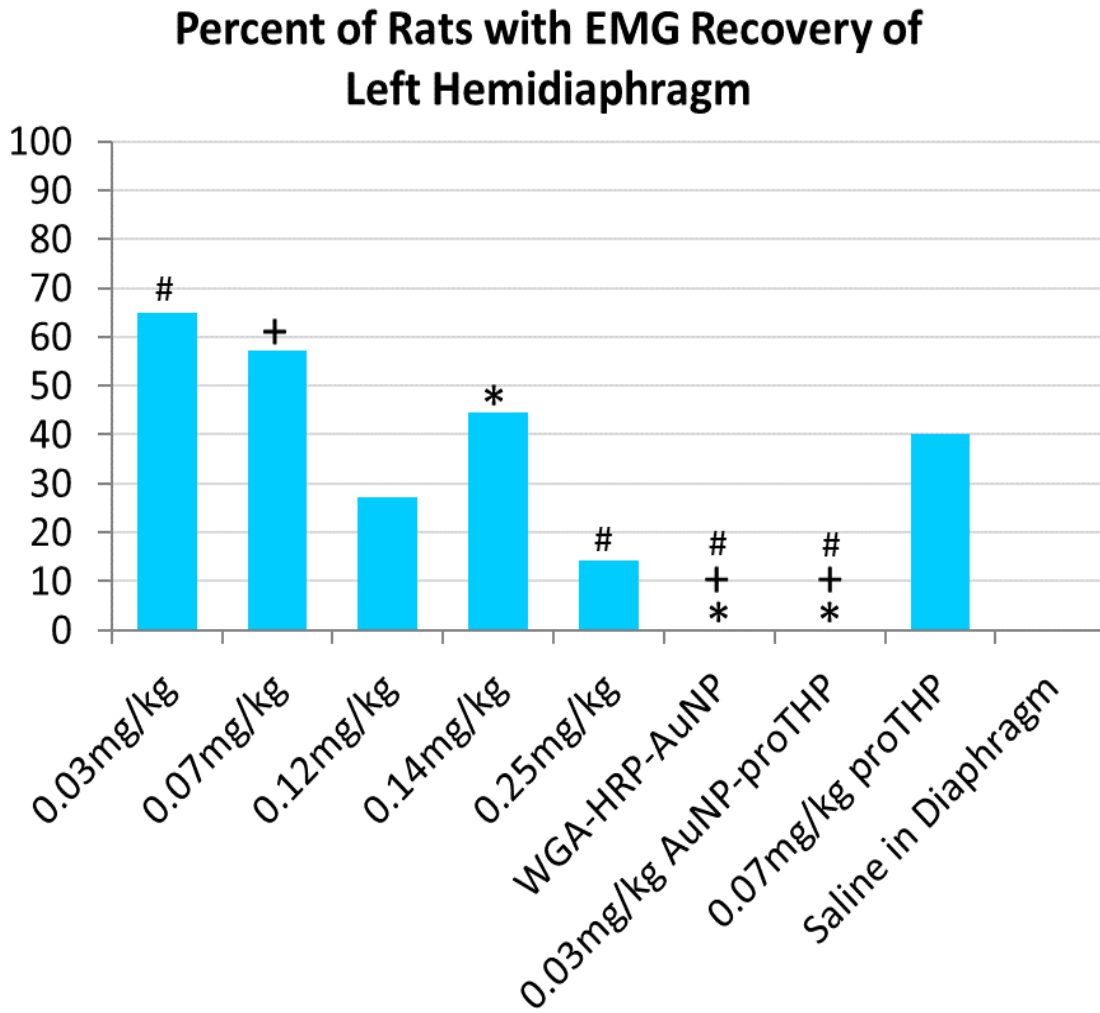


**Figure 40: Percent Recovery Detected by EMG.** The chart displays the percentage of rats in each group that had left hemidiaphragm recovery detected by EMG. Statistical analysis consisted of data from 120 rats. A Chi-square test was performed and significance was found between the proportions of observations (Yes/No) and the groups,  $X^2(9, N = 120) = 23.749$ ,  $p = 0.005$ . The Fisher exact test found significance between the following pairwise comparisons; 0.03mg/kg vs. 0.25mg/kg ( $p=0.033$ , #); 0.03mg/kg vs. WGA-HRP-AuNP ( $p=0.001$ , #); 0.03mg/kg vs. 0.03 AuNP-proTHP ( $p=0.002$ , #); 0.07mg/kg vs. 0.03 AuNP-proTHP ( $p=0.009$ , +); 0.07mg/kg vs. WGA-HRP-AuNP ( $p=0.004$ , +); 0.14mg/kg vs. 0.03AuNP-proTHP ( $p=0.031$ , \*); 0.14mg/kg vs. WGA-HRP-AuNP ( $p=0.026$ , \*).

Based on EMG data, the previously paralyzed hemidiaphragm can be stimulated following injection of the nanoconjugate. The return of hemidiaphragm function can be detected as early as day 2 post injection, and persists for the duration of the experiment, up to and including day 14 post injection. All five nanoconjugate doses produced recovery as detected by EMG.

Injection of control solutions containing saline, WGA-HRP-AuNP, or AuNP-proTHP were unable to stimulate any detectable hemidiaphragm activity. Interestingly, the remaining control solution proTHP dissolved in saline, injected intradiaphragmatically, did result in activity detectable by EMG. However, with data only from the EMG, it is unclear as to whether this is isolated muscle activity stimulated by the injection or proTHP (Bianchi 1961; Isaacson and Sandow, 1967; Kentera and Varagic, 1975; Jones et al., 1982; Creed et al., 1983; Supinski et al., 1984), or if it is a return of function mediated by the bulbospinal pathway via the phrenic nerve.

#### **Phrenic nerve response to WGA-HRP-AuNP-proTHP and control solutions**

Bilateral phrenic nerve recordings were used to quantify recovery on days 3, 7, and 14 following nanoconjugate injection of the three doses with the highest occurrence of diaphragm recovery as characterized by EMG. See Methods for details.

One-way ANOVA showed significant drug effect on day 3 between the 0.14mg/kg dose and the remaining two groups, 0.03mg/kg dose and 0.07mg/kg dose for the INT ( $p < 0.001$ ) and the MAX ( $p < 0.001$ ) (Fig. 41, Table 6). This data suggests that at the day 3-time point, the 0.14mg/kg dose nanoconjugate is the most effective at restoring LPN activity with  $5.1 \pm 0.8\%$  INT and  $8.2 \pm 1.4\%$  MAX LPN recovery.

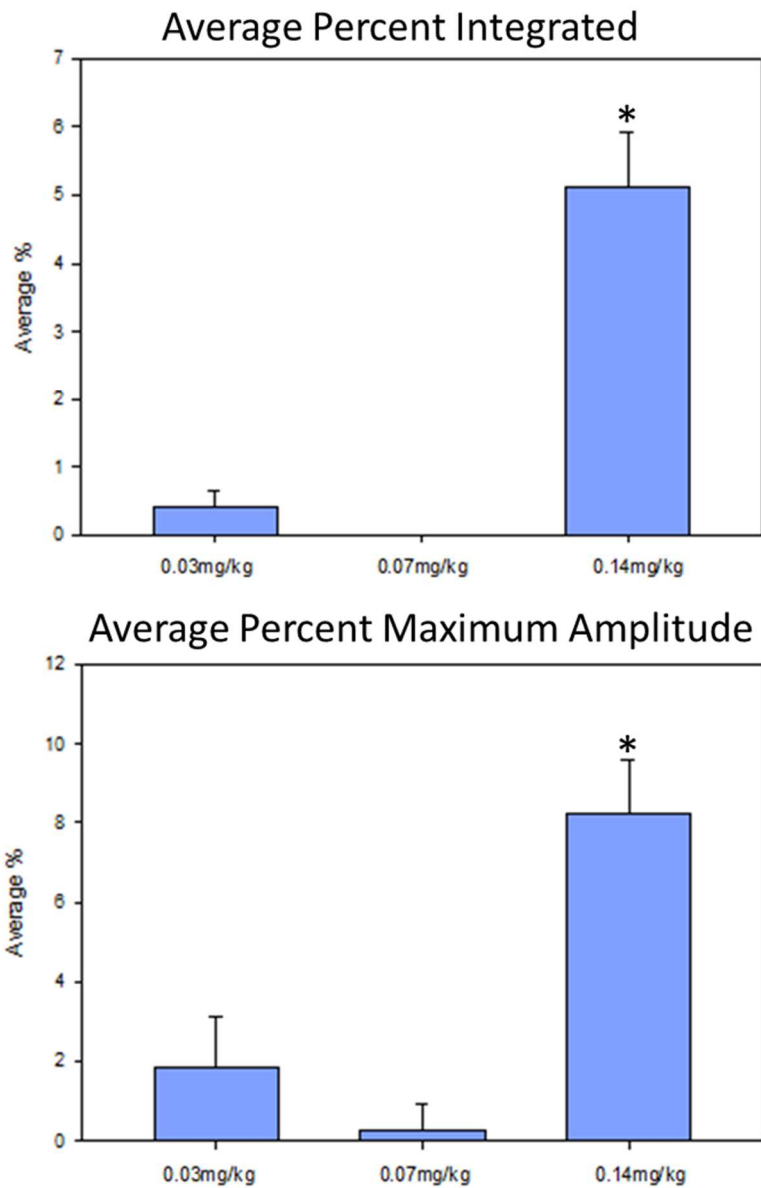


**Figure 41: Comparison of Day 3 Nerve Recordings.** The average percent integrated (top graph) and average percent maximum amplitude (bottom graph). Statistical data consisted of neurograms from 21 rats (Table 6). One-way ANOVA showed significant drug effect on day 3 between the 0.14mg/kg dose and the remaining two groups, 0.03mg/kg dose and 0.07mg/kg dose for the integrated waveform ( $p < 0.001$ ) and the maximal amplitudes ( $p < 0.001$ ).

Nanoconjugate Dose Administered	Percent INT	Percent MAX
0.03mg/kg	0.4±0.2%	1.8±1.2%
0.07mg/kg	0.002±0.005%	0.2±0.7%
0.14mg/kg	5.1±0.8%	8.2±1.4%

**Table 6: Left phrenic nerve percent recovery on day 3.** The percent integrated (INT) and percent maximum amplitude (MAX) of the left phrenic nerve compared to the right phrenic nerve. Statistical data consisted of neurograms from 21 rats. One-way ANOVA showed significant drug effect on day 3 between the 0.14mg/kg dose and the remaining two groups, 0.03mg/kg dose and 0.07mg/kg dose for the integrated waveform ( $p<0.001$ ) and the maximal amplitudes ( $p<0.001$ ).

One-way ANOVA showed no significant drug effect on day 7 for either the INT or the MAX (Fig. 42, Table 7). The dose 0.14mg/kg demonstrated the highest percent recovery following nanoconjugate administration with  $0.6\pm 1.3\%$  INT and  $3.8\pm 8.4\%$  MAX LPN recovery. The control solution 0.07mg/kg proTHP dissolved in saline, injected intradiaphragmatically demonstrated  $0.5\pm 0.1\%$  INT and  $1.5\pm 0.4\%$  MAX LPN recovery. The LPN signal was detected in the remaining two controls WGA-HRP-AuNP and AuNP-proTHP, however the amount was negligible;  $0.01\pm 0.02\%$  INT,  $0.6\pm 1.0\%$  MAX and  $0.004\pm 0.01\%$  INT,  $0.3\pm 1.0\%$  MAX respectively.

One-way ANOVA showed significant drug effect on day 14 for the INT between the 0.03mg/kg dose and the 0.07mg/kg dose ( $p=0.042$ ). There was also significant drug effect for the MAX between the 0.03mg/kg dose and the remaining two doses 0.07mg/kg ( $p<0.001$ ) and 0.14mg/kg ( $p<0.001$ ) (Fig. 43, Table 8). This data suggests that at the day 14-time point, the 0.03mg/kg dose nanoconjugate is the most effective at restoring LPN activity with  $2.3\pm 0.9\%$  INT and  $7.9\pm 2.2\%$  MAX LPN recovery

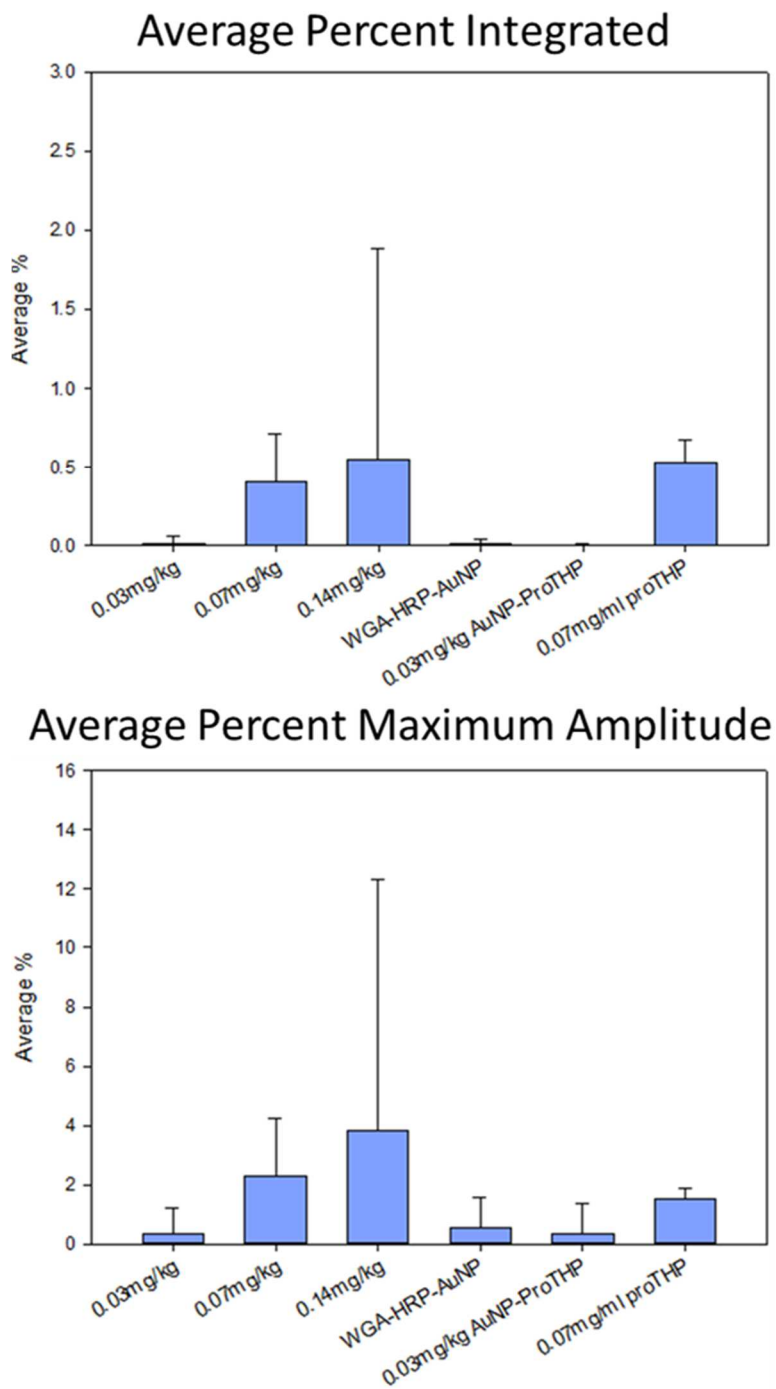


**Figure 42: Comparison of Day 7 Nerve Recordings.** The average percent integrated (top graph) and average percent maximum amplitude (bottom graph). Statistical data consisted of neurograms from 30 rats (Table 7). One-way ANOVA showed no significant drug effect on day 7 for the integrated waveform or the maximal amplitudes.

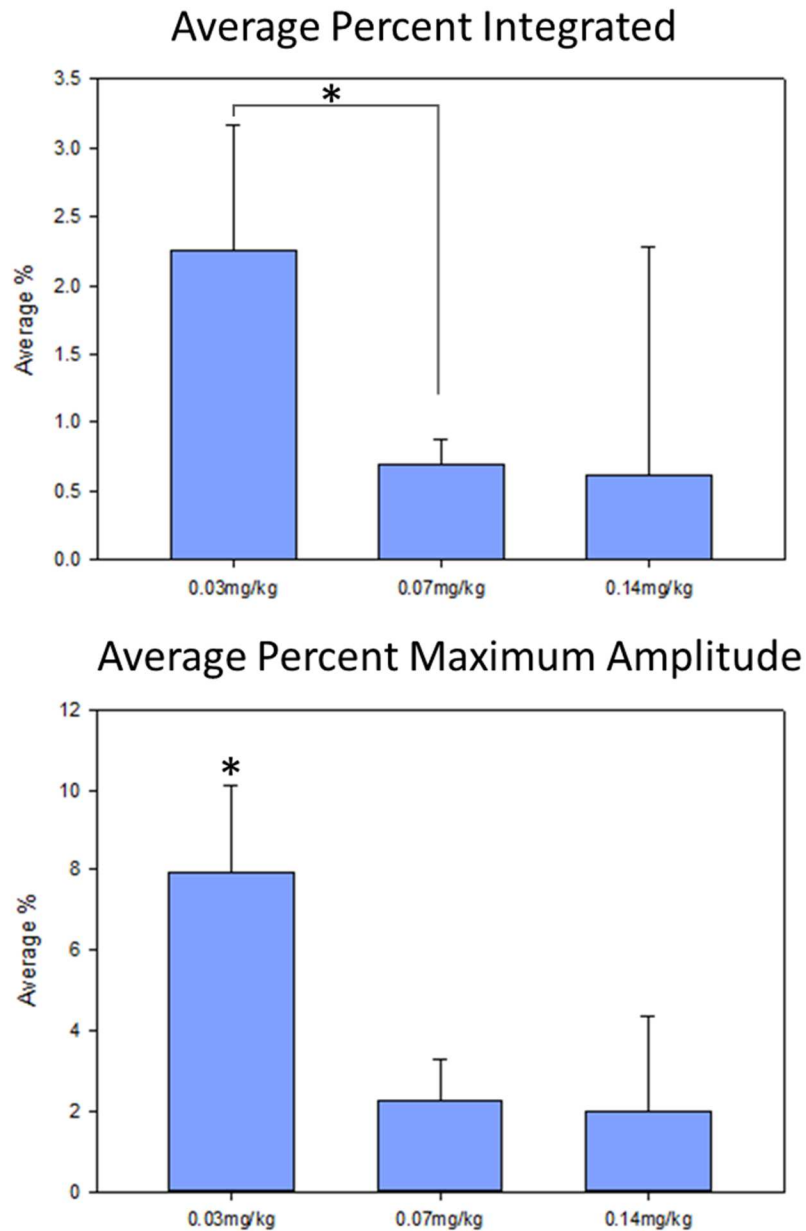


**Figure 43: Comparison of Day 14 Nerve Recordings.** The average percent integrated (top graph) and average percent maximum amplitude (bottom graph). Statistical data consisted of neurograms from 17 rats (Table 8). One-way ANOVA showed significant drug effect on day 14 for the integrated waveform between the 0.03mg/kg dose and the 0.07mg/kg dose ( $p=0.042$ ). There was also significant drug effect for the maximal amplitudes between the 0.03mg/kg dose and the remaining two doses 0.07mg/kg ( $p<0.001$ ) and 0.14mg/kg ( $p<0.001$ ).

Administered Solution	Percent INT	Percent MAX
0.03mg/kg nanoconjugate	0.01±0.04%	0.3±0.9%
0.07mg/kg nanoconjugate	0.4±0.3%	2.3±1.9%
0.14mg/kg nanoconjugate	0.6±1.3%	3.8±8.4%
WGA-HRP-AuNP	0.01±0.02%	0.6±1.0%
0.03mg/kg AuNP-proTHP	0.004±0.01%	0.3±1.0%
0.07mg/kg proTHP	0.5±0.1%	1.5±0.4%

**Table 7: Left phrenic nerve percent recovery on day 7.** The percent integrated (INT) and percent maximum amplitude (MAX) of the left phrenic nerve compared to the right phrenic nerve. Statistical data consisted of neurograms from 30 rats. One-way ANOVA showed no significant drug effect on day 7 for the integrated waveform or the maximal amplitudes.

Nanoconjugate Dose Administered	Percent INT	Percent MAX
0.03mg/kg	2.3±0.9%	7.9±2.2%
0.07mg/kg	0.7±0.2%	2.3±0.9%
0.14mg/kg	0.6±1.7%	1.9±2.4%

**Table 8: Left phrenic nerve percent recovery on day 14.** The percent integrated (INT) and percent maximum amplitude (MAX) of the left phrenic nerve compared to the right phrenic nerve. Statistical data consisted of neurograms from 17 rats. One-way ANOVA showed significant drug effect on day 14 for the integrated waveform between the 0.03mg/kg dose and the 0.07mg/kg dose ( $p=0.042$ ). There was also significant drug effect for the maximal amplitudes between the 0.03mg/kg dose and the remaining two doses 0.07mg/kg ( $p<0.001$ ) and 0.14mg/kg ( $p<0.001$ ).



Based on statistical analysis of the neurograms, both the 0.14mg/kg and 0.03mg/kg doses had a significant drug effect for different time points; day 3, day 14 respectively. This variance may demonstrate the effect of proTHP over time.

To determine the effect of proTHP over time, the neurograms sampled for each dose at the three time points, day 3, 7, and 14, were compared. The 0.03mg/kg dose group had a total of 20 rats. One-way ANOVA showed a significant drug effect on day 14 for both the integrated waveform and the maximal amplitudes  $p < 0.001$  (Fig. 44). This data suggests the dose 0.03mg/kg does not have an immediate effect but is more effective over time.

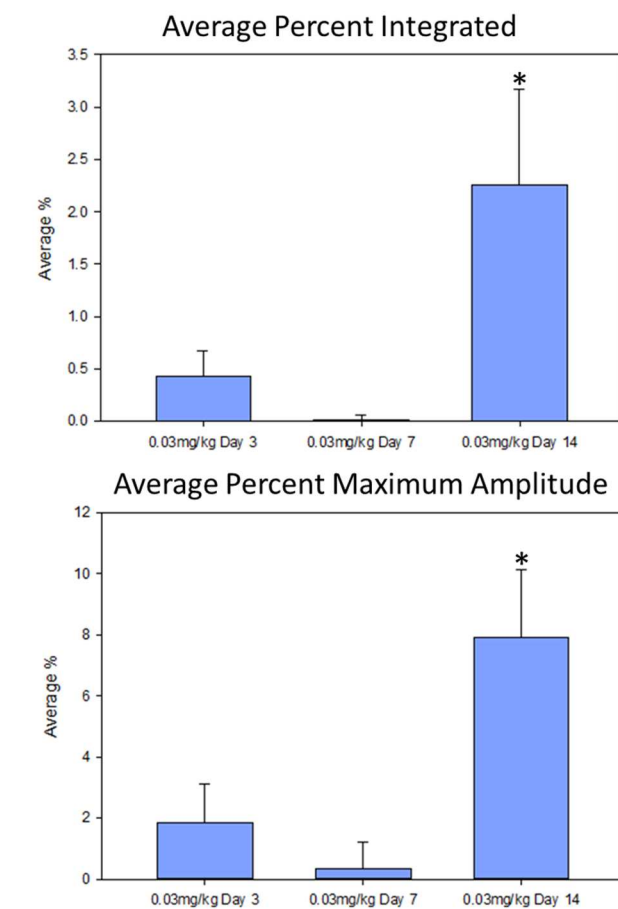


**Figure 44: Dose 0.03mg/kg Nerve Recordings.** The average percent integrated (top graph) and average percent maximum amplitude (bottom graph). Statistical data consisted of neurograms from 20 rats. One-way ANOVA showed significant drug effect on day 14 for both the integrated waveform or the maximal amplitudes  $p < 0.001$ .

The 0.07mg/kg dose group consisted of 14 rats. One-way ANOVA showed significant drug effect for the integrated waveform on day 14 for both the integrated waveform [day 3 vs. day 7 ( $p=0.003$ ); day 3 vs. day 14 ( $p<0.001$ ); day 7 vs. day 14 ( $p=0.014$ )], and the maximal amplitudes [day 3 vs. day 7 ( $p=0.048$ ); day 3 vs. day 14 ( $p=0.003$ )] (Fig. 45). This data suggests the dose 0.07mg/kg, similar to 0.03mg/kg, is more effective over time.

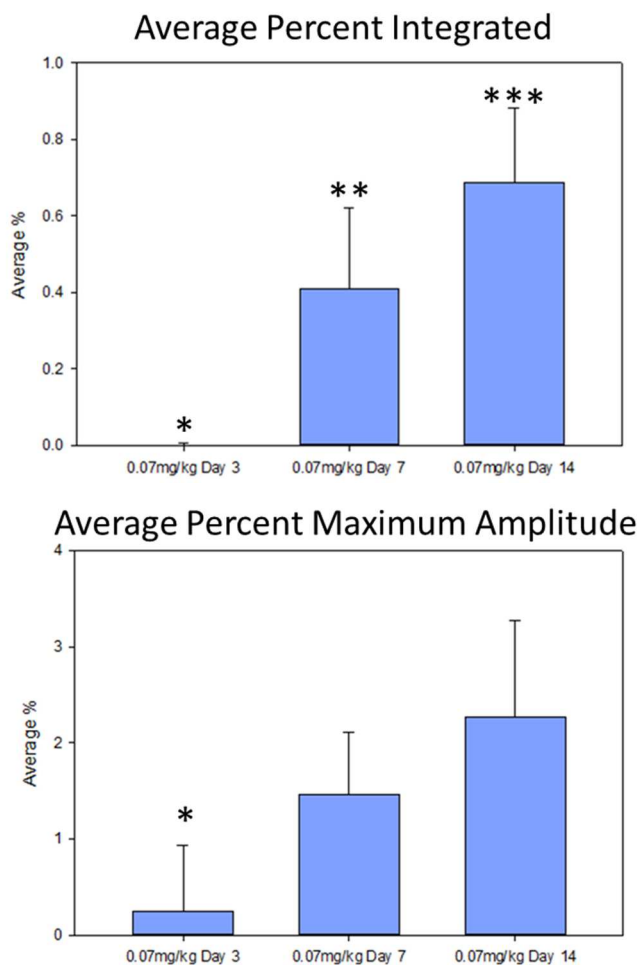


**Figure 45: Dose 0.07mg/kg Nerve Recordings.** The average percent integrated (top graph) and average percent maximum amplitude (bottom graph). Statistical data consisted of neurograms from 17 rats. One-way ANOVA showed significant drug effect for the integrated waveform between all days sampled, day 3 vs. day 7 ( $p=0.003$ ); day 3 vs. day 14 ( $p<0.001$ ); day 7 vs. day 14 ( $p=0.014$ ). The maximal amplitudes showed significance for day 3 only; vs. day 7 ( $p=0.048$ ); vs. day 14 ( $p=0.003$ ).

The 0.14mg/kg dose group consisted of 17 rats. One-way ANOVA showed significant drug effect for the integrated waveform on day 3 for the integrated waveform ( $p < 0.001$ ), but showed no significance for the maximal amplitudes (Fig. 46). This suggests that the 0.14mg/kg dose has an immediate effect that wears off over time. Alternatively, the decrease could be a result of overstimulation appearing as a decrease in LPN activity at the later time points (Nantwi et al, 1996).

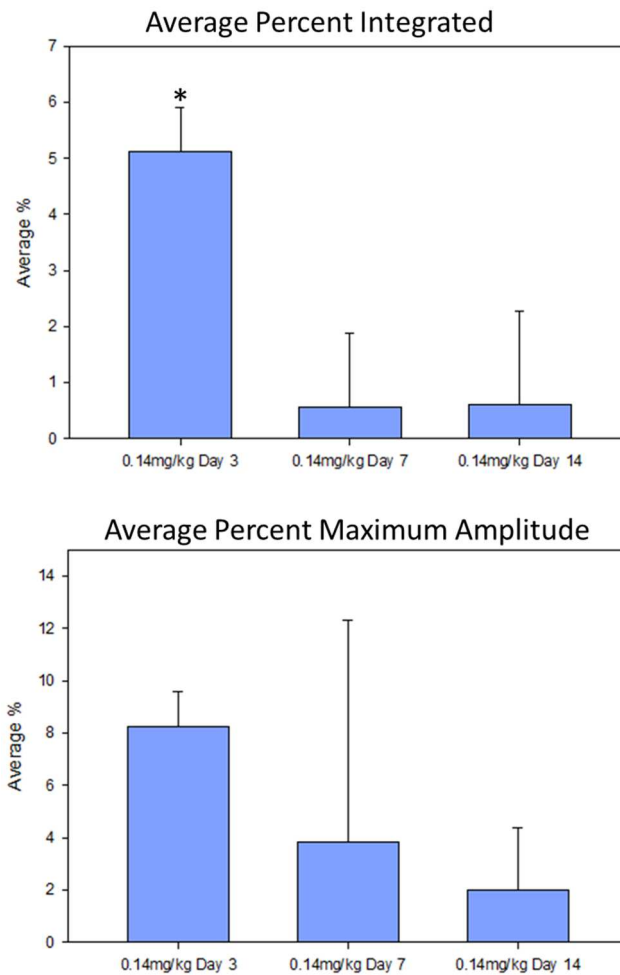


**Figure 46: Dose 0.14mg/kg Nerve Recordings.** The average percent integrated (top graph) and average percent maximum amplitude (bottom graph). Statistical data consisted of neurograms from 17 rats. One-way ANOVA showed significant drug effect for the integrated waveform on day 3 for the integrated waveform ( $p < 0.001$ ), but showed no significance for the maximal amplitudes.

## Discussion

### *Visualization*

WGA-HRP was chosen as the transporter to mediate the selective uptake of the nanoconjugate. This was accomplished by using the unique relationship between WGA and receptors on the phrenic motoneuron axon terminals at the neuromuscular junction. The role of HRP was to provide a method to visualize the WGA-HRP-AuNP component following injection. Unfortunately, the chemical reactions to visualize HRP were inconsistent. There was concern that the amount of HRP in the system was so miniscule, thus creating the challenge to consistently detect HRP. In an effort to amplify the signal, a technique to bind antibodies to the WGA component was implemented. The technique to visualize WGA proved to be stable and reproducible as demonstrated by the study investigating the DPCPX nanoconjugate (Minic et al., 2016). The establishment of a protocol to detect WGA suggests that HRP is dispensable, i.e. it is not important for the uptake of WGA at the phrenic neuromuscular terminals.

In this study, WGA was detected in the ipsilateral phrenic nuclei and bilaterally in the rVRGs on day 3 post nanoconjugate injection. Due to the permanent amide bond between WGA-HRP and AuNP, it is thought that the AuNPs are also located in the ipsilateral phrenic nuclei and bilateral rVRGs. In an effort to determine the AuNPs location(s) post injection, a biodistribution study is currently underway.

At this time, we are unable to visualize the proTHP portion of the nanoconjugate *in vivo*. The ester bond was designed to release proTHP intracellularly, ideally within the phrenic motoneurons and rVRG pre-motor neurons. The presence of proTHP would stimulate these neurons, resulting in recovery of the diaphragm. It has been confirmed in a solution of artificial cerebral spinal fluid, at a 12-hour time point, that the ester bonds are

broken and proTHP has been released. Further studies to detail the release of proTHP, and DPCPX, including release in a solution more similar to the intracellular environment and pH are underway. In addition, a study to identify where in the cell the ester bond is broken is being developed.

Interestingly in comparison to the WGA-HRP-AuNP-proTHP nanoconjugate, the WGA-HRP-AuNP-DPCPX nanoconjugate was also detected bilaterally in the rVRGs but was bilaterally detected in the PN (Minic et al., 2016). This is an interesting finding since both experiments followed the same protocol. At day 7 post injection, the highest average integrated waveform from the proTHP nanoconjugate was  $0.55 \pm 1.3\%$ , whereas the DPCPX nanoconjugate produced a staggering  $56.8 \pm 4.3\%$  recovery. Moreover, on day 14 the proTHP nanoconjugate produced  $2.26 \pm 0.9\%$  LPN recovery compared to the DPCPX nanoconjugate with  $72.4 \pm 7.3\%$  LPN recovery. In the DPCPX study, the presence of WGA in both phrenic nuclei, suggests the DPCPX nanoconjugate has greater mobility. This could play a part in the notable effectiveness of the DPCPX nanoconjugate compared to the proTHP nanoconjugate.

#### *EMG analysis*

The results from EMG analysis demonstrate that all five nanoconjugate doses were able to stimulate recovery of LHD activity detected as early as day 2 post injection and persisted up to 14 days. EMG results suggest the dose  $0.03\text{mg/kg}$  to be most effective as it produced a 65% recovery rate, higher than all remaining doses. Significance of the recovery percent rate was detected in between the nanoconjugate groups, and two of the controls WGA-HRP-AuNP and  $0.03\text{mg/kg}$  AuNP-proTHP. As reported in the results, sporadic (non-phasic) bursts were detected in the  $0.12\text{mg/kg}$  and  $0.14\text{mg/kg}$  groups, a possible effect of over stimulation (Nantwi et al., 1996). In addition, several of the  $0.14\text{mg/kg}$

dose rats presented difficulty when putting them under anesthesia for follow up procedures, often requiring supplemental anesthesia injections before beginning the procedure. Both of these observations suggest that 0.14mg/kg is over stimulating, or hyper-activating, the respiratory system. Following injection of the highest nanoconjugate dose of 0.25mg/kg, recovery was detected in 1 rat out of 7 (14%). The dose 0.25mg/kg resulted in the lowest percent recovery, suggesting a suppression of respiratory system activity when a higher dose of theophylline is administered (Nantwi et al., 1996).

The control solutions, WGA-HRP-AuNP and 0.03mg/kg AuNP-proTHP did not produce LHD recovery in any of the rats tested. It is interesting to note that AuNP-proTHP was unable to produce LHD recovery even though proTHP was present. The explanation behind this remains elusive; one possibility is that without the WGA-HRP, AuNP-proTHP remains within the muscle (extracellularly) until the conjugate is cleared. Remaining in the diaphragm could prevent the degradation of the ester bond which is designed to dissociate proTHP from AuNP in a pH similar to that found intracellularly, which is more acidic than the extracellular environment (Adler et al., 1965; Deutsch et al., 1982).

Interestingly the intradiaphragmatic injection of proTHP dissolved in saline was able to produce diaphragm activity in 40% of the rats, whereas saline alone was not. However, upon further investigation, injecting theophylline into the muscle may provoke a systemic response manifesting in muscle contractions (Bianchi 1961; Isaacson and Sandow, 1967; Kentera and Varagic, 1975; Jones et al., 1982; Creed et al., 1983; Supinski et al., 1984). It is important to point out that drug induced contractions within the diaphragm does not equate phrenic nerve activity. Being able to provoke contractions of the diaphragm following intradiaphragmatic injection of proTHP or the tripartite nanoconjugate highlights the importance of characterizing recovery with EMG *and* phrenic nerve recordings.

### *Bilateral Phrenic Nerve Recordings*

To better understand the effect of the nanoconjugate, quantification of bilateral nerve recordings under standardized conditions were compared between groups. Phrenic nerve recordings detected bilateral phrenic nerve activity in all groups. Beginning with the nerve recordings sampled on day 3, the 0.14mg/kg dose group produced a significantly greater percent recovery for the average percent integrated waveform, and the maximum amplitude. However, the average percent for the 0.14mg/kg integrated waveform was only  $5.12 \pm 0.8\%$  LPN activity compared to the RPN. On day 7, there was no significance detected between experimental and control groups. The 0.14mg/kg group was again the group with the highest integrated waveform, but the day 7 average integrated waveform decreased to  $0.55 \pm 1.3\%$  LPN activity compared to the RPN.

Interestingly on day 14 the 0.03mg/kg dose demonstrated significantly greater percent recovery than the 0.07mg/kg and 0.14mg/kg groups with an integrated waveform of  $2.26 \pm 0.9\%$  LPN activity. The variations of percent recovery for the 3 nanoconjugate doses over the course of the study might demonstrate the effect on respiration as proTHP is metabolized over time. The 0.03mg/kg dose is  $0.4 \pm 0.2\%$  on days 3 and 7, then jumps up to  $2.3 \pm 0.9\%$  on day 14. Similarly, the LPN percent recovery following a 0.07mg/kg dose is barely detectable on day 3, followed by a significant increase in percent recovery that continues to increase up to day 14. Conversely the 0.14mg/kg dose started out strong with  $5.1 \pm 0.8\%$  LPN recovery followed by a significant decline in activity for the remainder of the study. This pattern following the 0.14mg/kg dose, could depict a strong response from the initial proTHP exposure followed by an inhibitory effect in the subsequent days. The inhibition of phrenic nerve activity following a high dose of theophylline has been described

before (Nantwi et al., 1996; Nantwi et al., 2003b). However, this is the first time theophylline appears to stimulate phrenic nerve activity followed by an inhibition of activity.

Considering the results for both the EMG and phrenic nerve recordings following injection of the tripartite nanoconjugate and control solutions; it is possible that recovery following nanoconjugate injection is the result of a systemic effect following intradiaphragmatic injection, an effect of the release of proTHP in the PN and rVRGs following WGA mediated endocytosis, or a combination of both. The rationale behind a systemic effect is based on the observations following injection of the control proTHP in saline that demonstrated a 40% occurrence of LHD recovery detected by EMG, and  $0.5 \pm 0.1\%$  LPN activity compared to the RPN on day 7. The results produced by injection proTHP alone compared to the nanoconjugate at the same 0.07mg/kg dose, 57% occurrence of LHD and  $0.4 \pm 0.3\%$  LPN activity on day 7, suggests the recovery observed following nanoconjugate injection is primarily systemic. Visualization of WGA in the ipsilateral phrenic nuclei and bilaterally in the rVRGs confirms that the WGA component is able to mediate intracellular transport following injection, but the presence of proTHP in these locations are not confirmable at this time.

Regardless of where or how proTHP is acting, a maximum integrated waveform of  $5.12 \pm 0.8\%$  LPN activity following nanoconjugate injection is poor recovery. Fortunately, in addition to theophylline there are multiple drugs known to enhance respiration following high SCI including DPCPX, a specific  $A_1$  adenosine receptor antagonist (Nantwi et al., 1996; Goshgarian and Nantwi, 2001; Kajana and Goshgarian, 2008). As mentioned in the previous section, simultaneous to this study, AuNPs conjugated to WGA-HRP and DPCPX were being investigated. Injection of the DPCPX nanoconjugate produces an average percent recovery of 56.8% on day 7 and 72.4% on day 14 for the integrated waveforms of



the LPN compared to the RPN (Minic et al., 2016). Further investigation into the use of the DPCPX nanoconjugate is underway as results are more promising than those detailed in this study using proTHP.

Lastly, concerns about the high AuNP concentration of the proTHP nanoconjugate, and possible AuNP aggregation preventing endocytosis, has led to an experiment to investigate the rate of recovery following injection of greatly diluted proTHP nanoconjugate solution. If there is an aggregation of AuNPs, preventing the uptake of the nanoconjugate, reducing the concentration would reduce the chance of aggregation. This could increase the WGA mediated uptake, increasing the amount of proTHP exposed to the PN and rVRGs, in turn increasing the percent recovery of the LNP.

#### *Notes on the synthesis of the theophylline nanoconjugate*

Throughout this experiment the complexity of theophylline nanoconjugate synthesis became apparent. In order to bind theophylline to the AuNPs a hydroxymethyl group was added to the theophylline creating proTHP. A short length of time between proTHP synthesis and nanoconjugate synthesis was critical to make a functional nanoconjugate. The final product, proTHP, was originally stored in small vials containing room air. Over time the moisture in the air was able to dissociate the hydroxymethyl group, turning an unknown amount of proTHP back to THP. This dissociation made the chemical reaction to bind proTHP to the AuNPs less effective, resulting in various amounts of proTHP per AuNP. For example, when comparing 2 nanoconjugate batches with thermogravimetric analysis (TGA) a 5.697% weight variance was detected, which is the difference of 105 molecules of proTHP per AuNP and a change in proTHP concentration by 0.22mg/ml. The instability of the hydroxymethyl group made apparent the need to characterize every batch with TGA to verify uniformity and the actual drug concentration. Confirming the drug concentration with

TGA allows the appropriate adjustment in volume to ensure the reported dose is injected. The integrity of post-synthesis (ester) bond stability has been emphasized by others (Duncan and Gaspar, 2011), therefore It was decided to limit the use of the nanoconjugate for no longer than one-month post synthesis. To further protect proTHP, a technique of storing newly synthesized proTHP under a layer of argon gas to block moisture, was implemented. Further investigation into the effects of the proTHP bound nanoconjugate must employ all known methods to stabilize proTHP and must use methods such as TGA to verify the actual nanoconjugate drug load. A consideration for future studies is the use of a hydroxyethyl theophylline, commercially available from Sigma-Aldrich, in place of the hydroxymethyl theophylline synthesized by our collaborators and used in this study. The hydroxyethyl theophylline appears to be more stable than the hydroxymethyl theophylline and could reduce drug load variance complications. Studies are currently underway to determine differences between synthesis and the stability of nanoconjugates synthesized with hydroxyethyl theophylline compared to hydroxymethyl theophylline.

Interestingly the synthesis of the WGA-HRP-AuNP-DPCPX nanoconjugate used in the Minic et al., 2016 study did not encounter the same issues stated above. In comparison to theophylline, DPCPX has an extra 5 carbon ring causing DPCPX to be more hydrophobic, a characteristic that may contribute to the stability of DPCPX during nanoconjugate synthesis.

### **Closing Statement**

WGA-HRP-AuNP-proTHP nanoconjugates are capable of increasing the amount of LPN recovery when injected intradiaphragmatically immediately after C2Hx. Targeting drug delivery, reduces the therapeutic dose from 15mg/kg IV (Nantwi et al., 1996) to less than 0.2mg/kg. In doing so the restored left hemidiaphragm and left phrenic nerve function can

be detected as early as day 2 and persists up to day 14 post injection. However, the WGA-HRP-AuNP-proTHP nanoconjugate used in this study fails to induce the amount of recovery following the administration of the WGA-HRP-AuNP-DPCPX nanoconjugate (Minic et al., 2016).

Lastly, the application of the WGA-HRP-AuNP nanoconjugate is not limited to the phrenic motor system. WGA-HRP has been utilized for decades to identify neuromuscular pathways. In theory, injection of the WGA-HRP-AuNP nanoconjugate bound to a variety of substances could hold promise for applications in multiple disease and injury models.

### **CHAPTER 3: APPLICATION OF THE THEOPHYLLINE BOUND NANOCONJUGATE IN THE CHRONICALLY INJURED SPINAL CORD MODEL**

#### **Summary**

The chronically C2Hx rat exhibits injury induced plasticity of physiologically active synapses in the spinal cord and medullary respiratory centers. Over time, synaptic plasticity results in multiple connections to numerous nuclei in addition to those identified in the acute C2Hx model as demonstrated by WGA-Alexa 488 labeling (Buttry and Goshgarian, 2014). Due to the retrograde transsynaptic transport of WGA, following intradiaphragmatic injection, the nanoconjugate is expected to deliver the drug to the additional nuclei identified in the chronically C2Hx model. Following nanoconjugate injection, a variable effect in the descending respiratory drive was observed. However, the full effect of the proTHP bound nanoconjugate in the chronically C2Hx model remains uncertain due to the complex environment post injury and variability between individuals.

#### **Introduction**

Of the estimated 276,000 people living in the United States only 4.5% (12,500 people) are people with new injuries, meaning the vast majority have a chronic injury (NSCISC, 2015). In order for a drug therapy to be considered clinically, administration in chronically injured individuals must be considered as well as in the acutely injured. In this study chronically injured rats were defined as 12 weeks post C2Hx. This time frame provided an adequate recovery period for the central nervous system in the rat C2Hx injury model to adapt to the SCI (Nantwi et al., 1999; Golder et al., 2001b; Nantwi et al., 2003a; Fuller et al., 2008; Buttry and Goshgarian, 2014). It is well known that in the chronically C2Hx injury model the respiratory pathway, as well as accessory pathways discussed in Chapter 1, are in a hyperactive state (Goshgarian, 1979). This is critical information since the therapeutic dose (15 mg/kg theophylline, systemically administered) that stimulates

phrenic nerve activity in the acutely C2Hx rat has been shown to *inhibit* phrenic motor output when administered to the chronically C2Hx rat (Nantwi et al., 2003a). Moreover, reducing the dose in the chronically C2Hx rats to 5 mg/kg or 2.5 mg/kg also inhibit phrenic nerve output or have no effect (Nantwi et al., 2003a).

To characterize functional recovery in the chronically C2Hx rats following nanoconjugate injection, EMG analysis and phrenic nerve recordings were used as described in Chapter 2 (see methods for additional details). In previous studies spontaneous functional recovery of the diaphragm has been documented following C2Hx (Nantwi et al., 1999; Golder et al., 2001; Nantwi et al., 2003a; Fuller et al., 2008). However, based on the method of measurement, the time frame in which the spontaneous recovery occurs varies. In the Chapter 1 chronic studies, EMG recordings immediately prior to intradiaphragmatic tracer injections indicated spontaneous functional recovery of the diaphragm in 62% of the rats at the time point of 7 weeks post C2Hx or more. Also demonstrated in the Chapter 1 studies, in chronically injured rats, there is a change in the physiologically active synapses temporally associated with the activation of the diaphragm following a C2Hx based on the change in pattern of WGA-Alexa 488 labeling following intradiaphragmatic injection. In this study the nanoconjugate was applied to the chronic C2Hx injury model with the expectation of WGA mediated transport of the nanoconjugate to the nuclei observed in the Chapter 1 chronic C2Hx injury model. Plasticity of physiologically active synapses in the chronically C2Hx system has the potential to change the distribution of the nanoconjugate due to the properties of WGA receptor mediated transsynaptic transport. The change in proTHP distribution could induce recovery following 12 weeks post C2Hx or strengthen the spontaneously developed recovery. In contrast, the

nanoconjugate could have an inhibitory effect similar to systemic administration, blocking the descending drive in chronic C2Hx rats as demonstrated by Nantwi et al., 2003a.

### **Physiological response to WGA-HRP-AuNP-proTHP**

The chronic study was comprised of data from 27 C2Hx rats. After a 12-week recovery period all rats underwent a second EMG to test for spontaneous recovery prior to the injection of nanoconjugate. See methods for details.

Each rat underwent an EMG 3 to 6 days following nanoconjugate injection. Based on the EMG results, each rat was placed into a “Recovery/Improvement” or “No change/Loss” category. Recovery was defined as a return of diaphragm activity when prior to nanoconjugate injection there was a complete absence of diaphragm activity, i.e. no spontaneous recovery. An improvement upon spontaneous recovery was defined as activity appearing in 1 or more of the 3 diaphragm areas in addition to spontaneous activity. No change was defined as no observable activity regained in 1 or more of the 3 areas following injection. Lastly, a loss was defined as a loss of spontaneous activity in 1 or more of the 3 areas of the diaphragm following nanoconjugate injection. Five of the 12 rats (41.67%) resulted in improvement following injection of the nanoconjugate at the dose 0.07mg/kg. In an effort to increase the amount of rats that exhibited improvement following nanoconjugate administration, the dose was lowered to 0.06mg/kg. However, 0.06mg/kg resulted in improvement in 1 of 5 rats (20%). The last group to be tested received a dose of 0.02mg/kg, and resulted in improvement in 3 of 16 (18.75%). Similar to the EMG analysis in Chapter 2, the *occurrence* of “Recovery/Improvement” or “No change/Loss” were compared to determine the dose that produced the most recovery or improved upon existing spontaneous recover, however no significance was detected (Fig. 47).

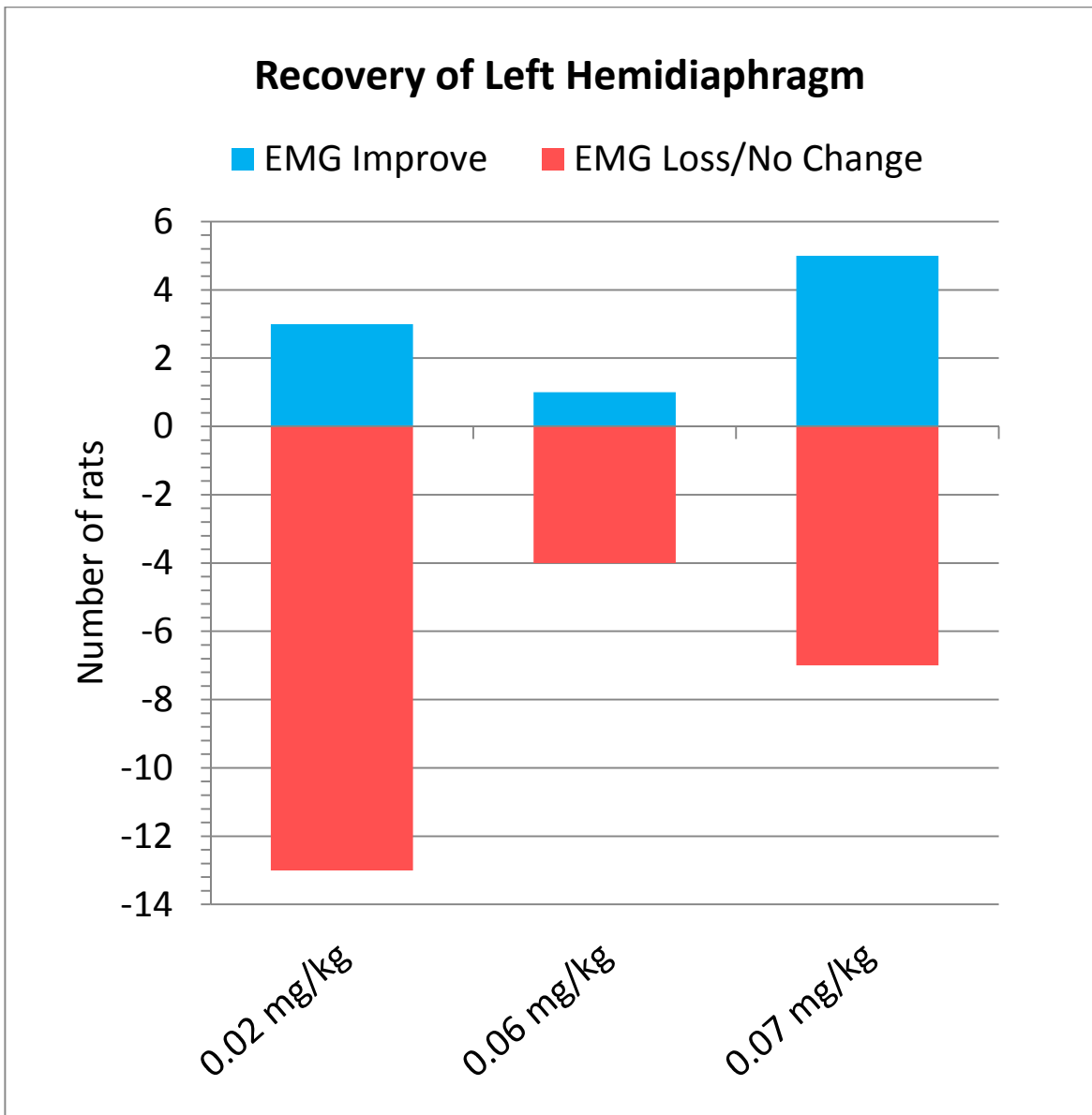


**Figure 47: Chronic C2Hx model EMG response to nanoconjugate dose.** At 12 weeks post C2Hx three groups were created based on the nanoconjugate dose injected: 0.02mg/kg (N=16), 0.06mg/kg (N=5), and 0.07mg/kg (N=4). Each rat underwent a second EMG in the days following injection. In the above graph groups are sub-divided into a “Recovery/Improvement” or “No change/Loss” category based on return of function or an improvement of spontaneous activity or no change or a loss of spontaneous activity. The percent of recovery/improvement for the three nanoconjugate doses were compared, no significance was found suggesting that proTHP has no effect on chronic animals.

Bilateral phrenic nerve recordings were sampled at 13 weeks (day 7 post nanoconjugate injection). Groups were compared to determine the dose that produced the most recovery or improvement upon existing spontaneous recovery; 0.02mg/kg (N=10), 0.06mg/kg (N=3), and 0.07mg/kg (N=3). One-way ANOVA with Holm-Sidak pairwise comparison showed a significant dose effect between the groups ( $p < 0.001$ ). Pairwise comparison showed significance between the 0.06mg/kg dose and the remaining two doses, 0.02mg/kg and 0.07mg/kg for both the integrated waveform ( $p < 0.001$ ) and maximal amplitudes ( $p < 0.001$ ) (Fig. 48). This suggests that on day 7 post nanoconjugate injection the 0.06mg/kg dose produces a higher percentage of left phrenic nerve activity than the remaining two doses.

#### **Influence of spontaneous activity on recovery**

At 12 weeks post C2Hx, 22 of the 27 rats had spontaneous activity, prior to nanoconjugate injection, detected by EMG. The WGA component of the nanoconjugate is activity dependent and requires muscle activity of the diaphragm to undergo receptor mediated endocytosis. Rats that had spontaneous activity prior to injection at 12 weeks post C2Hx could have an advantage over rats with no spontaneous activity. Interestingly analysis of the occurrence of "Recovery/Improvement" vs. "No change/Loss" based on EMG recordings showed no significance for all 3 doses; 0.02mg/kg, 0.06mg/kg, and 0.07mg/kg. However, the data from the phrenic nerve recordings revealed that the 0.2mg/kg dose group showed significance with the One-way ANOVA with Holm-Sidak pairwise comparison ( $p < 0.001$ ) for the integrated waveform ( $p < 0.001$ ), but not for the maximal amplitudes ( $p = 0.003$ ) (Fig. 49).



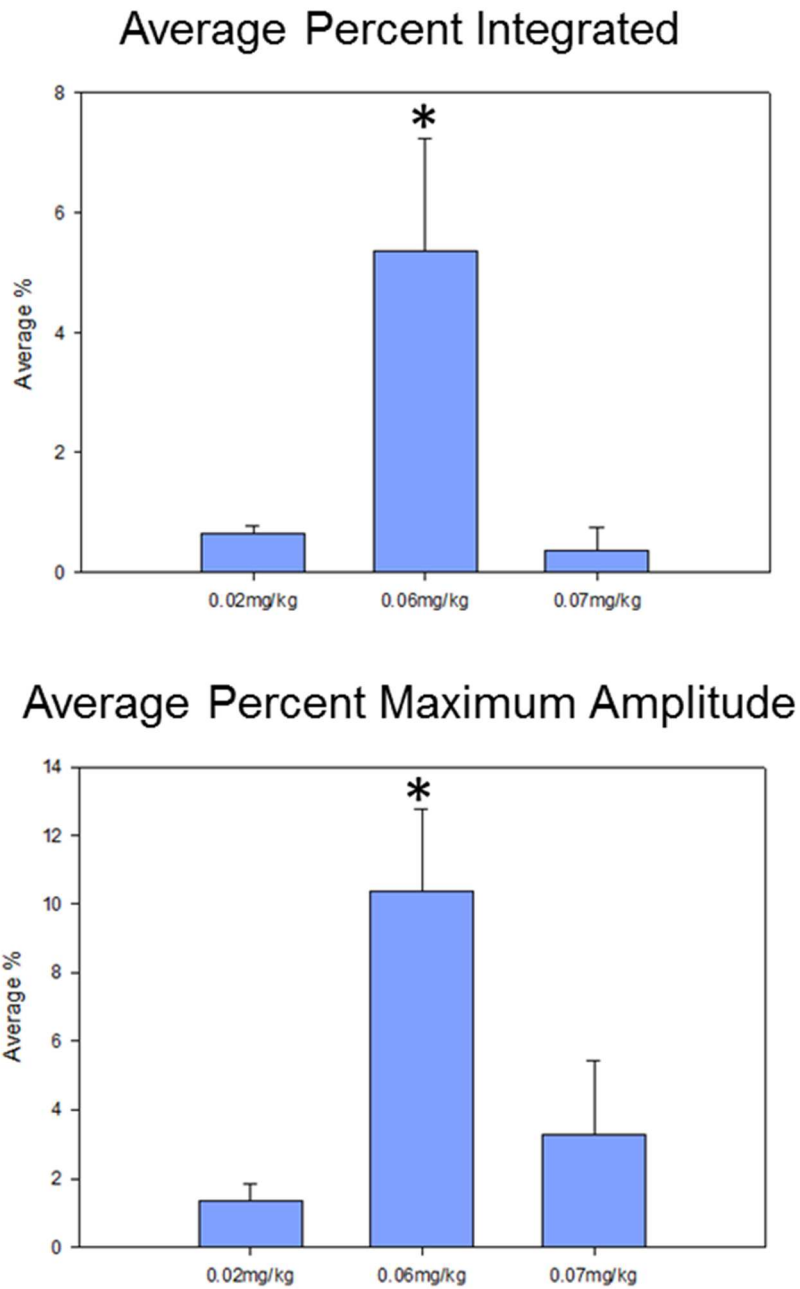


**Figure 48: Nerve recording dose comparison in chronically C2Hx.** Comparison of the average percent integrated (top graph) and average percent maximum amplitude (bottom graph) for the chronic groups. Statistical data consisted of neurograms from 17 rats. One-way ANOVA with Holm-Sidak pairwise comparison showed significant dose effect between the groups ( $p < 0.001$ ). Pairwise comparison showed significance between the 0.06mg/kg dose and the remaining two doses, 0.02mg/kg and 0.07mg/kg for both the integrated waveform ( $p < 0.001$ ) and maximal amplitudes ( $p < 0.001$ ).

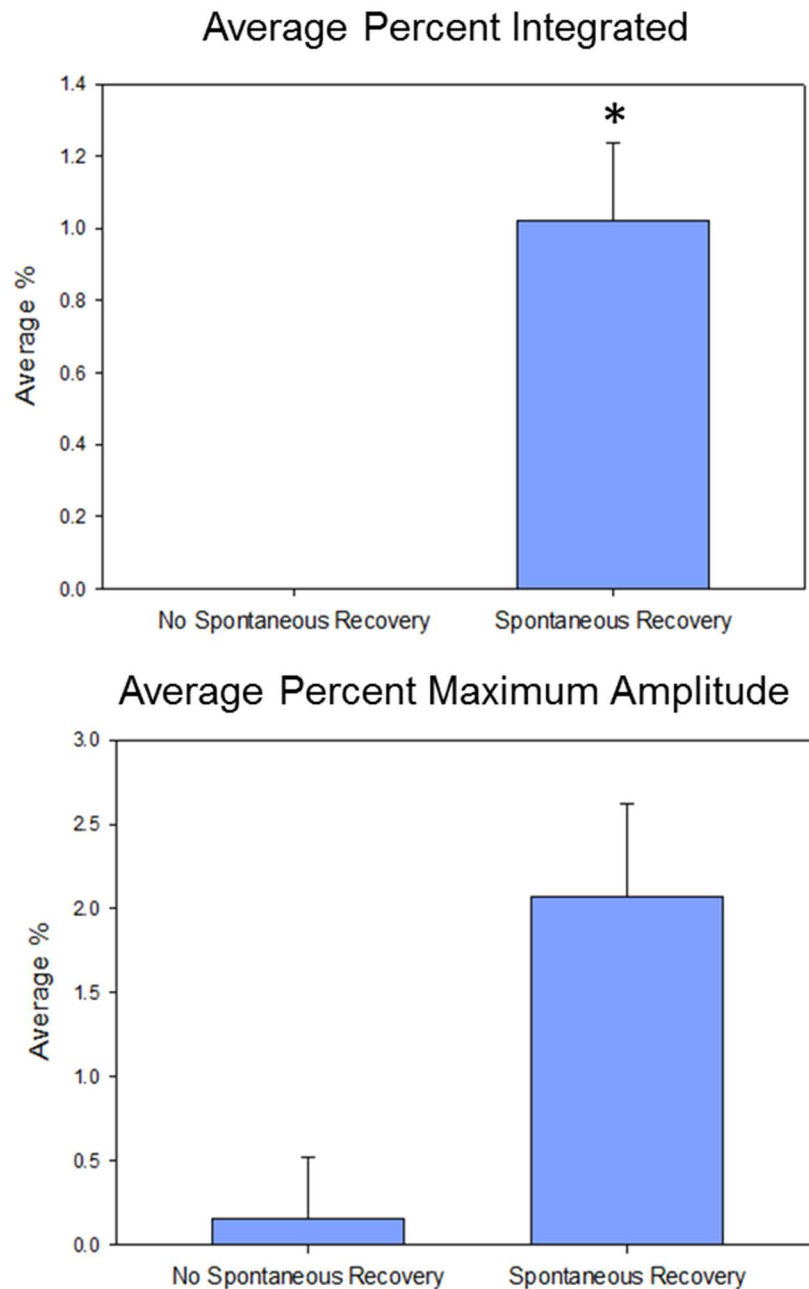


**Figure 49: Effect of spontaneous recovery on nerve recordings in nanoconjugate injected chronically C2Hx rats.** Comparison of the average percent integrated (top graph) and average percent maximum amplitude (bottom graph) for the chronic group that received the 0.02mg/kg dose. Statistical data consisted of neurograms from 8 rats. One Way ANOVA with Holm-Sidak pairwise comparison showed significant effect between rats with spontaneous recovery vs. those with no spontaneous recovery ( $p < 0.001$ ). Pairwise comparison showed significance between groups for the integrated waveform ( $p < 0.001$ ), but not for the maximal amplitudes ( $p = 0.003$ ).

## Discussion

Application of any drug intended to increase respiratory drive following SCI must be characterized in both the acute and chronically injured systems. There are numerous differences in the spinal cord and medulla following injury including changes in cell to cell connections (Lane et al., 2009; Buttry and Goshgarian, 2014) and how respiration reacts to drug intervention (Nantwi et al., 2003a). Plasticity of physiologically active synapses in the chronically C2Hx system, as discussed in Chapter 1, has the potential to change the distribution of the nanoconjugate due to the properties of WGA receptor mediated transsynaptic transport (Buttry and Goshgarian, 2014). Qualitative analysis of the occurrence of recovery or improvement upon spontaneous recovery following nanoconjugate injection produced no significance between the doses injected. However quantitative analysis of phrenic nerve recordings reported a significant increase in the amount of left phrenic nerve (LPN) activity following injection of the 0.06mg/kg dose compared to 0.02mg/kg and 0.07mg/kg. In addition, chronic rats that had spontaneous activity as determined by EMG analysis at 12 weeks post-op followed by injection of 0.02mg/kg had a significant increase in the amount of LPN activity compared to rats without spontaneous activity at 12 weeks post-op followed by injection of 0.02mg/kg nanoconjugate. This suggests that the amount of activity present prior to injection may influence the effectiveness of the activity dependent WGA mediated endocytosis. Increased WGA mediated endocytosis of the nanoconjugate would increase the targeted release of proTHP, resulting in a higher delivered drug concentration.

The chronic results suggest that the targeted drug delivery nanoconjugate based approach can be applied to the chronic system to stimulate LPN activity. The chronic study consisted of 27 rats and just scratched the surface of the work required to fully characterize

the nanoconjugate in the chronically injured system. Further investigation of the doses reported in this study as well as control solutions are needed to move forward with chronic applications.

## OVERALL SUMMARY

The studies presented in Chapter 1 examined the respiratory pathways prior to and after a cervical SCI. First, utilizing the selective, activity dependent uptake of WGA (Harrison et al., 1984, 1986; Jankowska, 1985; Schwab et al., 1979), spinal cord and brain stem nuclei were identified with a fluorescent neuronal tracer, WGA-Alexa 488. WGA-Alexa 488 has an advantage over the traditionally used WGA-HRP since the Alexa 488 portion is readily identified with fluorescent microscopy. Eliminating the need for chemical reactions to visualize HRP has provided a method to visualize the neurons responsible for diaphragm activity while maintaining the integrity of the tissue for further biochemical or molecular analysis.

Injection of WGA-Alexa 488 into the ipsilateral hemidiaphragm following a C2Hx resulted in bilateral labeling of the phrenic motoneurons in the cervical spinal cord as well as the premotor rVRG neurons in the medulla. However, following WGA-Alexa 488 exposure to the isolated ipsilateral phrenic nerve following a C2Hx, labeling was only identified in the ipsilateral phrenic nuclei. This observation suggests that WGA-Alexa 488 must be exposed to the phrenic axon terminal at the neuromuscular junction in order for transsynaptic transport to occur.

Once the labeling properties of WGA-Alexa 488 were identified and found to be reproducible in the acute C2Hx model, the tracer was then characterized in the chronically injured system. Following a C2Hx, the ipsilateral diaphragm is paralyzed with the exception of intermittent activity stimulated by the crossed phrenic pathway (CPP). Over time the diaphragm can regain phasic activity, this is referred to as spontaneous recovery (Nantwi et al., 1999). Since the CPP circuitry is already in place, it would seem that spontaneous recovery is a result of strengthening the CPP. To determine the nuclei associated with

spontaneous recovery, rats underwent a C2Hx followed by a 12-week recovery period. At 12-weeks WGA-Alexa 488 was injected into the ipsilateral hemidiaphragm. Interestingly not only was WGA-Alexa 488 identified bilaterally in the phrenic nuclei and the rVRGs but was also identified in numerous spinal cord and brain stem nuclei. The change in labeling demonstrates injury induced plasticity following SCI. Many of the labeled nuclei have been linked to respiration as motor nuclei for accessory respiratory muscle, or nuclei that help regulate and coordinate respiration with body functions. Therefore, the presence of WGA-Alexa 488 in the nuclei (forelimb motoneurons, RST, DSCT, and VSCT) unique to the chronically injured model is likely caused by hyperactivity of existing pathways. WGA-Alexa 488 labeling in the medulla for the acutely C2Hx and chronically C2Hx were strikingly different. The acutely C2Hx rats displayed WGA-Alexa 488 labeling isolated to the rVRGs. However, the chronically C2Hx rats, in addition to the rVRGs, displayed labeling in the raphe, hypoglossal, spinal trigeminal, parvicellular reticular, gigantocellular reticular, and intermediate reticular nuclei. All of these have been previously demonstrated, using alternative tracers, to be associated with respiratory control in acutely hemisected or non-injured rats. It is important to point out that WGA-Alexa 488 only labels these nuclei in the chronically injured system. This further emphasizes the selective activity-mediated uptake of WGA bound conjugates.

Similar to the chronically C2Hx rats, the sham C2Hx rats also displayed bilateral WGA-Alexa 488 labeled interneurons primarily in laminae VII and VIII of the cervical and thoracic cord and bilateral labeled intercostal motoneurons in the thoracic spinal cord. These results imply that the sham C2Hx surgery including laminectomy of C2, durotomy, and laparotomy had an impact on the spinal cord environment. Interestingly, the supraspinal nuclei appeared unaffected by the sham C2Hx and presented WGA-Alexa 488 labeling

indistinguishable from the acute C2Hx rats. Thus, we can conclude that hemisection of the spinal cord induces changes in the supraspinal circuitry. The use of WGA-Alexa 488 as a neuronal tracer to detect changes in physiologically active synapses post injury proves to be a valuable tool to identify areas of injury induced plasticity.

In the last study of Chapter 1, WGA-Alexa Fluorochromes were administered to acutely C2Hx and non-injured rats by intradiaphragmatic and intrapleural injections. Intrapleural injections were investigated as an alternative method to the invasive procedure required to administer intradiaphragmatic injections. Following intrapleural injection, the PN, intercostal SC nuclei, rVRGs, and unexpectedly the nucleus ambiguus (NA) were all bilaterally labeled. A direct connection from the NA to the PN has yet to be defined, suggesting that WGA-Alexa fluorochromes are capable of undergoing transsynaptic transport across at least 2 synapses. This finding is of interest especially in respect to the application of WGA-Alexa in the chronically injured system. Understanding the order of activation may help determine the role each nuclei plays in spontaneous recovery. The availability of neuronal tracers capable of crossing one, multiple, select, or all synapses allows investigators to implement these techniques to ask questions related to neuronal synapses and changes following injury and treatment.

In the final two chapters, following an acute or chronic SCI, a novel nanoconjugate was administered to stimulate activation of the phrenic nuclei and diaphragm. Following a C2Hx there is a loss of ipsilateral hemidiaphragm function. In the rodent injury model adenosine antagonists, such as theophylline, are able to stimulate the functionally latent CPP and restore hemidiaphragm function. However, in humans the therapeutic dose of theophylline results in hyperactivity of many non-target nuclei. To reduce the administered dose, theophylline was conjugated to the neuronal tracer WGA-HRP, using a gold

nanoparticle (AuNP) as a coupler. Following intradiaphragmatic injection of the tripartite nanoconjugate, WGA-HRP is expected to mediated endocytosis at the axon terminal of phrenic motoneurons. Once the nanoconjugate is endocytosed, the transient ester bond linking the drug to the AuNP is degraded, freeing the drug. By targeting the drug to only the neurons associated with diaphragm function, the dose needed to stimulate hemidiaphragm activity is greatly reduced.

To investigate the effectiveness of the tripartite nanoconjugate in the acutely injured system, rats were subjected to a C2Hx followed by intradiaphragmatic injection of the theophylline bound nanoconjugate. Although the nanoconjugate was able to induce recovery at the level of the phrenic nerve and the diaphragm, the amount of recovery was rather small with a maximum average percent recovery of  $5.12 \pm 0.8\%$ .

It is known that the nanoconjugate is able to undergo receptor mediated endocytosis, due to identification of the WGA portion of the nanoconjugate post injection in the phrenic nucleus and rVRGs. However, the amount of nanoconjugate uptake needs to increase. Several areas for improvement have been identified, including the injection of a diluted nanoconjugate solution to determine if aggregation of the AuNPs are creating an issue with uptake. These studies are planned and are not within the scope of this dissertation. Regardless of the complications with the theophylline version of the nanoconjugate, it is still important to point out that the nanoconjugate is capable of undergoing WGA mediated endocytosis followed by transsynaptic transport. There are numerous options as to what drug can be bound to the AuNPs. For example, replacing proTHP with DPCPX induces a superior recovery of LPN activity.

Lastly, the final chapter examines the application of the tripartite nanoconjugate in the chronically C2Hx rat model. The WGA-Alexa 488 chronic study provided an



exceptionally detailed anatomical picture of the spinal and supraspinal nuclei that undergo injury induced plasticity and synaptic activity modification. Based on WGA mediated uptake, the nanoconjugate is expected to undergo transport to the nuclei identified with WGA-Alexa 488 in the chronic C2Hx model. The chronically injured system has remained challenging to work with and responds differently to drugs than the acutely injured system (Nantwi et al., 2003a). The 0.06mg/kg dose showed a significant effect over the remaining two doses based on phrenic nerve recordings. However, rats with spontaneous recovery of the diaphragm also showed a significant advantage over those with no spontaneous recovery when comparing the average percent integrated waveforms. Endocytosis of WGA has been shown to be activity dependent. Thus suggesting rats exhibiting spontaneous recovery following chronic injury would have enhanced transport of the nanoconjugate, increasing drug exposure. Application of the tripartite nanoconjugate in the chronically injured system requires additional in-depth investigations to fine tune the drug dose, AuNP concentration, and alternative drugs. With these findings, utilizing WGA to selectively deliver drugs has potential clinical applications to increase respiratory output following SCI.

These studies show that WGA is able to selectively transport WGA-bound conjugates, specifically Alexa fluorochromes and drug bound AuNPs, to nuclei that regulate diaphragm function in the non-injured and acutely and chronically C2Hx rat models. In addition to the respiratory motor pathway, WGA has been investigated in numerous neuronal pathways. The findings presented here, have the potential for applications in any system demonstrated to facilitate the selective uptake of WGA.

## **MATERIALS AND METHODS**

### **Animal Use**

Adult male Sprague Dawley rats were used in these studies. All animal studies were approved by the Wayne State University School of Medicine Institutional Animal Care and Use Committee.

### **Second Cervical Segment Spinal Cord Hemisection (C2Hx)**

All rats were injected with atropine sulfate (0.04mg/kg, im) 10 minutes prior to anesthesia induction to reduce mucus secretions during the subsequent aseptic survival surgery. Anesthesia was a mixture of ketamine (70mg/kg, ip) and xylazine (7mg/kg, ip). After anesthesia induction, bupivacaine (2mg/kg, sc) a local anesthetic was injected into the dorsal neck. The dorsal aspect of the neck was shaved and prepared for aseptic surgery. An incision was made on the dorsal neck to expose the second cervical vertebra (CV2). The paravertebral muscles were cut and retracted along the midline axis. All muscle attachments to CV2 were cut to expose the spinous processes, laminae, and the intervertebral space between CV1/CV2 and CV2/CV3. A bilateral laminectomy was completed at the level of CV2 to expose the spinal cord. A durotomy was performed with spring micro-scissors. After locating the C2 and C3 dorsal roots, the left half of the spinal cord was cut just to the left of midline and continued to the lateral aspect of the cord caudal to the C2 dorsal root. Care was taken to avoid cutting the large dorsal blood vessel that typically courses along the midline of the spinal cord. The location of the hemisection also avoids the anterior spinal artery on the ventral aspect of the spinal cord. The functional completeness of the injury was confirmed with EMG of the diaphragm (see EMG Analysis). The dorsal neck muscles were closed using 4-0 absorbable sutures (Vicryl, Ethicon) followed by wound clips (Reflex® 9mm) for the skin. Following the cleaning of the cervical

incision, the rats were injected with Buprenorphine (0.01mg/kg, sc) in 10ml saline for pain control and yobine (2mg/kg, ip) to reverse xylazine. The following 48 hours, post-operative rats were given additional injections of Buprenorphine (0.01mg/kg, sc) every 8-12 hours for pain management. The rats recovered on a heating blanket on their back to limit pressure on the diaphragm. When the rats were able to ambulate, they were returned to clean litter-lined cages with food and water provided ad libitum on the floor of the cage to minimize neck movement during recovery. The rats were also given peanut butter and cereal as an enticement to eat.

### **Sham Second Cervical Segment Spinal Cord Hemisection**

Rats underwent an identical hemisection surgical procedure described above up to and including the durotomy, but the spinal cord was not cut.

### **Electromyography Analysis**

Immediately following the left C2Hx or sham C2Hx, paralysis of the ipsilateral hemidiaphragm was confirmed by EMG analysis. The abdominal surface of the diaphragm was exposed by a 6-8 cm horizontal incision made approximately 0.5 cm caudal and parallel to the costal margin. Bipolar platinum wire electrodes (Grass F-E2) were inserted intramuscularly within each side of the diaphragm to detect muscle activity. Signals were amplified (20,000X) and band pass-filtered (30Hz-3kHz) by Grass amplifiers (model P511 AC, Astro-Med, Inc., West Warwick, RI) and raw EMG signals were recorded by a Cambridge Electronic Design (CED, Cambridge, England) data acquisition system integrated with CED Spike 2® software. Recordings were taken from three areas of the left hemidiaphragm: anterior (sternal), lateral (costal) and posterior (crural). Only rats that showed a complete absence of activity in all three areas were included in the study.

In all chronic rats a second EMG to test for spontaneous recovery was assessed immediately prior to the injection of WGA-Alexa fluor conjugates, nanoconjugate, or control solutions.

Rats that received a nanoconjugate or control solution were assessed with EMG analysis an additional 1-3 times depending on the length of the experiment. All subsequent EMG recordings were performed under ketamine/xylazine anesthesia while spontaneously breathing.

Following the EMG, the abdominal cavity was closed using 4-0 absorbable sutures (Vicryl, Ethicon) followed by wound clips (Reflex® 9mm) for the skin. Postoperative care for the first 48 hours was identical to the care described above after C2Hx.

### **Acute Studies**

Acute is defined as up to 14 days following SCI. Dependent on the study, rats survived a minimum of 48 hours or up to 14 days.

### **Chronic Studies**

Hemisected rats recovered for a period of at least 7 weeks with no intervention with respect to respiratory function. Several rats required medical attention for issues such as wounds associated with the incision site or eye, or autophagy of the right hind paw. When needed and as prescribed by the veterinarian, topical application of triple antibiotic ointment, silver sulfadiazine, or Columbia powder was used to manage wounds. In addition, Buprenorphine (0.01mg/kg, sc) or Carprofen (5mg/kg, sc) was administered for pain management. To prevent autophagy of the right rear paw a topical mixture of New Skin and metronidazole (500mg/mL MP Biomedicals 0215571005) was applied to the right rear paw weekly (Zhang et al., 2001). Prior to implementing the topical paw treatment, several rats had to be euthanized prior to completion of the study due to the severity of rear paw wounds.

### **Intradiaphragmatic injections of WGA-Alexa fluor conjugates**

Intradiaphragmatic injections of WGA-Alexa fluor conjugates were administered; i) following a laparotomy to expose the abdominal surface of the diaphragm (non-injured), ii) following EMG confirmation of hemidiaphragm paralysis (acutely injured), iii) following an EMG at 12 weeks post C2Hx (chronically injured). All injections were administered using a 28 gauge Hamilton syringe (catalog # 7637-01, and # 7803-02). Rats were injected with either 2% WGA- Alexa 594 (Life Technologies Cat. # W11262) saline solution or 2% WGA-Alexa 488 (Life Technologies Cat. # W11261) in saline solution into the left hemidiaphragm. A total of 50µl was administered to each rat in 10µl increments. The amount of tracer injected was based on a previous study (Moreno et al., 1992) which determined that five 10µl injections distributed from the anterior to posterior region of the hemidiaphragm were sufficient to label the phrenic nucleus that spans the C3-C6 segments of the cervical spinal cord. All rats were sutured as described in the EMG analysis section and survived for 48 hours.

### **Intradiaphragmatic injections of nanoconjugate or control solutions**

A detailed description of the synthesis of the proTHP nanoconjugates can be found in the following manuscript: “Transporter protein and drug-conjugated gold nanoparticles capable of bypassing the blood-brain barrier” Zhang et al., 2016. Intradiaphragmatic injections of the nanoconjugate or a control solution; i) WGA-HRP-AuNP, ii) AuNP-ProTHP, iii) ProTHP were administered following EMG confirmation of hemidiaphragm paralysis (acutely injured), or following an EMG at 8-12 weeks post C2Hx (chronically injured). All injections were administered using a 28 gauge Hamilton syringe (catalog # 7637-01, and # 7803-02). The total volume of the solution injected was weight based and dependent on the concentration of the drug in the solution. Volume of the control solutions were calculated

identical to the drug based solutions to eliminate variance based on volume. All solutions were injected in 10 $\mu$ l increments or less and were distributed from the anterior to posterior region of the hemidiaphragm (Fig. 50). Following injection, the needle was slowly retracted to prevent any leaks at the injection site. Rats survived for 3-14 days depending on the timeline for each experimental group.

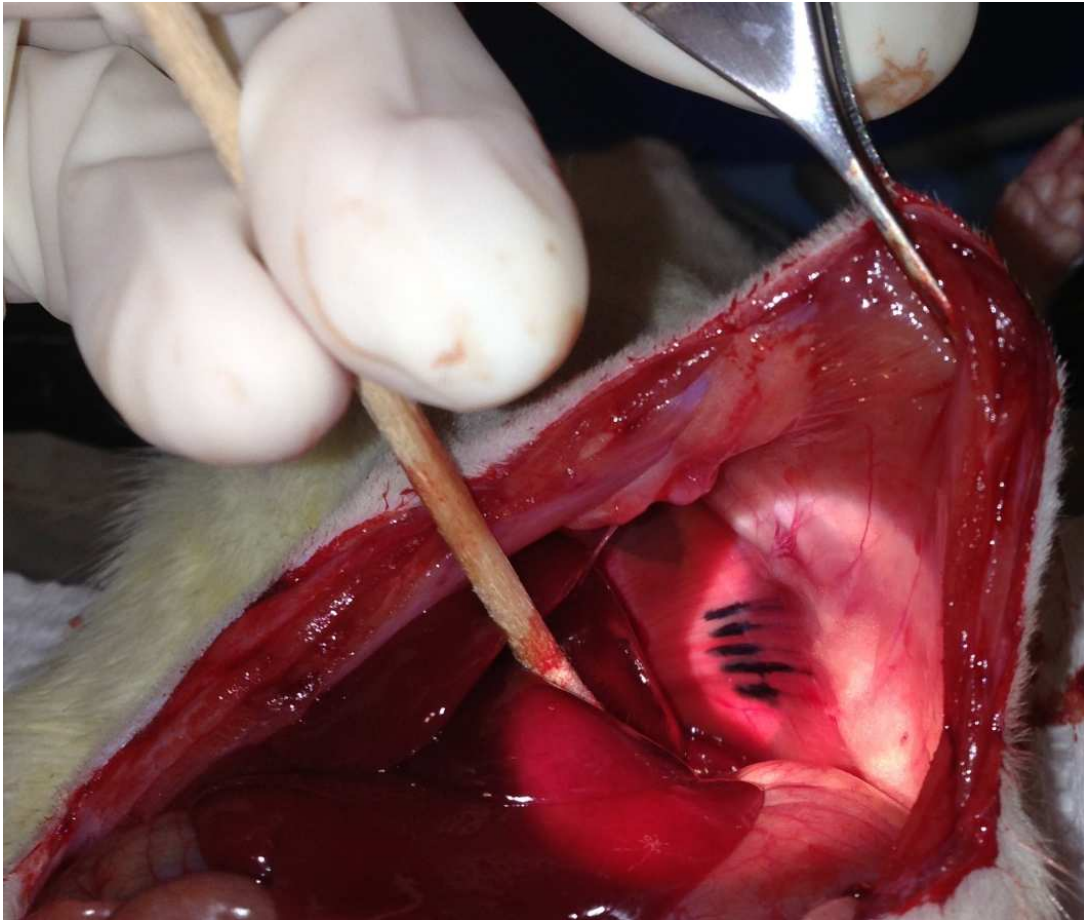


**Figure 50: Intraoperative view of nanoconjugate injection sites.** Exposure of the abdominal surface of the left hemidiaphragm following injections of the WGA-HRP-AuNP-proTHP nanoconjugate into the left hemidiaphragm. Injection sites are clearly visualized due to the black coloration of the nanoconjugate solution.

#### **Intact Phrenic Nerve Soak**

Rats received a soak treatment of 2% WGA-Alexa 488 applied to the isolated left phrenic nerve for 1 hour immediately after a C2Hx or sham surgery. The cervical phrenic

nerve was approached ventrally and isolated from the underlying brachial plexus with fine forceps and cotton swabs. The sheath of the nerve was carefully removed with fine forceps. Photographic images of the nerve were captured at 40X on an Olympus C-5050 digital camera attached to a Zeiss surgical microscope (Fig. 8). A cup created by cutting off the bottom of a 1.5ml microcentrifuge tube was placed under the phrenic nerve. Small pieces of bench top paper were placed around the cup to absorb fluid produced by the surrounding tissue during the 1-hour treatment. 1.5µl of 2% WGA-Alexa 488 were placed in the cup with a micropipette. The surgical field was covered with a piece of gauze moistened in sterile saline to prevent tissues from drying out during treatment. After 1 hour, the remaining WGA-Alexa 488, the cup and the bench paper was removed and the area was gently swabbed to remove excess fluid. The muscles were sutured with 4-0 absorbable suture (Vicryl, Ethicon) followed by 4-0 non-absorbable nylon suture (Ethilon, Ethicon) to close the skin. The rats survived for 48 hours.

### **Intrapleural Injection**

Rats received a transcutaneous intrapleural injection administered through the fifth intercostal space into the thoracic cavity on the right side as described by Mantilla et al., 2009. All rats received 50µl of 2% WGA-Alexa 488 saline solution administered with a 25 gauge by 5/8" needle syringe (Buttry and Goshgarian, 2015). It is important to note that advancing the needle too far will result in an injection into the lung parenchyma.

### **Vagus Nerve Injection**

The right vagus nerve was exposed by an incision of the ventral neck. The vagus nerve was identified based on the anatomical relationship with the jugular vein and the carotid artery. A Hamilton syringe was used to inject 1µl of a neuronal tracer into the right vagus nerve; rats were injected with 5% True blue chloride (TB, Santa Cruz Biotechnology,

Inc. Cat. # sc-216026) aqueous solution, or a 2% WGA-Alexa 594 (Life Technologies Cat. # W11262) saline solution. The surrounding area was examined for any signs of leakage. The neck muscles were sutured with 4-0 absorbable sutures (Vicryl) followed by closure of the skin with 4-0 non-absorbable nylon sutures (Ethilon).

### **Tissue preparation of WGA-Alexa fluor conjugate injected rats**

Forty-eight hours after injections, rats were anesthetized with urethane (1.6 g/kg, ip) and transcardially perfused with 150 mL saline followed by 300 mL of 4% paraformaldehyde in 0.1M phosphate-buffered saline (pH 7.4). The spinal cord (cervical through thoracic) and medulla were removed and an insect pin was inserted along the longitudinal axis of both on the left to differentiate the left from the right side. The medullary and spinal tissue was then post-fixed in the perfusate overnight and cryoprotected 2-3 days in 30% sucrose in 0.1M PBS until the tissue sank. Transverse, horizontal, or sagittal sections through the medulla and spinal cord were cut in 40 $\mu$ m thick sections with a cryostat and collected in 0.1M PBS. Every section from the medulla was saved, whereas every 3rd spinal cord section was saved. Sections were then washed in 0.1M PBS and mounted on Poly-L-lysine treated slides. The sections were cover slipped with Fluoromount (Sigma cat. # F4680) and examined with a Zeiss Axiophot fluorescent microscope using the 488 filter (green), 594 filter (red), and the Dapi filter (blue). Images were captured using the Axio Vision Rel. 4.8 Program.

Autofluorescence is not problematic when examining WGA-Alexa tracers due to the distinct granulation within the WGA-Alexa labeled cells (Goshgarian and Buttry, 2014). However, True blue labeled cells have a hazy appearance throughout the cell body. To reduce the chance of counting false positive True blue labeled cells, images were captured with exposure times that resulted in a dark background. For cell counts, cells were



considered labeled with True blue if the cell body was clearly identifiable and brightly illuminated compared to the dark background. Cells were considered labeled with WGA-Alexa fluor conjugate if the cell body was clearly identifiable and displayed granulation characteristic of the tracer. Neurons labeled with WGA-Alexa fluor conjugates are exceptionally bright and can be easily seen at low magnification. Positively labeled neurons always have distinct granules that can be seen clearly at higher magnification. Non-labeled neurons do not display granulation within the cell boundaries. Cells on every other section from the medulla were counted since every section was saved after sectioning the tissue; this was to avoid counting the same cell body twice. Since every 3rd section from the spinal cord was saved, cells were counted on every spinal cord section saved. A cell was considered labeled if the cell body with a nucleus was identifiable.

### **Bilateral Phrenic Nerve Recordings/Electrophysiology**

The groups designated for bilateral phrenic nerve recordings included rats with varying doses of nanoconjugate, and rats that received injection of one of the control solutions; i) WGA-HRP-Au, ii) AuNP-ProTHP, iii) WGA-HRP-AuNP-ProTHP intravenous, iv) proTHP intradiaphragmatic. Bilateral phrenic nerve recordings were sampled at day 3, 7, and 14 for acute studies and at 13 weeks for chronic studies. The rats were injected with atropine sulfate (0.06mg/kg, im) 10 minutes prior to anesthesia induction to reduce mucus secretions during the procedure. The initial dose of anesthesia was a mixture of ketamine (70mg/kg, ip) and xylazine (7mg/kg, ip). A supplement of ketamine (17mg/kg, ip) and xylazine (2mg/kg, ip) was provided as needed. The femoral vein was cannulated for drug and fluid delivery. The femoral artery was cannulated to monitor blood pressure (World Precision Instruments, #SYS-BP1). The blood pressure was maintained in the range of 90-105 mmHg by injection of Lactated Ringer's (Baxter) as needed. The right and left phrenic

nerve were exposed by an incision to the ventral neck. The phrenic nerves were dissected from the underlying brachial plexus and carefully de-sheathed with fine forceps and cotton swabs. The right and left vagus nerves were dissected and the trachea was dissected to prepare for a tracheotomy. The rats were ventilated with a mixture of room air and oxygen. A bilateral vagotomy and phrenicotomy was performed. The phrenic nerves were cut to eliminate afferent activity. The proximal portions of the cut right and left phrenic nerves were then placed on bipolar platinum electrodes (Grass F-E2). Signals were amplified (20,000X) and band pass-filtered (30Hz-3kHz) by Grass amplifiers (model P511 AC, Astro-Med, Inc., West Warwick, RI), raw and integrated signals were recorded by a Cambridge Electronic Design (CED, Cambridge, England) data acquisition system integrated with CED Spike 2® software. Once the phrenic nerves were stable in the setup, standardized conditions were achieved. The rats were paralyzed with pancuronium bromide (0.5mg/kg iv); and the apneic threshold was determined. To determine the apneic threshold (the lowest PaCO<sub>2</sub> at which a subject will remain apneic (temporary stop breathing)), the ventilator frequency was slowly turned up until the phrenic nerve signal disappeared (ventilator is doing all the work and the system is flooded with O<sub>2</sub> therefore the brain stem does not need to send a signal to contract diaphragm/breath and rid the body of CO<sub>2</sub>). The ventilator was then turned down slowly until the recruitment threshold was found and the rat began to breathe again (bursting signal re-appears on neurogram). The CO<sub>2</sub> level was maintained at the recruitment threshold, 3 to 5 mmHg above the apneic threshold (Fig. 51). Once the rat was stable under standardized conditions the bilateral phrenic nerve recordings and blood pressure were recorded on the Spike 2® software. Blood pressure was monitored and intravenous fluids (Lactated Ringers) were provided as needed.

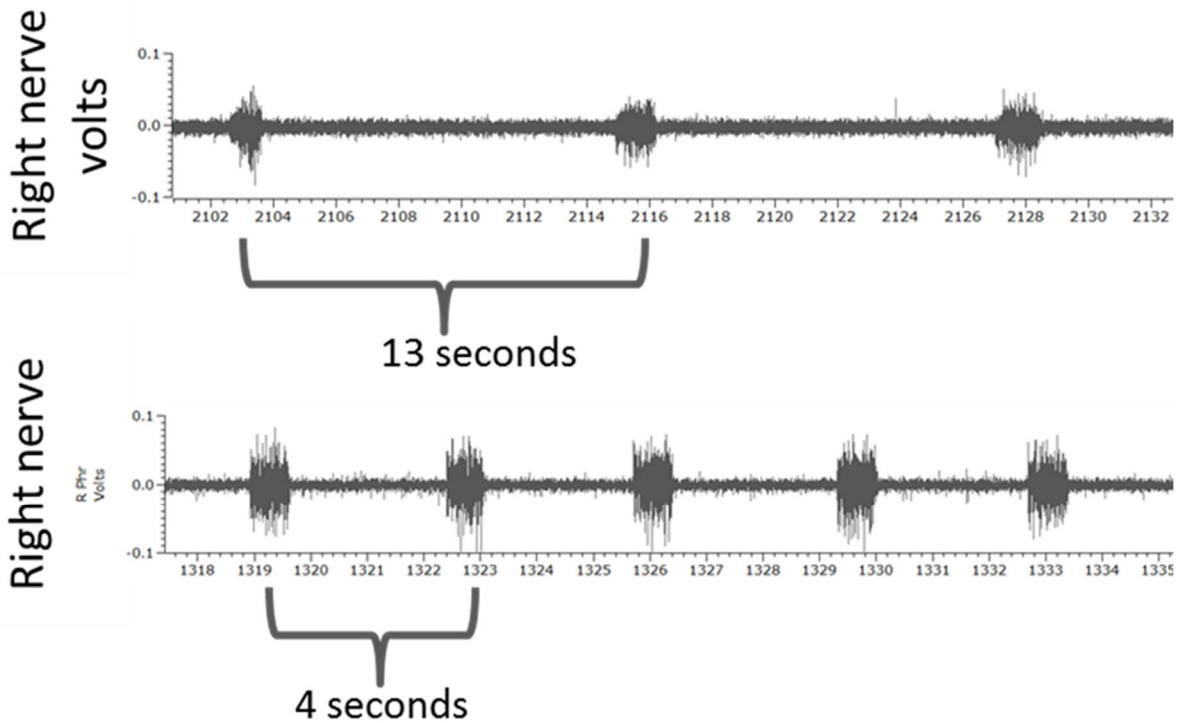


**Figure 51: Example neurograms identifying the apneic and recruitment thresholds.** The top trace displays a neurogram of the right phrenic nerve demonstrating the bursting pattern used to identify the apneic threshold. When the level of oxygen is increased the descending signal from the rVRG is inhibited resulting in an absence of phrenic nerve activity. An absence of signal for a minimum of 7 seconds is used to identify apnea, above is a 13 second pause. Once apnea is identified, the end tidal CO<sub>2</sub> level is set 3-5mmHG higher by slowly decreasing the oxygen to the ventilator. The bottom trace displays a neurogram after the apneic threshold had been identified and the end tidal CO<sub>2</sub> levels were adjusted. The stimuli to breath is stable and consistent as demonstrated by the consistent bursting pattern displayed on the neurogram.

The rats were tested for presence or absence of recovered phrenic nerve activity followed by quantification of the neurograms that demonstrate bilateral phrenic nerve activity (see statistical analysis below).

#### **Tissue preparation to visualize WGA**

Three days after intradiaphragmatic injection of WGA-HRP-AuNP-proTHP, rats were anesthetized with a mixture of ketamine (70mg/kg, ip) and xylazine (7mg/kg, ip). The

rats were transcardially perfused with 150 mL of heparinized saline followed by 350 mL of 4% Formaldehyde in 0.1M phosphate-buffered saline (pH 7.4). The spinal cord (C3-C6) and medulla were removed and an insect pin was inserted along the longitudinal axis of both on the right to differentiate the left from the right side. The medullary and spinal tissues were post-fixed in the perfusate overnight and cryoprotected 2-3 days in 30% sucrose in 0.1M PBS until the medulla sinks. Transverse sections (50microns) through the medulla and spinal cord were cut with a cryostat and collected in 0.1M PBS.

Tissue sections were washed in immunobuffer for 10 minutes (x3) followed by incubation in 10% Normal Horse Serum (NHS) blocking solution for 30 minutes. Sections were incubated in a primary antibody, anti-WGA made in goat (Vector labs, batch 2024) with a 1:200 concentrations in 10% NHS. Sections remained in the primary antibody for 72 hours. Sections were then washed in Tris-PBS for 10 minutes (x3). Sections were then incubated in a secondary antibody, Biotin-Donkey anti-goat (Jackson ImmunoResearch, batch 113055) with a 1:400 concentrations in 1%NHS. Sections remained in the secondary antibody for 24 hours. The sections were washed in Tris-PBS for 10 minutes (x3). Sections were then incubated in Cy 3 Streptavidin (Jackson ImmunoResearch) diluted in immunobuffer with a 1:1000 concentration for 4 hours. After the addition of Cy 3 Streptavidin the sections were covered in foil to limit exposure to lights. Sections were washed in Tris-PBS for 10 minutes (x3) and mounted on slides. Buffered glycerol (pH 8.6) was placed on to the sections and covered slipped (Strack and Loewy, 1990). Tissue sections were examined on a Zeiss Axioimager.M2 fluorescent microscope using the red filter. Images were captured using the Zen 2 pro Blue edition program.

### **Statistical analysis of EMG and neurogram recordings**

All statistical test of EMG data was performed in SigmaPlot 13.0. Qualitative analysis of EMG data was performed as described by Minic et al., 2016. As stated by Minic et al., 2016 only the incidence of recovery was quantitated not the amount of recovery. Treatment groups were divided into a Yes or No category based on recovery (return of function to the left hemidiaphragm) or the absence of activity respectfully. Recovery was classified as a return of activity in any two sections of the left hemidiaphragm (anterior, lateral, posterior). For comparison between two groups, the Fisher exact test was performed to determine if the ratio of Yes/No for each group was statistically different. When more than two groups were being compared, the Chi-square test with  $\alpha = 0.010$  was performed to determine if there was significance within the group as a whole. In addition to the Chi-square, each group was compared pairwise with the Fisher exact test to identify significance between each pair of groups. All graphs for EMG data were made in Excel.

Data was obtained from the bilateral phrenic nerve recording procedure once the apneic threshold was established and the rat was stabilized near the recruitment threshold. Once stabilized 10 consecutive breaths were sampled (Fig. 52). The sampled data from Spike was exported to Excel. The baselines (noise) for the 10 breaths of the right and left neurograms, determined in Spike, were subtracted from the right a left set of data points respectfully in Excel. The area under the curves (AUC) from the right and left rectified and integrated waveforms (INT) were calculated. The percent recovery of the left INT compared to the right INT (right=100%) was calculated for each breath, then the average % INT was calculated. Then the maximum amplitude was identified for each of the 10 breaths. The percent maximum amplitude (MAX) of the left compared to the right (right=100%) was calculated for each breath, then the average % MAX was calculated. The average % INT and the average % MAX for each group was averaged. The average percent recovery for

INT and MAX from each group was then compared and subjected to statistical examination using SigmaPlot 13.0. All groups underwent One-way ANOVA ( $\alpha=0.050$ ) followed by Holm-Sidak pairwise comparison to determine the effect of the injected solution on the percent recovery and percent max recovery. All graphs for neurogram data were made in SigmaPlot 13.0.

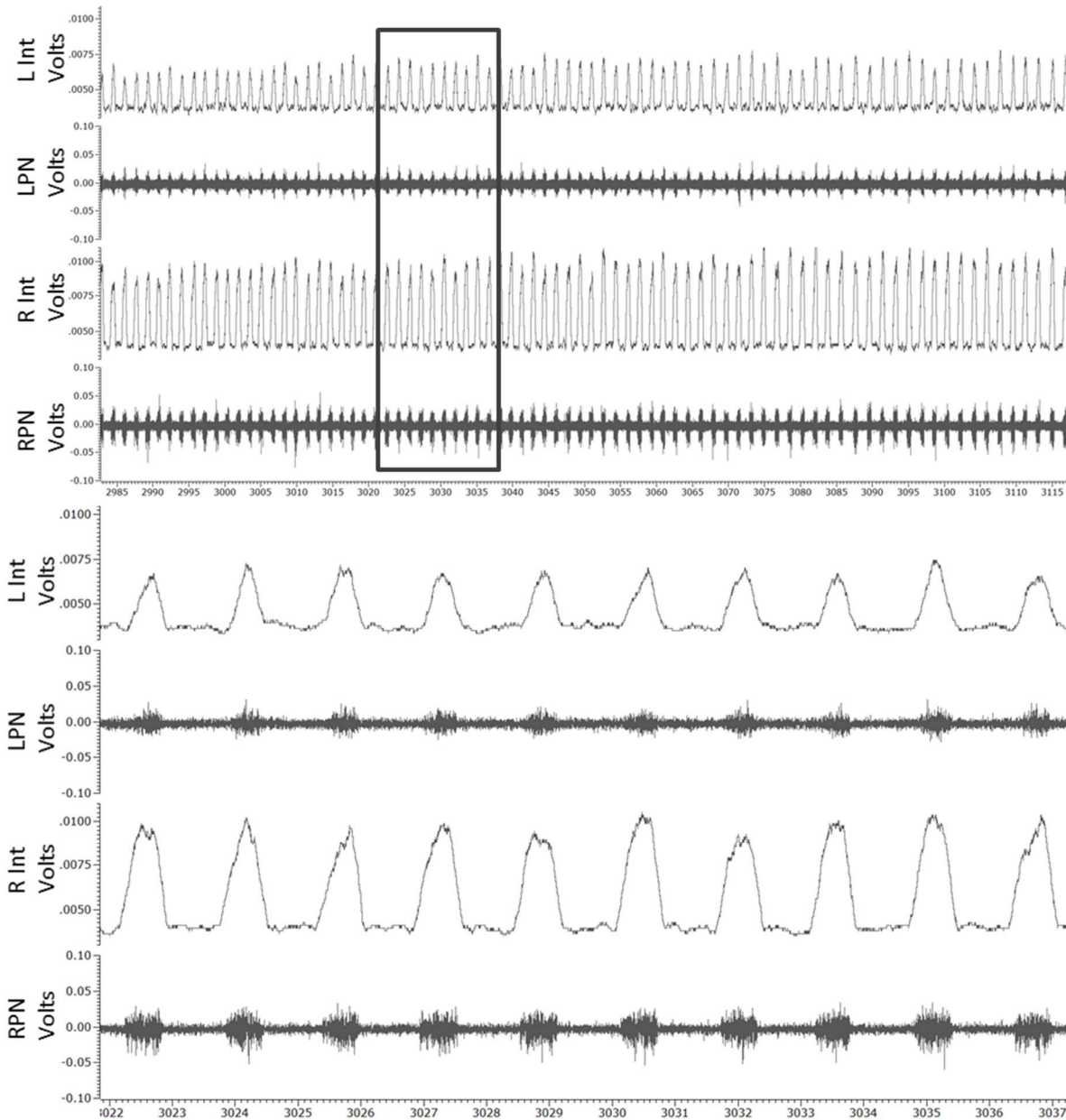


**Figure 52: Phrenic nerve tracing.** The neurogram displayed here was recorded on day 7 post injection. L Int, integrated left waveform; LPN, left phrenic nerve signal in volts; R Int, integrated right waveform; RPN, right phrenic nerve signal in volts. The top trace is a sample of the neurogram that spans over 130 seconds. The bottom trace is a sample of 10 breaths from the boxed area in the top trace. To calculate LPN recovery, background was subtracted from the integrated waveforms. Then the area under the curve was calculated for the R and LPN. Left was expressed as a percentage of right. In addition, the maximum amplitude for each burst was calculated from the R and L integrated waveforms and the left was expressed as a percentage of right.

**APPENDIX****Nanoconjugate Patent Information**

The work presented herein has been submitted for patenting: “Transporter Protein-Coupled Nanodevices for Targeted Drug Delivery”, First Named Inventor/Applicant Name: Harry Goshgarian (co-inventors: Guangzhao Mao, Yanhua Zhang). Original Assignee: Wayne State University. Application number: 14/534,994, Application type: Utility/Design using an application data sheet (37 CFR 1.76), Date Filed: November 6, 2014. Publication number: US20150125926 A1.



## REFERENCES

- Adler S, Roy A, Relman AS (1965) Intracellular acid-base regulation. II. The interaction between CO<sub>2</sub> tension and extracellular bicarbonate in the determination of muscle cell pH. *J Clin Invest* 44:21-30.
- Atoji Y, Kusindarta DL, Hamazaki N, Kaneko A (2005) Innervation of the rat trachea by bilateral cholinergic projections from the nucleus ambiguus and direct motor fibers from the cervical spinal cord: a retrograde and anterograde tracer study. *Brain Res* 1031:90-100.
- Aubier M, De Troyer A, Sampson M, Macklem PT, Roussos C (1981) Aminophylline improves diaphragmatic contractility. *N Engl J Med* 305:249-252.
- Baker-Herman TL, Mitchell GS (2002) Phrenic long-term facilitation requires spinal serotonin receptor activation and protein synthesis. *J Neurosci* 22:6239-6246.
- Barbalho-Moulim MC, Miguel GP, Forti EM, César MeC, Azevedo JL, Costa D (2011) Silicone-ring Roux-en-Y gastric bypass in the treatment of obesity: effects of laparoscopic versus laparotomic surgery on respiration. *Obes Surg* 21:194-199.
- Barker JR, Thomas CF, Behan M (2009) Serotonergic projections from the caudal raphe nuclei to the hypoglossal nucleus in male and female rats. *Respir Physiol Neurobiol* 165:175-184.
- Barnes PJ (2013) Theophylline. *Am J Respir Crit Care Med* 188:901-906.
- Bascom AT, Lattin CD, Aboussouan LS, Goshgarian HG (2005) Effect of acute aminophylline administration on diaphragm function in high cervical tetraplegia: a case report. *Chest* 127:658-661.

- Basterra J, Dilly PN, Chumbley C (1987) The sympathetic innervation of the vocal cord. An experimental study in the guinea pig. *J Laryngol Otol* 101:1040-1045.
- Bellingham MC (1999) Synaptic inhibition of cat phrenic motoneurons by internal intercostal nerve stimulation. *J Neurophysiol* 82:1224-1232.
- Bianchi CP (1961) The Effect of Caffeine on Radiocalcium Movement in Frog Sartorius. *J Gen Physiol* 44:845-858.
- Borges LF, Sidman RL (1982) Axonal transport of lectins in the peripheral nervous system. *J Neurosci* 2:647-653.
- Bosco G, Poppele RE (2001) Proprioception from a spinocerebellar perspective. *Physiol Rev* 81:539-568.
- Boulenguez P, Gestreau C, Vinit S, Stamegna JC, Kastner A, Gauthier P (2007) Specific and artifactual labeling in the rat spinal cord and medulla after injection of monosynaptic retrograde tracers into the diaphragm. *Neurosci Lett* 417:206-211.
- Broadwell RD, Balin BJ (1985) Endocytic and exocytic pathways of the neuronal secretory process and trans-synaptic transfer of wheat germ agglutinin-horseradish peroxidase in vivo. *J Comp Neurol* 242:632-650.
- Butcher RW, Sutherland EW (1962) Adenosine 3',5'-phosphate in biological materials. I. Purification and properties of cyclic 3',5'-nucleotide phosphodiesterase and use of this enzyme to characterize adenosine 3',5'-phosphate in human urine. *J Biol Chem* 237:1244-1250.
- Buttry JL, Goshgarian HG (2014) Injection of WGA-Alexa 488 into the ipsilateral hemidiaphragm of acutely and chronically C2 hemisectioned rats reveals activity-dependent synaptic plasticity in the respiratory motor pathways. *Exp Neurol* 261:440-450.

- Buttry JL, Goshgarian HG (2015) WGA-Alexa transsynaptic labeling in the phrenic motor system of adult rats: Intrapleural injection versus intradiaphragmatic injection. *J Neurosci Methods* 241:137-145.
- Cabot JB, Alessi V, Carroll J, Ligorio M (1994) Spinal cord lamina V and lamina VII interneuronal projections to sympathetic preganglionic neurons. *J Comp Neurol* 347:515-530.
- Center NSCIS (2015) National Spinal Cord Injury Statistical Center Annual Report. In: University of Alabama at Birmingham.
- Chen YS, Hung YC, Liao I, Huang GS (2009) Assessment of the In Vivo Toxicity of Gold Nanoparticles. *Nanoscale Res Lett* 4:858-864.
- Cheng J, Gu YJ, Cheng SH, Wong WT (2013) Surface functionalized gold nanoparticles for drug delivery. *J Biomed Nanotechnol* 9:1362-1369.
- Creed KE, Ishikawa S, Ito Y (1983) Electrical and mechanical activity recorded from rabbit urinary bladder in response to nerve stimulation. *J Physiol* 338:149-164.
- Cunningham ET, Sawchenko PE (1989) A circumscribed projection from the nucleus of the solitary tract to the nucleus ambiguus in the rat: anatomical evidence for somatostatin-28-immunoreactive interneurons subserving reflex control of esophageal motility. *J Neurosci* 9:1668-1682.
- Darlot F, Cayetanot F, Gauthier P, Matarazzo V, Kastner A (2012) Extensive respiratory plasticity after cervical spinal cord injury in rats: axonal sprouting and rerouting of ventrolateral bulbospinal pathways. *Exp Neurol* 236:88-102.
- De Jong WH, Hagens WI, Krystek P, Burger MC, Sips AJ, Geertsma RE (2008) Particle size-dependent organ distribution of gold nanoparticles after intravenous administration. *Biomaterials* 29:1912-1919.

- Deutsch C, Taylor JS, Wilson DF (1982) Regulation of intracellular pH by human peripheral blood lymphocytes as measured by  $^{19}\text{F}$  NMR. *Proc Natl Acad Sci U S A* 79:7944-7948.
- DeVries KL, Goshgarian HG (1989) Spinal cord localization and characterization of the neurons which give rise to the accessory phrenic nerve in the adult rat. *Exp Neurol* 104:88-90.
- Ditunno JF, Little JW, Tessler A, Burns AS (2004) Spinal shock revisited: a four-phase model. *Spinal Cord* 42:383-395.
- Dobbins EG, Feldman JL (1994) Brainstem network controlling descending drive to phrenic motoneurons in rat. *J Comp Neurol* 347:64-86.
- Dougherty BJ, Lee KZ, Lane MA, Reier PJ, Fuller DD (2012a) Contribution of the spontaneous crossed-phrenic phenomenon to inspiratory tidal volume in spontaneously breathing rats. *J Appl Physiol* 112:96-105.
- Dougherty BJ, Lee KZ, Gonzalez-Rothi EJ, Lane MA, Reier PJ, Fuller DD (2012b) Recovery of inspiratory intercostal muscle activity following high cervical hemisection. *Respir Physiol Neurobiol* 183:186-192.
- Dreaden EC, Mackey MA, Huang X, Kang B, El-Sayed MA (2011) Beating cancer in multiple ways using nanogold. *Chem Soc Rev* 40:3391-3404.
- Dreaden EC, Alkilany AM, Huang X, Murphy CJ, El-Sayed MA (2012) The golden age: gold nanoparticles for biomedicine. *Chem Soc Rev* 41:2740-2779.
- Duncan B, Kim C, Rotello VM (2010) Gold nanoparticle platforms as drug and biomacromolecule delivery systems. *J Control Release* 148:122-127.
- Eldridge FL, Millhorn DE, Kiley JP (1985) Antagonism by theophylline of respiratory inhibition induced by adenosine. *J Appl Physiol* (1985) 59:1428-1433.

- Eldridge FL, Millhorn DE, Waldrop TG, Kiley JP (1983) Mechanism of respiratory effects of methylxanthines. *Respir Physiol* 53:239-261.
- Ellenberger HH, Feldman JL (1988) Monosynaptic transmission of respiratory drive to phrenic motoneurons from brainstem bulbospinal neurons in rats. *J Comp Neurol* 269:47-57.
- Ellenberger HH, Feldman JL (1990a) Brainstem connections of the rostral ventral respiratory group of the rat. *Brain Res* 513:35-42.
- Ellenberger HH, Feldman JL (1990b) Subnuclear organization of the lateral tegmental field of the rat. I: Nucleus ambiguus and ventral respiratory group. *J Comp Neurol* 294:202-211.
- Fabian RH, Coulter JD (1985) Transneuronal transport of lectins. *Brain Res* 344:41-48.
- Fay RA, Norgren R (1997) Identification of rat brainstem multisynaptic connections to the oral motor nuclei using pseudorabies virus. III. Lingual muscle motor systems. *Brain Res Brain Res Rev* 25:291-311.
- Feldman JL, Ellenberger HH (1988) Central coordination of respiratory and cardiovascular control in mammals. *Annu Rev Physiol* 50:593-606.
- Feldman JL, Loewy AD, Speck DF (1985) Projections from the ventral respiratory group to phrenic and intercostal motoneurons in cat: an autoradiographic study. *J Neurosci* 5:1993-2000.
- Ferguson G, Khanchandani N, Lattin C, Goshgarian H (1999) Clinical effects of theophylline on inspiratory muscle drive in tetraplegia. In, pp 191-197. *Neurorehabil Neural Repair*.

- Fontán JJ, Diec CT, Velloff CR (2000) Bilateral distribution of vagal motor and sensory nerve fibers in the rat's lungs and airways. *Am J Physiol Regul Integr Comp Physiol* 279:R713-728.
- Fuller DD, Johnson SM, Olson EB, Mitchell GS (2003) Synaptic pathways to phrenic motoneurons are enhanced by chronic intermittent hypoxia after cervical spinal cord injury. *J Neurosci* 23:2993-3000.
- Fuller DD, Golder FJ, Olson EB, Mitchell GS (2006) Recovery of phrenic activity and ventilation after cervical spinal hemisection in rats. *J Appl Physiol* 100:800-806.
- Fuller DD, Doperalski NJ, Dougherty BJ, Sandhu MS, Bolser DC, Reier PJ (2008) Modest spontaneous recovery of ventilation following chronic high cervical hemisection in rats. *Exp Neurol* 211:97-106.
- Furicchia JV, Goshgarian HG (1987) Dendritic organization of phrenic motoneurons in the adult rat. *Exp Neurol* 96:621-634.
- Gaytán SP, Pásaro R (1998) Connections of the rostral ventral respiratory neuronal cell group: an anterograde and retrograde tracing study in the rat. *Brain Res Bull* 47:625-642.
- Gjerdrum LM, Abrahamsen HN, Villegas B, Sorensen BS, Schmidt H, Hamilton-Dutoit SJ (2004) The influence of immunohistochemistry on mRNA recovery from microdissected frozen and formalin-fixed, paraffin-embedded sections. *Diagn Mol Pathol* 13:224-233.
- Golder FJ, Reier PJ, Bolser DC (2001a) Altered respiratory motor drive after spinal cord injury: supraspinal and bilateral effects of a unilateral lesion. *J Neurosci* 21:8680-8689.

- Golder FJ, Reier PJ, Davenport PW, Bolser DC (2001b) Cervical spinal cord injury alters the pattern of breathing in anesthetized rats. *J Appl Physiol* 91:2451-2458.
- Golder FJ, Fuller DD, Davenport PW, Johnson RD, Reier PJ, Bolser DC (2003) Respiratory motor recovery after unilateral spinal cord injury: eliminating crossed phrenic activity decreases tidal volume and increases contralateral respiratory motor output. *J Neurosci* 23:2494-2501.
- Goshgarian HG (1979) Developmental plasticity in the respiratory pathway of the adult rat. *Exp Neurol* 66:547-555.
- Goshgarian HG (2003) The crossed phrenic phenomenon: a model for plasticity in the respiratory pathways following spinal cord injury. *J Appl Physiol* 94:795-810.
- Goshgarian HG, Rafols JA (1981) The phrenic nucleus of the albino rat: a correlative HRP and Golgi study. *J Comp Neurol* 201:441-456.
- Goshgarian HG, Rafols JA (1984) The ultrastructure and synaptic architecture of phrenic motor neurons in the spinal cord of the adult rat. *J Neurocytol* 13:85-109.
- Goshgarian HG, Ellenberger HH, Feldman JL (1991) Decussation of bulbospinal respiratory axons at the level of the phrenic nuclei in adult rats: a possible substrate for the crossed phrenic phenomenon. *Exp Neurol* 111:135-139.
- Goshgarian HG, Buttry JL (2014) The pattern and extent of retrograde transsynaptic transport of WGA-Alexa 488 in the phrenic motor system is dependent upon the site of application. *J Neurosci Methods* 222:156-164.
- Hadley SD, Goshgarian HG (1997) Altered immunoreactivity for glial fibrillary acidic protein in astrocytes within 1 h after cervical spinal cord injury. *Exp Neurol* 146:380-387.

- Hadziefendic S, Haxhiu MA (1999) CNS innervation of vagal preganglionic neurons controlling peripheral airways: a transneuronal labeling study using pseudorabies virus. *J Auton Nerv Syst* 76:135-145.
- Harrison PJ, Jankowska E, Zytnicki D (1986) Lamina VIII interneurons interposed in crossed reflex pathways in the cat. *J Physiol* 371:147-166.
- Harrison PJ, Hultborn H, Jankowska E, Katz R, Storai B, Zytnicki D (1984) Labelling of interneurons by retrograde transsynaptic transport of horseradish peroxidase from motoneurons in rats and cats. *Neurosci Lett* 45:15-19.
- Hatten ME, Schachner M, Sidman RL (1979) Histochemical characterization of lectin binding in mouse cerebellum. *Neuroscience* 4:921-935.
- Haxhiu MA, Loewy AD (1996) Central connections of the motor and sensory vagal systems innervating the trachea. *J Auton Nerv Syst* 57:49-56.
- Hayakawa T, Takanaga A, Tanaka K, Maeda S, Seki M (2002) Organization and distribution of the upper and lower esophageal motoneurons in the medulla and the spinal cord of the rat. *Okajimas Folia Anat Jpn* 78:263-279.
- Hayakawa T, Takanaga A, Tanaka K, Maeda S, Seki M (2004) Ultrastructure of the rostral ventral respiratory group neurons in the ventrolateral medulla of the rat. *Brain Res* 1027:94-102.
- He Y, Revel M, Loty B (1995) A quantitative model of post-laminectomy scar formation. Effects of a nonsteroidal anti-inflammatory drug. *Spine (Phila Pa 1976)* 20:557-563; discussion 579-580.
- Hershman S, Cuellar VG, Bendo JA (2013) Delayed presentation of incidental durotomy. *Bull Hosp Jt Dis* (2013) 71:231-234.



- Hilaire G, Monteau R (1997) Brainstem and spinal control of respiratory muscles during breathing. In, pp 91–105. Neural control of the respiratory muscles: Miller AD, Bianchi AL, Bishop BP, editors. CRC; New York: .
- Hirai N, Nakashima H, Tanaka Y (1988) Activity of dorsal spinocerebellar tract neurones in the thoracic spinal cord in relation to respiratory movement. *Brain Res* 475:385-388.
- Hoffman MS, Golder FJ, Mahamed S, Mitchell GS (2010) Spinal adenosine A2(A) receptor inhibition enhances phrenic long term facilitation following acute intermittent hypoxia. *J Physiol* 588:255-266.
- Horn JP, McAfee DA (1977) Modulation of cyclic nucleotide levels in peripheral nerve without effect on resting or compound action potentials. *J Physiol* 269:753-766.
- Hosono N, Yonenobu K, Ono K (1995) Postoperative cervical pseudomeningocele with herniation of the spinal cord. *Spine (Phila Pa 1976)* 20:2147-2150.
- Isaacson A, Sandow A (1967) Quinine and caffeine effects on <sup>45</sup>Ca movements in frog sartorius muscle. *J Gen Physiol* 50:2109-2128.
- Jain KK (2010) Advances in the field of nanooncology. *BMC Med* 8:83.
- Jankowska E (1985) Further indications for enhancement of retrograde transneuronal transport of WGA-HRP by synaptic activity. *Brain Res* 341:403-408.
- Jones DA, Howell S, Roussos C, Edwards RH (1982) Low-frequency fatigue in isolated skeletal muscles and the effects of methylxanthines. *Clin Sci (Lond)* 63:161-167.
- Kajana S, Goshgarian HG (2008a) Administration of phosphodiesterase inhibitors and an adenosine A1 receptor antagonist induces phrenic nerve recovery in high cervical spinal cord injured rats. *Exp Neurol* 210:671-680.

- Kajana S, Goshgarian HG (2008b) Spinal activation of the cAMP-PKA pathway induces respiratory motor recovery following high cervical spinal cord injury. *Brain Res* 1232:206-213.
- Kajana S, Goshgarian HG (2009) Systemic administration of rolipram increases medullary and spinal cAMP and activates a latent respiratory motor pathway after high cervical spinal cord injury. *J Spinal Cord Med* 32:175-182.
- Kentera D, Varagić VM (1975) The effects of cyclic N-2-O-dibutyl- adenosine 3',5'-monophosphate, adrenaline and aminophylline on the isometric contractility of the isolated hemidiaphragm of the rat. *Br J Pharmacol* 54:375-381.
- Kobler JB, Datta S, Goyal RK, Benecchi EJ (1994) Innervation of the larynx, pharynx, and upper esophageal sphincter of the rat. *J Comp Neurol* 349:129-147.
- Lalley PM, Mifflin SW (2012) Opposing effects on the phrenic motor pathway attributed to dopamine-D1 and -D3/D2 receptor activation. *Respir Physiol Neurobiol* 181:183-193.
- Lane MA, Lee KZ, Fuller DD, Reier PJ (2009) Spinal circuitry and respiratory recovery following spinal cord injury. *Respir Physiol Neurobiol* 169:123-132.
- Lane MA, White TE, Coutts MA, Jones AL, Sandhu MS, Bloom DC, Bolser DC, Yates BJ, Fuller DD, Reier PJ (2008) Cervical prephrenic interneurons in the normal and lesioned spinal cord of the adult rat. *J Comp Neurol* 511:692-709.
- Laskowski MB, Sanes JR (1987) Topographic mapping of motor pools onto skeletal muscles. *J Neurosci* 7:252-260.
- Lee JI, Sollars PJ, Baver SB, Pickard GE, Leelawong M, Smith GA (2009) A herpesvirus encoded deubiquitinase is a novel neuroinvasive determinant. *PLoS Pathog* 5:e1000387.

- Lipski J, Duffin J, Kruszewska B, Zhang X (1993) Upper cervical inspiratory neurons in the rat: an electrophysiological and morphological study. *Exp Brain Res* 95:477-487.
- Lipski J, Zhang X, Kruszewska B, Kanjhan R (1994) Morphological study of long axonal projections of ventral medullary inspiratory neurons in the rat. *Brain Res* 640:171-184.
- Luo P, Zhang J, Yang R, Pendlebury W (2006) Neuronal circuitry and synaptic organization of trigeminal proprioceptive afferents mediating tongue movement and jaw-tongue coordination via hypoglossal premotor neurons. *Eur J Neurosci* 23:3269-3283.
- MacFarlane PM, Mitchell GS (2008) Respiratory long-term facilitation following intermittent hypoxia requires reactive oxygen species formation. *Neuroscience* 152:189-197.
- MacFarlane PM, Satriotomo I, Windelborn JA, Mitchell GS (2009) NADPH oxidase activity is necessary for acute intermittent hypoxia-induced phrenic long-term facilitation. *J Physiol* 587:1931-1942.
- Macki M, Lo SF, Bydon M, Kaloostian P, Bydon A (2014) Post-surgical thoracic pseudomeningocele causing spinal cord compression. *J Clin Neurosci* 21:367-372.
- Manaker S, Tischler LJ, Bigler TL, Morrison AR (1992) Neurons of the motor trigeminal nucleus project to the hypoglossal nucleus in the rat. *Exp Brain Res* 90:262-270.
- Mantilla CB, Zhan WZ, Sieck GC (2009) Retrograde labeling of phrenic motoneurons by intrapleural injection. *J Neurosci Methods* 182:244-249.
- Matsushita M, Gao X (1997) Projections from the thoracic cord to the cerebellar nuclei in the rat, studied by anterograde axonal tracing. *J Comp Neurol* 386:409-421.
- Mieszawska AJ, Mulder WJ, Fayad ZA, Cormode DP (2013) Multifunctional gold nanoparticles for diagnosis and therapy of disease. *Mol Pharm* 10:831-847.

- Minic Z, Zhang Y, Mao G, Goshgarian HG (2016) Transporter Protein-Coupled DPCPX Nanoconjugates Induce Diaphragmatic Recovery after SCI by Blocking Adenosine A1 Receptors. *J Neurosci* 36:3441-3452.
- Minkels RF, Jüch PJ, Ter Horst GJ, Van Willigen JD (1991) Projections of the parvocellular reticular formation to the contralateral mesencephalic trigeminal nucleus in the rat. *Brain Res* 547:13-21.
- Model MA, Reese JL, Fraizer GC (2009) Measurement of wheat germ agglutinin binding with a fluorescence microscope. *Cytometry A* 75:874-881.
- Mogoseanu D, Smith AD, Bolam JP (1993) Monosynaptic innervation of trigeminal motor neurones involved in mastication by neurones of the parvicellular reticular formation. *J Comp Neurol* 336:53-65.
- Moreno DE, Yu XJ, Goshgarian HG (1992) Identification of the axon pathways which mediate functional recovery of a paralyzed hemidiaphragm following spinal cord hemisection in the adult rat. *Exp Neurol* 116:219-228.
- Moro S, Gao ZG, Jacobson KA, Spalluto G (2006) Progress in the pursuit of therapeutic adenosine receptor antagonists. *Med Res Rev* 26:131-159.
- Mouledous L, Hunt S, Harcourt R, Harry JL, Williams KL, Gutstein HB (2002) Lack of compatibility of histological staining methods with proteomic analysis of laser-capture microdissected brain samples. *J Biomol Tech* 13:258-264.
- Nantwi KD, Goshgarian HG (1998) Theophylline-induced recovery in a hemidiaphragm paralyzed by hemisection in rats: contribution of adenosine receptors. *Neuropharmacology* 37:113-121.

- Nantwi KD, Goshgarian HG (2002) Actions of specific adenosine receptor A1 and A2 agonists and antagonists in recovery of phrenic motor output following upper cervical spinal cord injury in adult rats. *Clin Exp Pharmacol Physiol* 29:915-923.
- Nantwi KD, El-Bohy A, Goshgarian HG (1996) Actions of systemic theophylline on hemidiaphragmatic recovery in rats following cervical spinal cord hemisection. *Exp Neurol* 140:53-59.
- Nantwi KD, Basura GJ, Goshgarian HG (2003a) Adenosine A1 receptor mRNA expression and the effects of systemic theophylline administration on respiratory function 4 months after C2 hemisection. *J Spinal Cord Med* 26:364-371.
- Nantwi KD, Basura GJ, Goshgarian HG (2003b) Effects of long-term theophylline exposure on recovery of respiratory function and expression of adenosine A1 mRNA in cervical spinal cord hemisected adult rats. *Exp Neurol* 182:232-239.
- Nantwi KD, El Bohy A, Schrimsher GW, Reier PJ, Goshgarian HG (1999) Spontaneous functional recovery in paralyzed hemidiaphragm following upper cervical spinal cord injury in adult rats. *Neurorehabil Repair* 13:225-234.
- Nathan PW (1963) The Descending Respiratory Pathway In Man. *J Neurol Neurosurg Psychiatry* 26:487-499.
- Nathan PW, Smith M, Deacon P (1996) Vestibulospinal, reticulospinal and descending propriospinal nerve fibres in man. *Brain* 119 ( Pt 6):1809-1833.
- Notsu K, Tsumori T, Yokota S, Sekine J, Yasui Y (2008) Posterior lateral hypothalamic axon terminals are in contact with trigeminal premotor neurons in the parvicellular reticular formation of the rat medulla oblongata. *Brain Res* 1244:71-81.
- Nozaki S, Iriki A, Nakamura Y (1993) Trigeminal premotor neurons in the bulbar parvocellular reticular formation participating in induction of rhythmical activity of

- trigeminal motoneurons by repetitive stimulation of the cerebral cortex in the guinea pig. *J Neurophysiol* 69:595-608.
- Panchuk-Voloshina N, Haugland RP, Bishop-Stewart J, Bhalgat MK, Millard PJ, Mao F, Leung WY (1999) Alexa dyes, a series of new fluorescent dyes that yield exceptionally bright, photostable conjugates. *J Histochem Cytochem* 47:1179-1188.
- Payne JN (1987) Comparisons between the use of true blue and diamidino yellow as retrograde fluorescent tracers. *Exp Brain Res* 68:631-642.
- Peterson BW, Maunz RA, Pitts NG, Mackel RG (1975) Patterns of projection and branching of reticulospinal neurons. *Exp Brain Res* 23:333-351.
- Porter WT (1895) The Path of the Respiratory Impulse from the Bulb to the Phrenic Nuclei. *J Physiol* 17:455-485.
- Pérez Fontán JJ, Velloff CR (2001) Labeling of vagal motoneurons and central afferents after injection of cholera toxin B into the airway lumen. *Am J Physiol Lung Cell Mol Physiol* 280:L152-164.
- Qin C, Farber JP, Chandler MJ, Foreman RD (2002) Chemical activation of C(1)-C(2) spinal neurons modulates activity of thoracic respiratory interneurons in rats. *Am J Physiol Regul Integr Comp Physiol* 283:R843-852.
- Reeber SL, Gebre SA, Sillitoe RV (2011a) Fluorescence mapping of afferent topography in three dimensions. *Brain Struct Funct* 216:159-169.
- Reeber SL, Gebre SA, Filatova N, Sillitoe RV (2011b) Revealing neural circuit topography in multi-color. *J Vis Exp*.
- Richerson GB (2004) Serotonergic neurons as carbon dioxide sensors that maintain pH homeostasis. *Nat Rev Neurosci* 5:449-461.

- Robertson B (1990) Wheat germ agglutinin binding in rat primary sensory neurons: a histochemical study. *Histochemistry* 94:81-85.
- Ruda M, Coulter JD (1982) Axonal and transneuronal transport of wheat germ agglutinin demonstrated by immunocytochemistry. *Brain Res* 249:237-246.
- Sahara Y, Hashimoto N, Nakamura Y (1996) Hypoglossal premotor neurons in the rostral medullary parvocellular reticular formation participate in cortically-induced rhythmical tongue movements. *Neurosci Res* 26:119-131.
- Sawchenko PE, Swanson LW (1981a) A method for tracing biochemically defined pathways in the central nervous system using combined fluorescence retrograde transport and immunohistochemical techniques. *Brain Res* 210:31-51.
- Sawchenko PE, Swanson LW (1981b) Central noradrenergic pathways for the integration of hypothalamic neuroendocrine and autonomic responses. *Science* 214:685-687.
- Saywell SA, Ford TW, Meehan CF, Todd AJ, Kirkwood PA (2011) Electrophysiological and morphological characterization of propriospinal interneurons in the thoracic spinal cord. *J Neurophysiol* 105:806-826.
- Schultze-Werninghaus G, Meier-Sydow J (1982) The clinical and pharmacological history of theophylline: first report on the bronchospasmolytic action in man by S. R. Hirsch in Frankfurt (Main) 1922. *Clin Allergy* 12:211-215.
- Schwab ME, Suda K, Thoenen H (1979) Selective retrograde transsynaptic transfer of a protein, tetanus toxin, subsequent to its retrograde axonal transport. *J Cell Biol* 82:798-810.
- Shammah-Lagnado SJ, Costa MS, Ricardo JA (1992) Afferent connections of the parvocellular reticular formation: a horseradish peroxidase study in the rat. *Neuroscience* 50:403-425.

- Shannon R, Freeman D (1981) Nucleus retroambigualis respiratory neurons: responses to intercostal and abdominal muscle afferents. *Respir Physiol* 45:357-375.
- Shrestha SS, Bannatyne BA, Jankowska E, Hammar I, Nilsson E, Maxwell DJ (2012) Excitatory inputs to four types of spinocerebellar tract neurons in the cat and the rat thoraco-lumbar spinal cord. *J Physiol* 590:1737-1755.
- Sieck GC, Fournier M (1989) Diaphragm motor unit recruitment during ventilatory and nonventilatory behaviors. *J Appl Physiol* 66:2539-2545.
- Simonyan K, Feng X, Henriquez VM, Ludlow CL (2012) Combined laryngeal inflammation and trauma mediate long-lasting immunoreactivity response in the brainstem sensory nuclei in the rat. *Front Integr Neurosci* 6:97.
- Soja PJ, Fragoso MC, Cairns BE, Oka JI (1995) Dorsal spinocerebellar tract neuronal activity in the intact chronic cat. *J Neurosci Methods* 60:227-239.
- Spyer KM (2009) To breathe or not to breathe? That is the question. *Exp Physiol* 94:1-10.
- Stecina K, Fedirchuk B, Hultborn HR (2013) Information to cerebellum on spinal motor networks mediated by the dorsal spinocerebellar tract. *J Physiol*.
- Strack AM, Loewy AD (1990) Pseudorabies virus: a highly specific transneuronal cell body marker in the sympathetic nervous system. *J Neurosci* 10:2139-2147.
- Stuesse SL, Powell KS (1982) Cardiac vagal preganglionic fibers in neonatal rats: a comparison with cervical vagal components. *Neurosci Lett* 34:7-12.
- Supinski GS, Deal EC, Kelsen SG (1984) The effects of caffeine and theophylline on diaphragm contractility. *Am Rev Respir Dis* 130:429-433.
- Tanaka Y, Hirai N (1994) Physiological studies of thoracic spinocerebellar tract neurons in relation to respiratory movement. *Neurosci Res* 19:317-326.



- Tanaka Y, Abla D, Hirai N (1990) Activity of crossed spinocerebellar tract neurones in the thoracic spinal cord in relation to the central respiratory rhythm. *Brain Res* 532:339-341.
- Ter Horst GJ, Copray JC, Liem RS, Van Willigen JD (1991) Projections from the rostral parvocellular reticular formation to pontine and medullary nuclei in the rat: involvement in autonomic regulation and orofacial motor control. *Neuroscience* 40:735-758.
- Thakor AS, Jokerst J, Zavaleta C, Massoud TF, Gambhir SS (2011) Gold nanoparticles: a revival in precious metal administration to patients. *Nano Lett* 11:4029-4036.
- Tian GF, Duffin J (1996) Connections from upper cervical inspiratory neurons to phrenic and intercostal motoneurons studied with cross-correlation in the decerebrate rat. *Exp Brain Res* 110:196-204.
- Travers JB, Norgren R (1983) Afferent projections to the oral motor nuclei in the rat. *J Comp Neurol* 220:280-298.
- Tsumori T, Qin Y, Yokota S, Niu JG, Yasui Y (2010) Central amygdaloid axon terminals are in contact with retrorubral field neurons that project to the parvocellular reticular formation of the medulla oblongata in the rat. *Brain Res* 1306:18-28.
- Tzelepis GE, Bascom AT, Safwan Badr M, Goshgarian HG (2006) Effects of theophylline on pulmonary function in patients with traumatic tetraplegia. *J Spinal Cord Med* 29:227-233.
- Valle MS, Bosco G, Poppele R (2000) Information processing in the spinocerebellar system. *Neuroreport* 11:4075-4079.
- Viala D, Fretton E (1983) Evidence for respiratory and locomotor pattern generators in the rabbit cervico-thoracic cord and for their interactions. *Exp Brain Res* 49:247-256.

- Vinit S, Kastner A (2009) Descending bulbospinal pathways and recovery of respiratory motor function following spinal cord injury. *Respir Physiol Neurobiol* 169:115-122.
- Wang H, Owens JD, Shih JH, Li MC, Bonner RF, Mushinski JF (2006) Histological staining methods preparatory to laser capture microdissection significantly affect the integrity of the cellular RNA. *BMC Genomics* 7:97.
- Watson C, Paxinos G, Kayalioglu G (2009) *The Spinal Cord, First Edition Edition*: Academic Press.
- Wilkerson JE, Mitchell GS (2009) Daily intermittent hypoxia augments spinal BDNF levels, ERK phosphorylation and respiratory long-term facilitation. *Exp Neurol* 217:116-123.
- Yamazaki H, Ohi Y, Haji A (2009) Mu-opioid and N-methyl-D-aspartate receptors are localized at laryngeal motoneurons of guinea pigs. *Biol Pharm Bull* 32:293-296.
- Yang CC, Chan JY, Chan SH (1995) Excitatory innervation of caudal hypoglossal nucleus from nucleus reticularis gigantocellularis in the rat. *Neuroscience* 65:365-374.
- Yang TY, Chen HJ, Sung FC, Kao CH (2015) The association between spinal cord injury and acute myocardial infarction in a nationwide population-based cohort study. *Spine (Phila Pa 1976)* 40:147-152.
- Yasui Y, Tsumori T, Oka T, Yokota S (2004) Amygdaloid axon terminals are in contact with trigeminal premotor neurons in the parvicellular reticular formation of the rat medulla oblongata. *Brain Res* 1016:129-134.
- Zhang J, Luo P (2003) Ultrastructural features of synapse from dorsal parvocellular reticular formation neurons to hypoglossal motoneurons of the rat. *Brain Res* 963:262-273.

Zhang Y, Buttry Walker J, Minic Z, Liu F, Goshgarian H, Mao G (2016) Transporter protein and drug-conjugated gold nanoparticles capable of bypassing the blood-brain barrier. *Sci Rep* 6:25794.

Zhang YP, Onifer SM, Burke DA, Shields CB (2001) A topical mixture for preventing, abolishing, and treating autophagia and self-mutilation in laboratory rats. *Contemp Top Lab Anim Sci* 40:35-36.

Zhou C, Yang S, Liu J, Yu M, Zheng J (2013) Luminescent gold nanoparticles: A new class of nanoprobes for biomedical imaging. *Exp Biol Med* (Maywood).

**ABSTRACT****AN ANALYSIS OF PLASTICITY IN THE RAT RESPIRATORY SYSTEM FOLLOWING  
CERVICAL SPINAL CORD INJURY AND THE APPLICATION OF  
NANOTECHNOLOGY TO INDUCE OR ENHANCE RECOVERY OF DIAPHRAGM**

by

**JANELLE WALKER****August 2016****Advisor:** Dr. Harry Goshgarian**Major:** Anatomy and Cell Biology**Degree:** Doctor of Philosophy

Second cervical segment spinal cord hemisection (C2Hx) results in ipsilateral hemidiaphragm paralysis. However, the intact latent crossed phrenic pathway can restore function spontaneously over time or immediately following drug administration.

WGA bound fluorochromes were administered to identify nuclei associated with diaphragm function in both the acute and chronic C2Hx models. WGA is unique in that it undergoes receptor mediated endocytosis and is transsynaptically transported across select physiologically active synapses. Comparison of labeling in the acutely injured to the chronically injured rat provided an anatomical map of spinal and supraspinal injury induced synaptic plasticity. The plasticity occurs over time in the chronic C2Hx model in an effort to adapt to the loss of hemidiaphragm function.

Utilizing the selectivity of WGA, a nanoconjugate was developed to target drug delivery to nuclei involved in diaphragm function post C2Hx in an effort to restore lost function. Theophylline was selected due to its established history as a respiratory stimulant. Theophylline was attached to gold nanoparticles by a transient bond designed to degrade intracellularly. The gold nanoparticles were then permanently attached to WGA-HRP.

Following intradiaphragmatic injection, the WGA portion was identified in the ipsilateral phrenic nuclei and bilaterally in the rVRGs. The location of WGA should reflect the location of the AuNP since the peptide bond between them is permanent.

The effectiveness of the nanoconjugate was verified with EMG analysis of the diaphragm and recordings from the phrenic nerves. All doses administered in the acute C2Hx model resulted in resorted hemidiaphragm and phrenic nerve activity. A dose of 0.14mg/kg had a significantly higher percent recovery on day 3, whereas 0.03mg/kg was significantly higher on day 14. The change in most effective dose over time is likely due to the availability or concentration of the drug and location of drug release. Administration of the nanoconjugate was also characterized in the chronically C2Hx model. The dose 0.06mg/kg resulted in significant recovery when injected 12 weeks post-C2Hx. This data suggests that WGA bound nanoconjugates are able to undergo endocytosis. In addition, the theophylline bound nanoconjugate is capable of restoring hemidiaphragm and phrenic nerve activity.

## AUTOBIOGRAPHICAL STATEMENT

### Education

- 2011 – 2016 Wayne State University School of Medicine, Detroit, MI  
Ph.D., Anatomy and Cell Biology
- 2003 – 2007 Oakland University, Rochester, MI  
Bachelor of Science, Biology

### Training

- 2010 – 2011 Physician Education and Medical Informatics  
Detroit Medical Center
- 2008 – 2009 Laboratory Associate, Eye Research Institute
- 2004 – 2007 Undergraduate Research Assistant, Oakland University  
Mouse embryonic stem cell and derivative cell line research

### Awards/Service

- 2012 Graduate Student Research Day committee member
- 2013 – 2014 Thomas C. Rumble Graduate Fellowship Recipient
- 2013 – 2015 Wayne State University Student Neuroscience Society
- 2014 – 2015 Thomas C. Rumble Graduate Fellowship Renewal
- 2014 – 2015 Physiology Journal Club
- 2016 Anatomy and Cell Biology Graduate Student Research Forum